Supporting Information

Threading of various 'U' shaped bidentate axles into a heteroditopic macrocyclic wheel *via* Ni^{II}/ Cu^{II} templation

Mandira Nandi, Saikat Santra, Bidyut Akhuli, Pradyut Ghosh*

Indian Association for the Cultivation of Science, 2A & 2B Raja S. C. Mullick Road, Kolkata 700 032, India. Fax: (+91) 33-2473-2805

E-mail: icpg@iacs.res.in

Table of Contents

Scheme 1S. Synthesis of **Axle2**

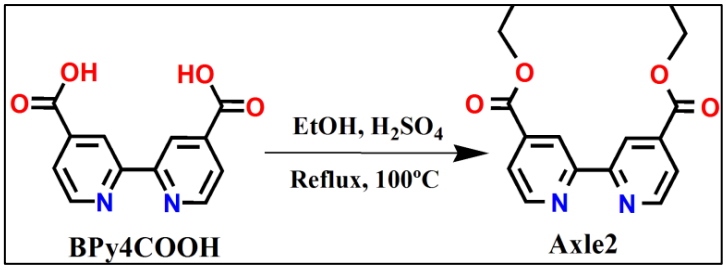

Scheme 2S. Synthesis of **Axle3**

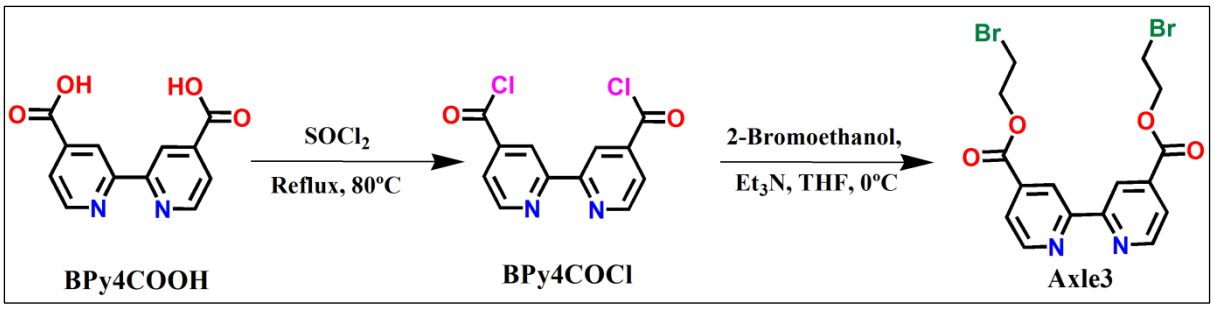

Scheme 3S. Synthesis of **Axle4**

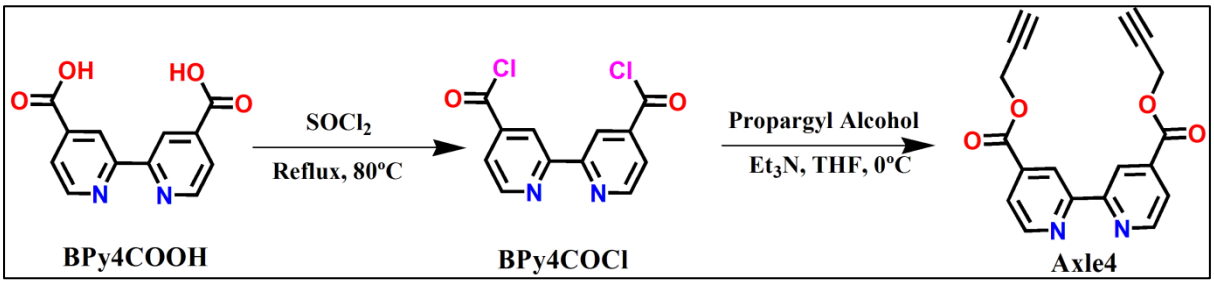

Scheme 4S. Synthesis of **Axle5**

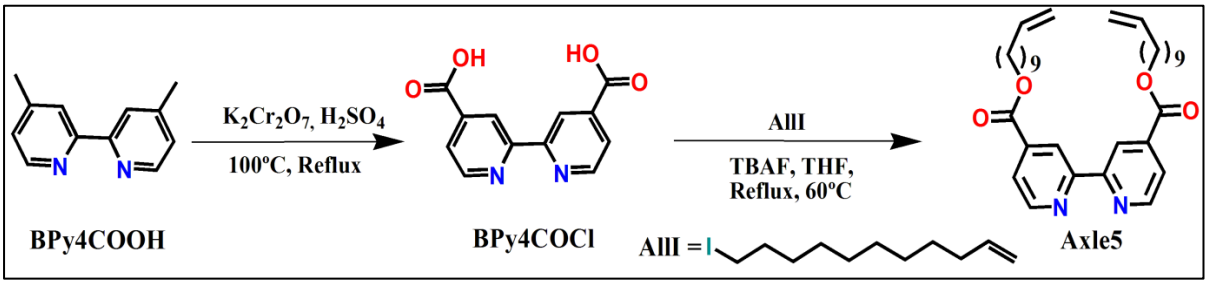

Scheme 5S. Synthesis of **Axle6**

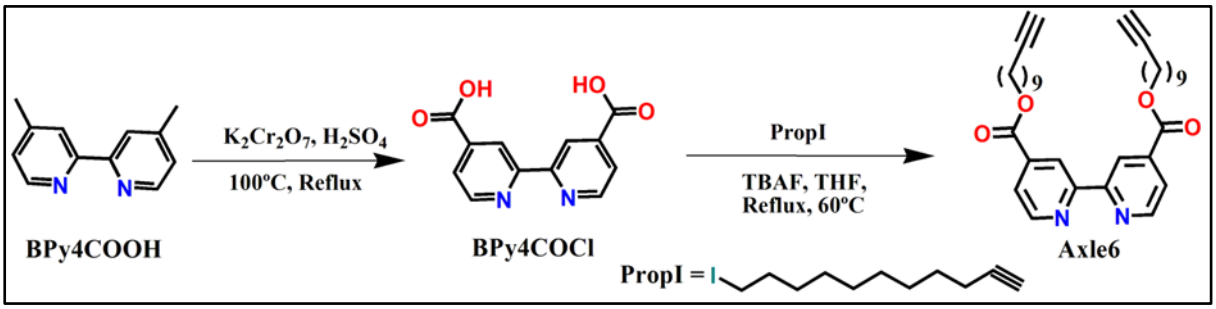

Scheme 6S. Synthesis of **Axle7**

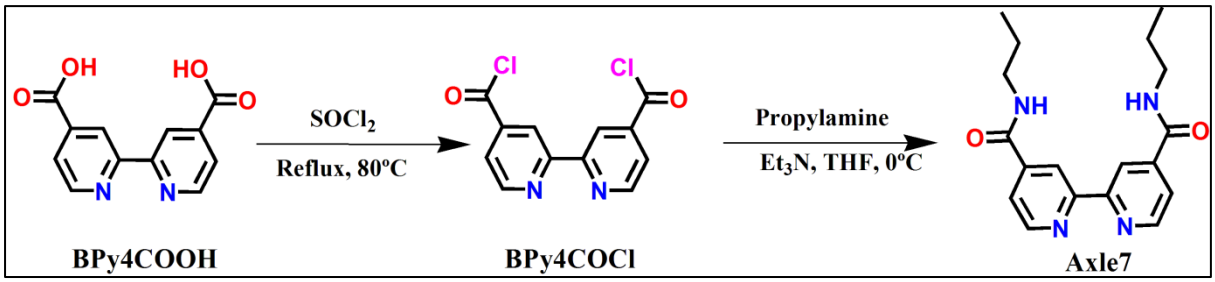

Scheme 7S. Synthesis of **Axle8**

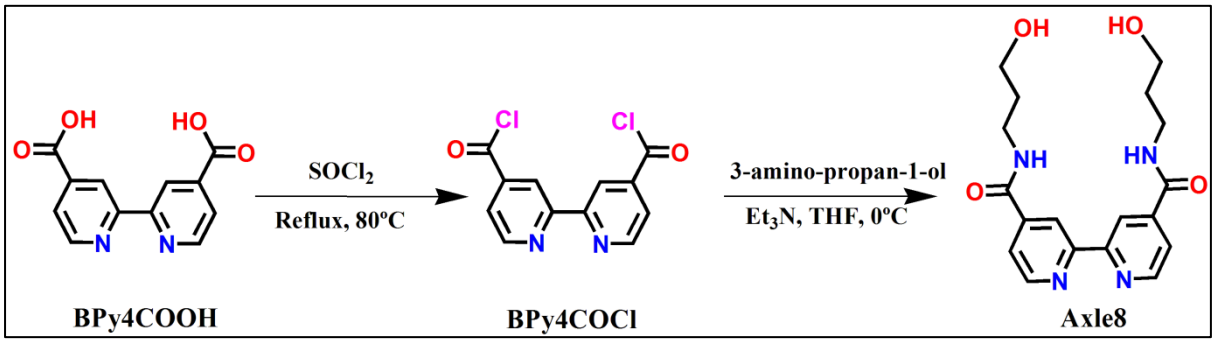

Scheme 8S. Synthesis of **Axle9**

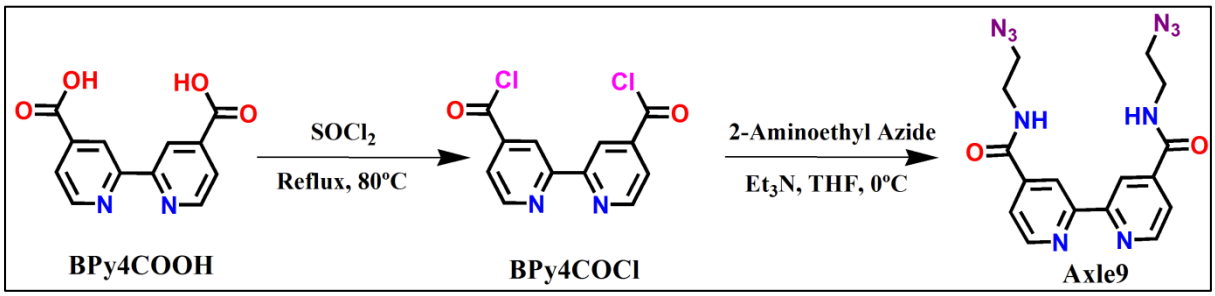

Scheme 9S: Synthesis of **Axle10**

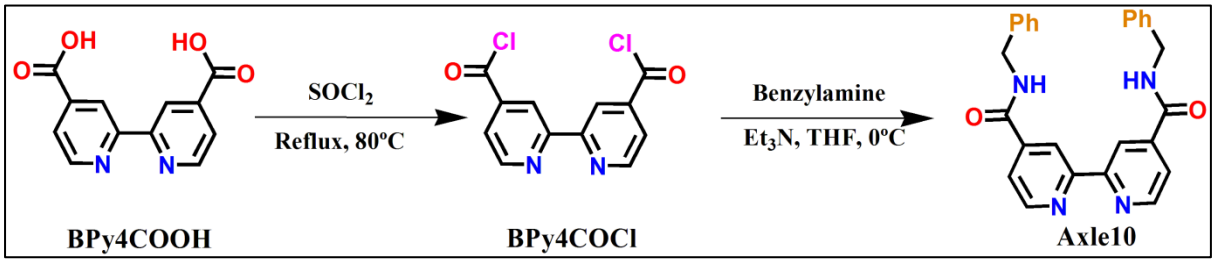

Figure 1S: ESI-MS of **Axle3**

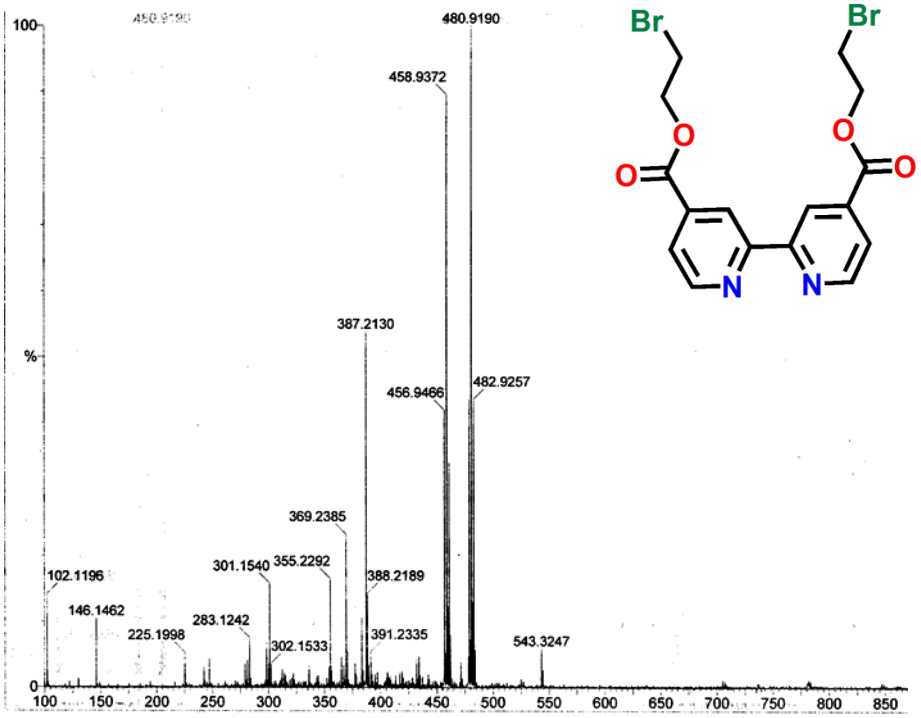

Figure 2S: ^{1}H-NMR Spectrum of **Axle3** in $CDCl_3$ (400 MHz)

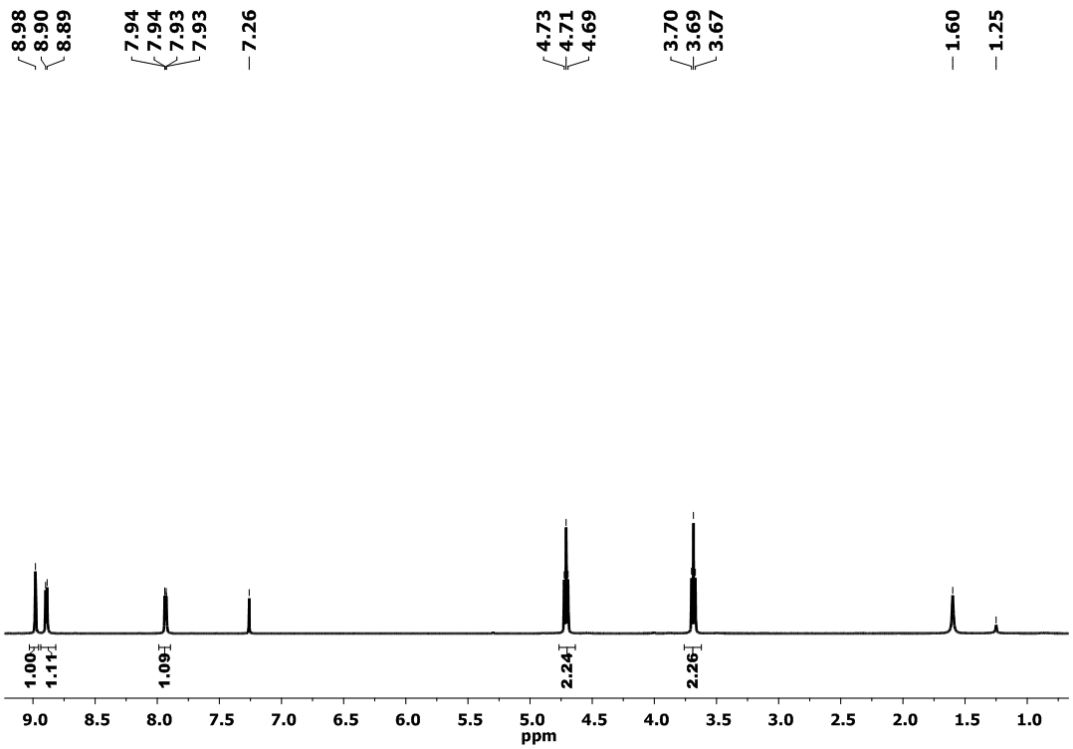

Figure 3S: ^{13}C-NMR Spectrum of **Axle3** in $CDCl_3$ (400 MHz).

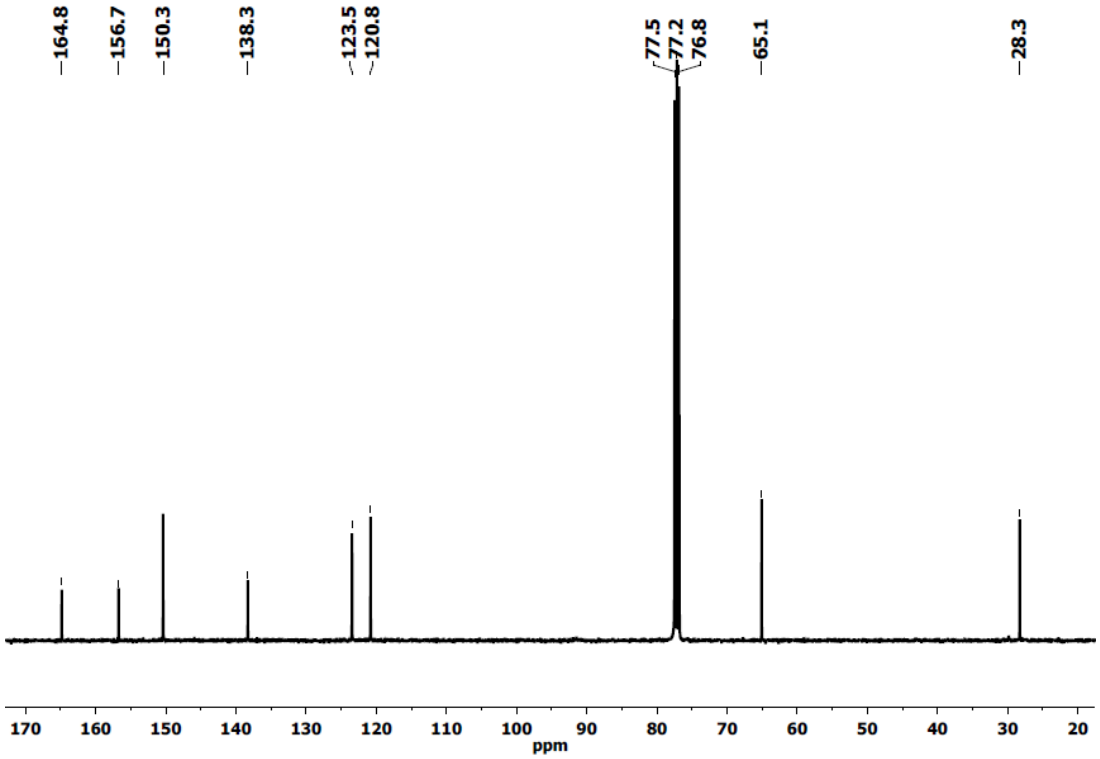

Figure 4S: FT-IR Spectrum of **Axle3**

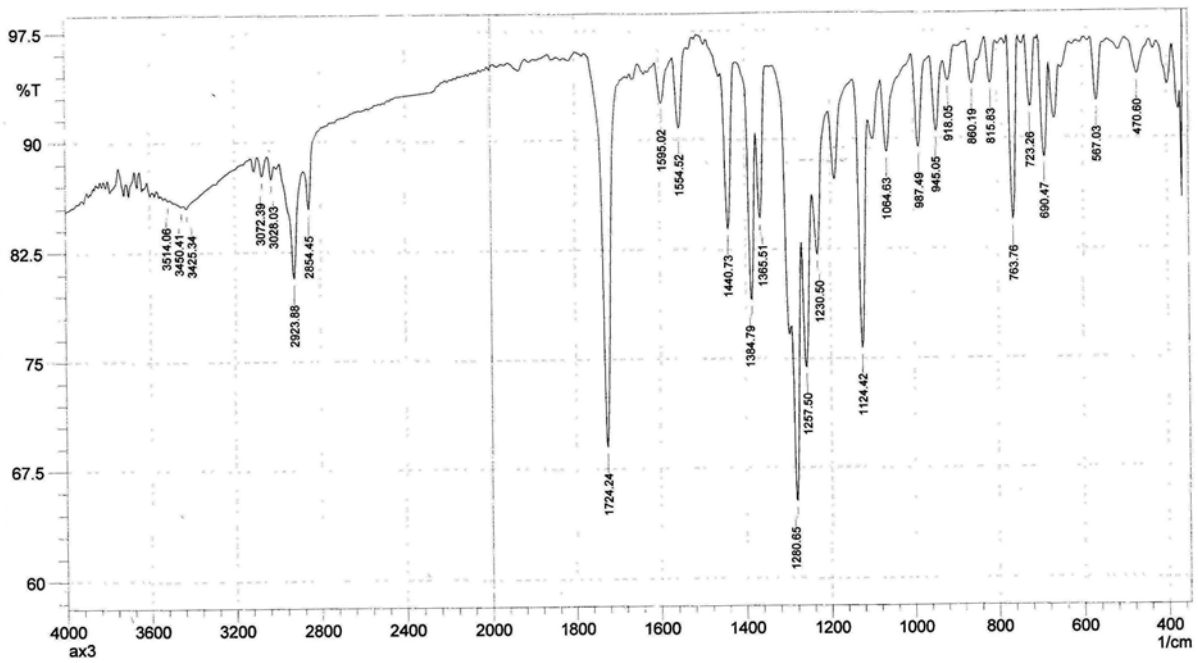

Figure 5S: ESI-MS of **Axle4**

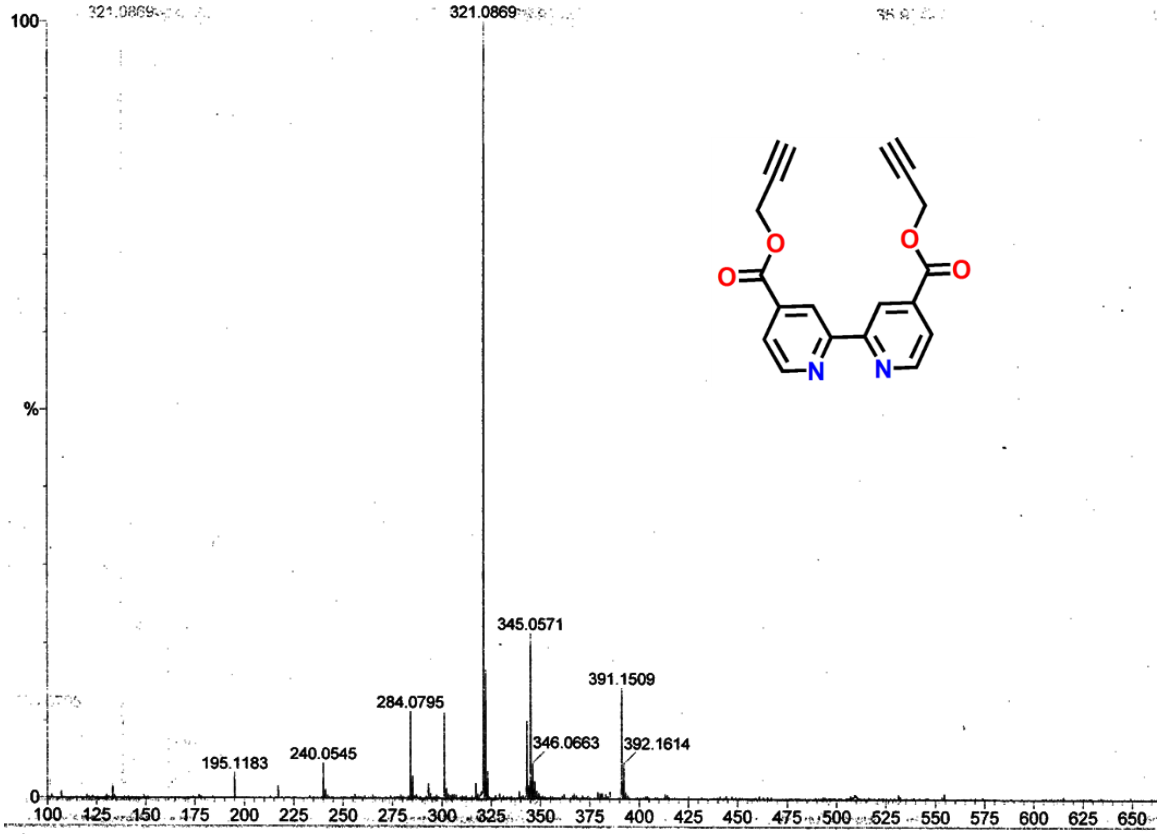

Figure 6S. ^{1}H-NMR Spectrum of **Axle4** in $CDCl_3$ (400 MHz).

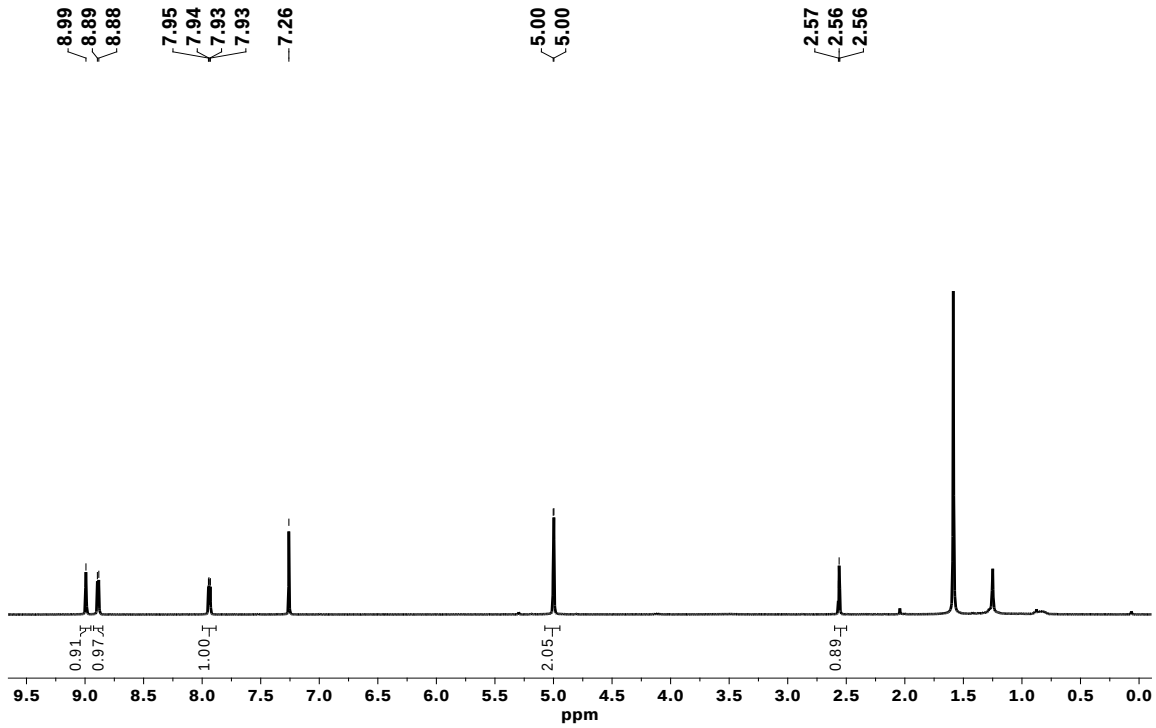

Figure 7S: ^{13}C - NMR Spectrum of **Axle4** in $CDCl_3$ (400 MHz).

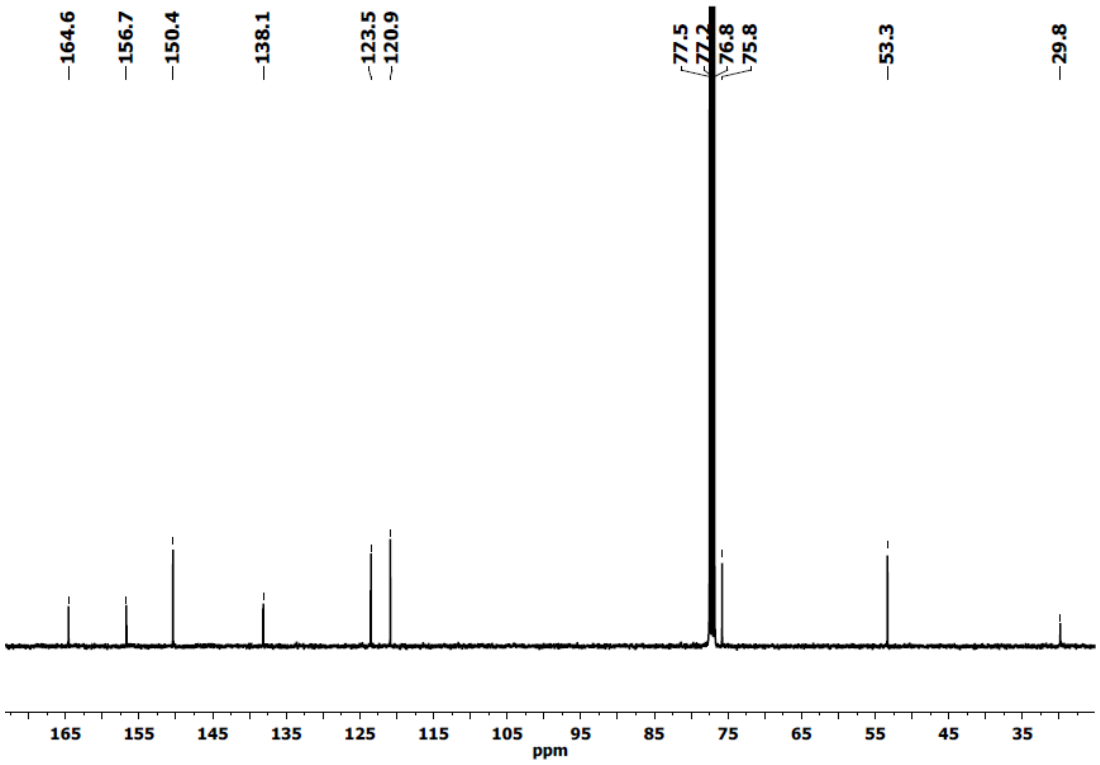

Figure 8S: FT-IR Spectrum of **Axle4**

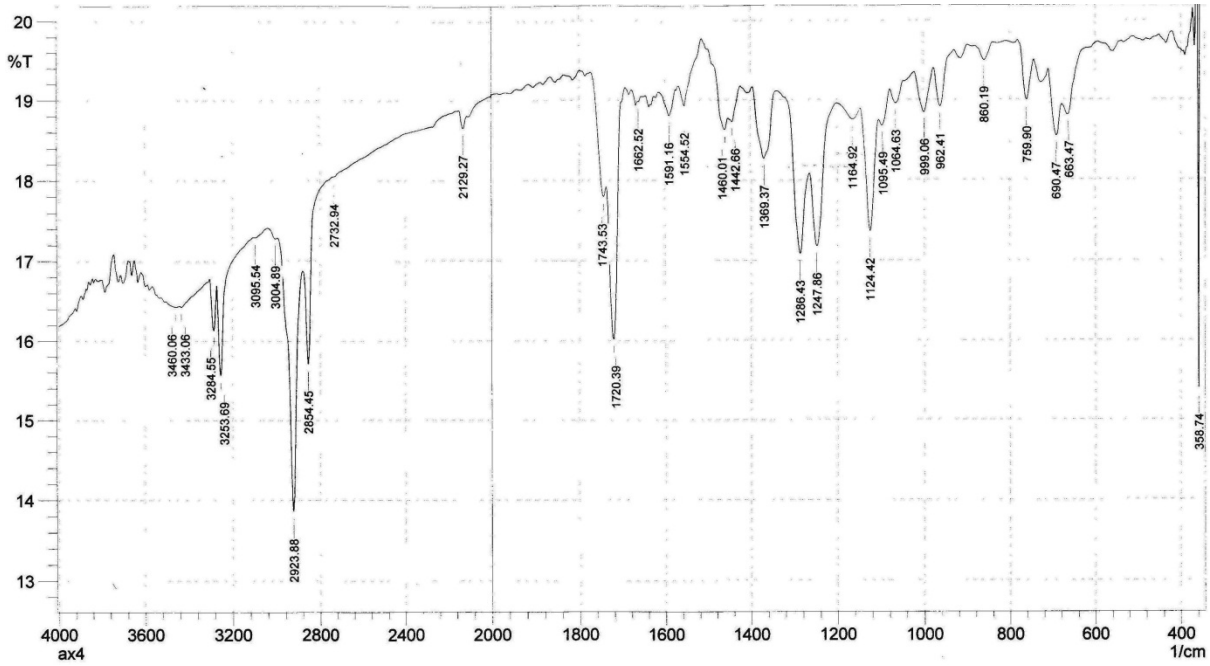

Figure 9S: ESI-MS of **Axle5**

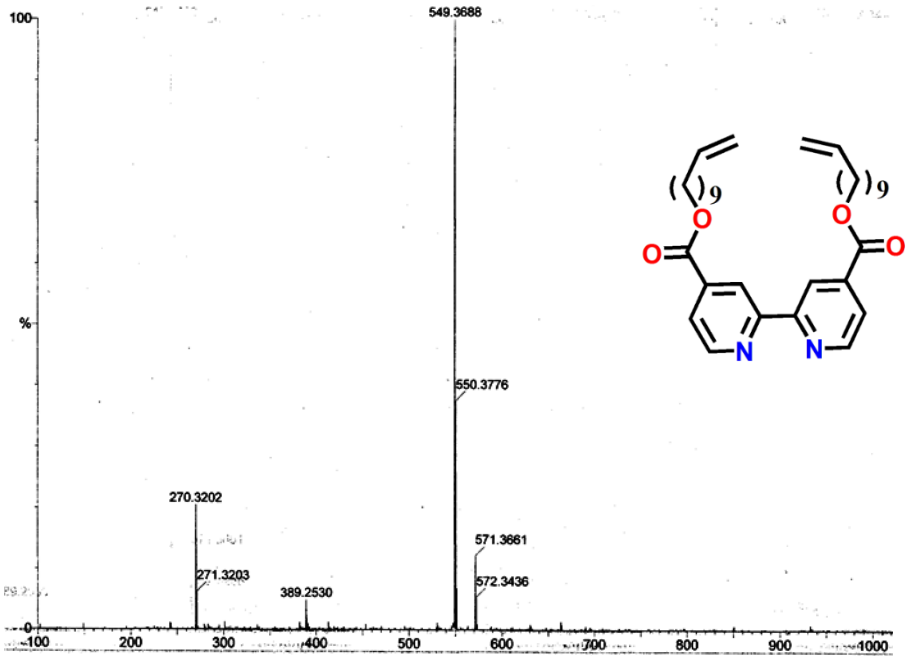

Figure 10S: ^{1}H-NMR Spectrum of **Axle5** in $CDCl_3$ (400 MHz)

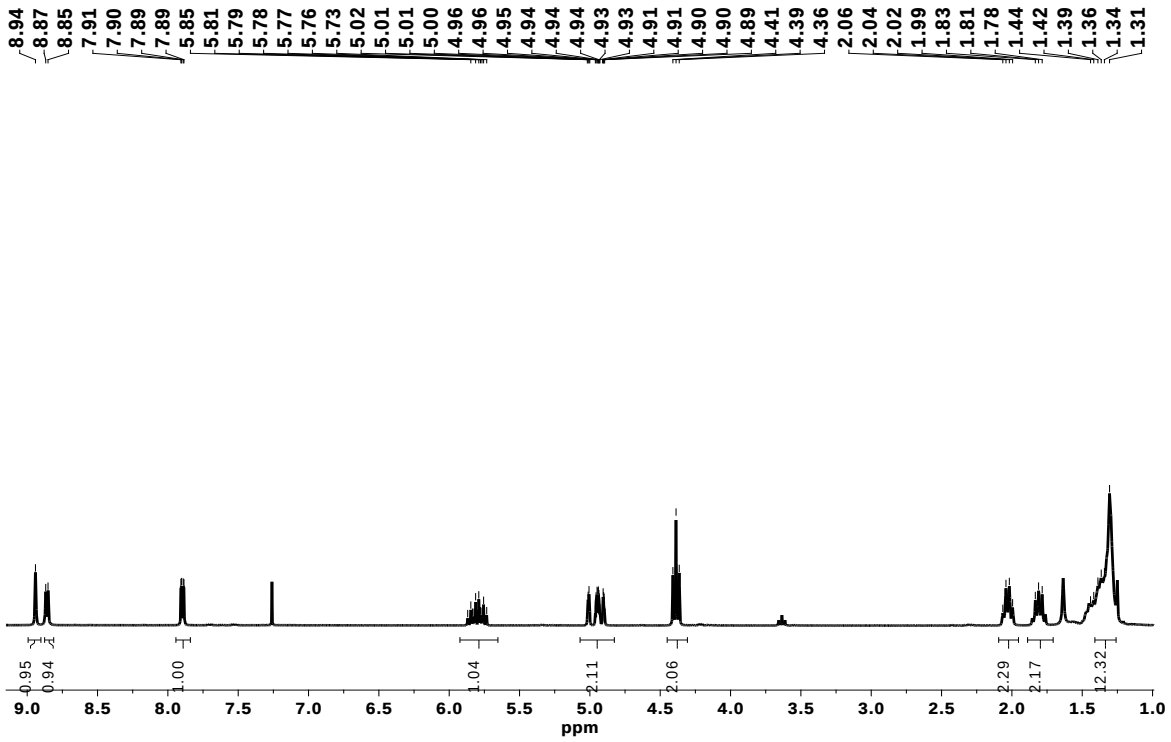

Figure 11S: ^{13}C-NMR Spectrum of **Axle5** in $CDCl_3$ (400 MHz).

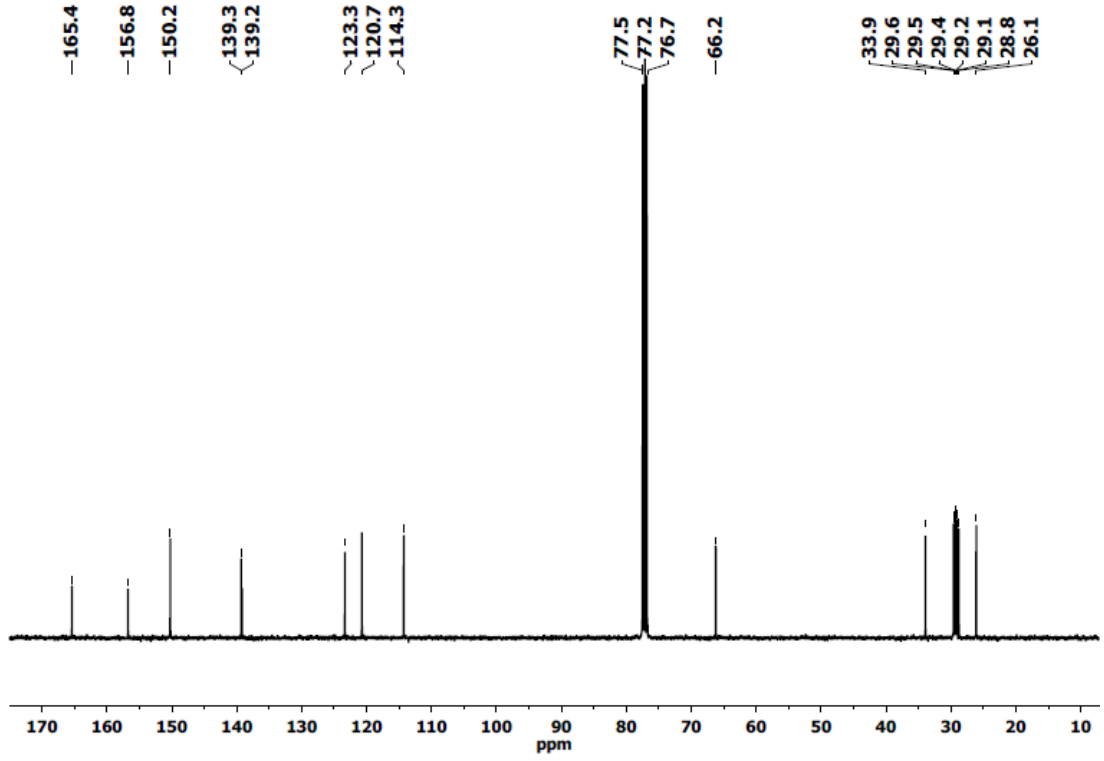

Figure 12S: FT-IR Spectrum of **Axle5**

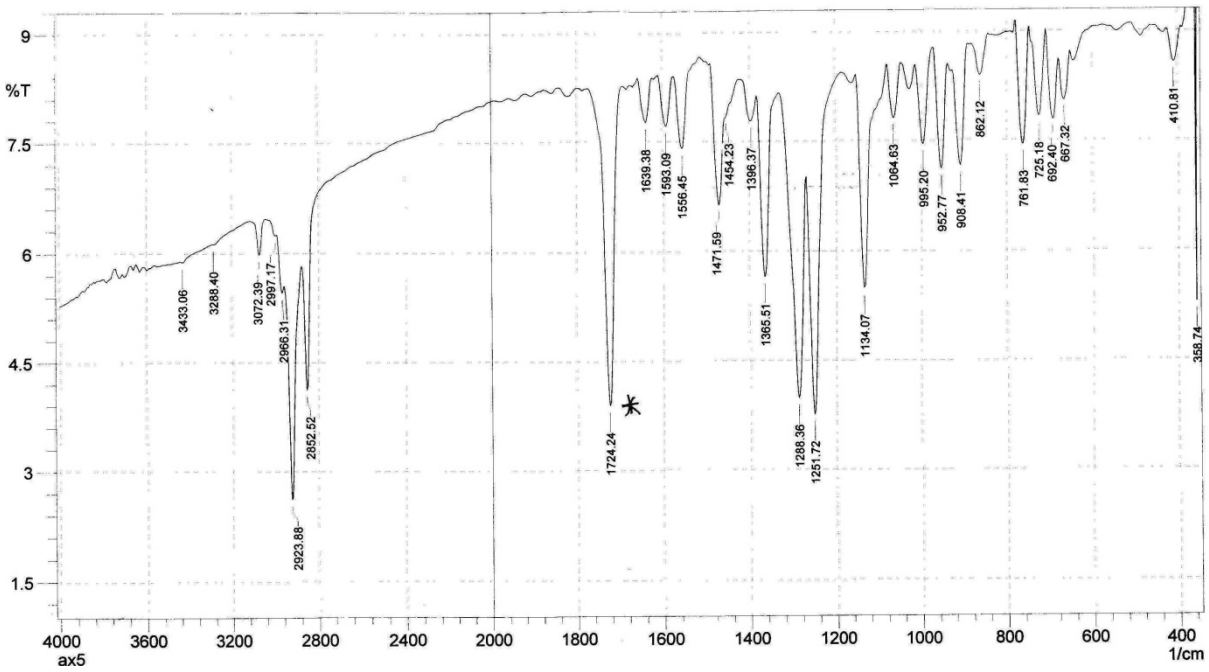

Figure 13S: ESI- MS of **Axle6**

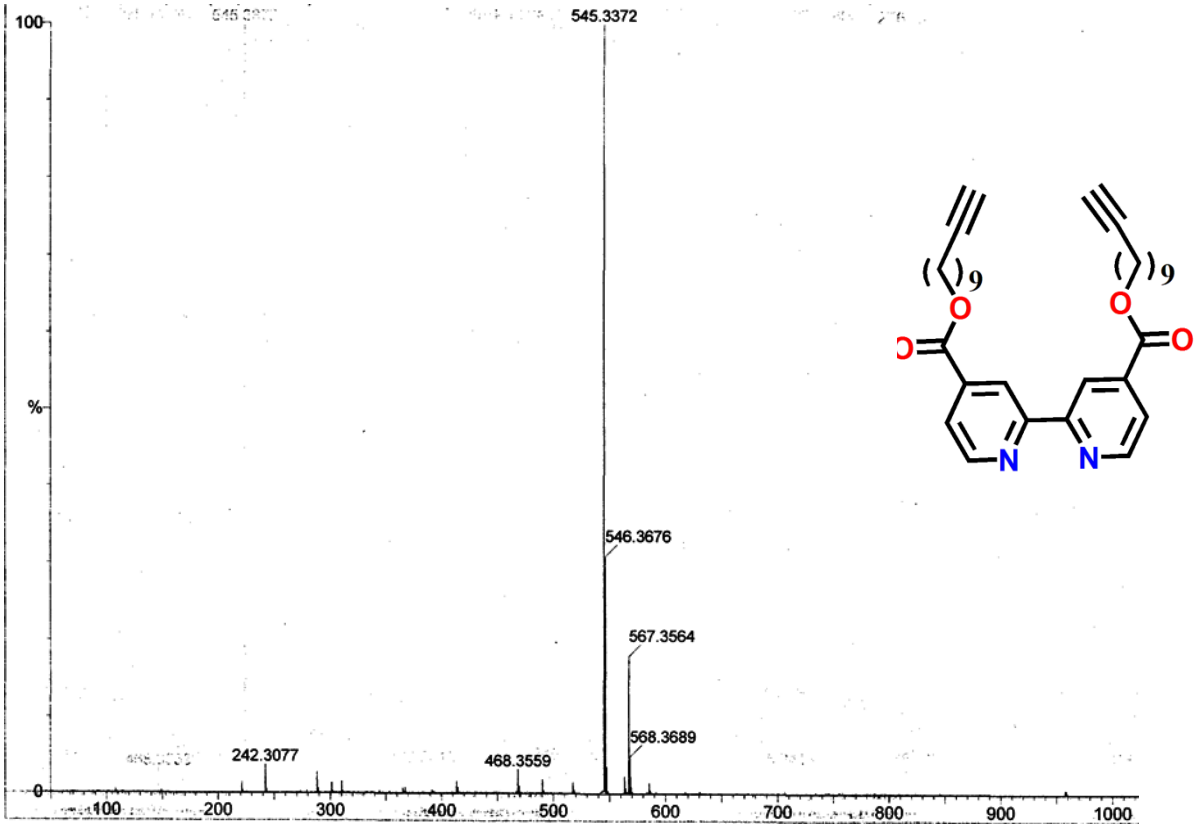

Figure 14S: ^{1}H-NMR Spectrum of **Axle6** in $CDCl_3$ (500 MHz).

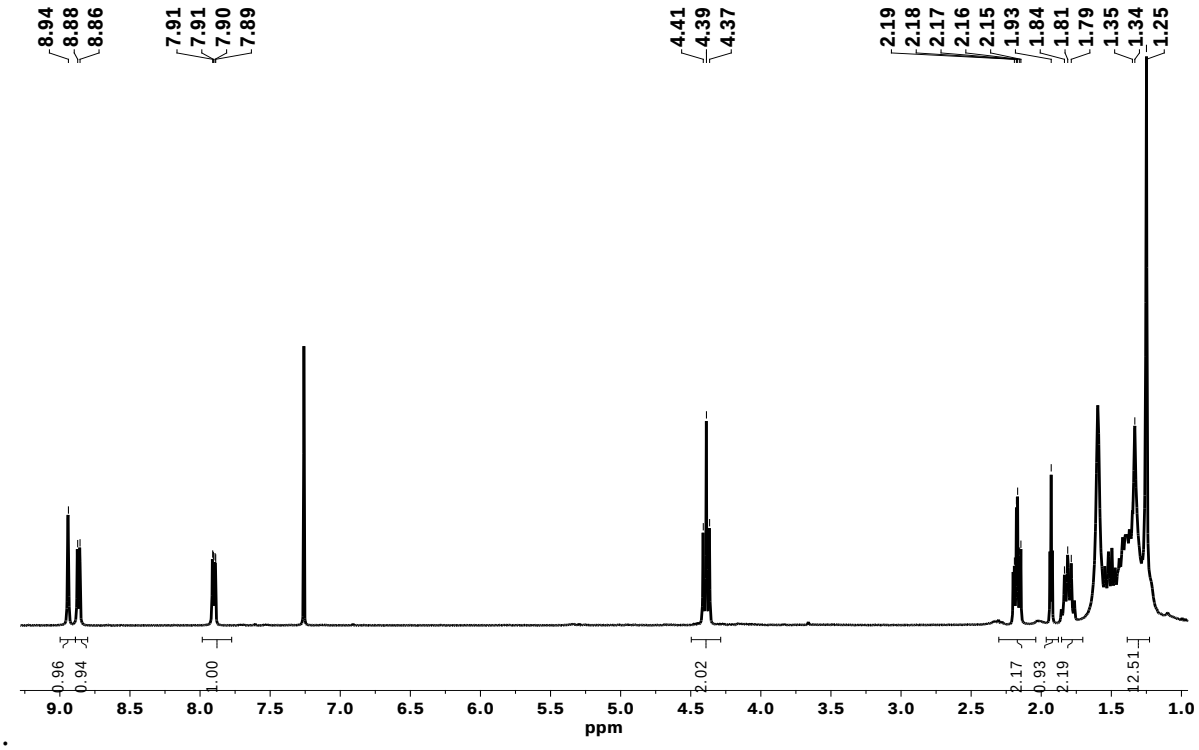

Figure 15S: ^{13}C-NMR Spectrum of **Axle6** in $CDCl_3$ (400 MHz).

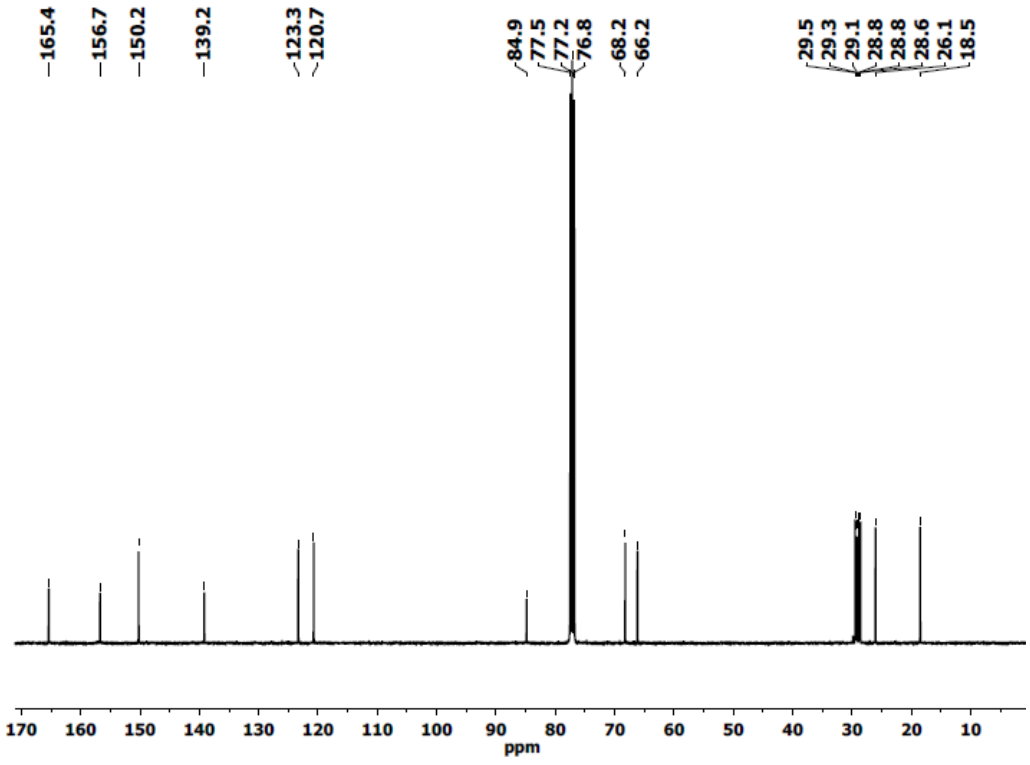

Figure 16S: FT-IR Spectrum of **Axle6**

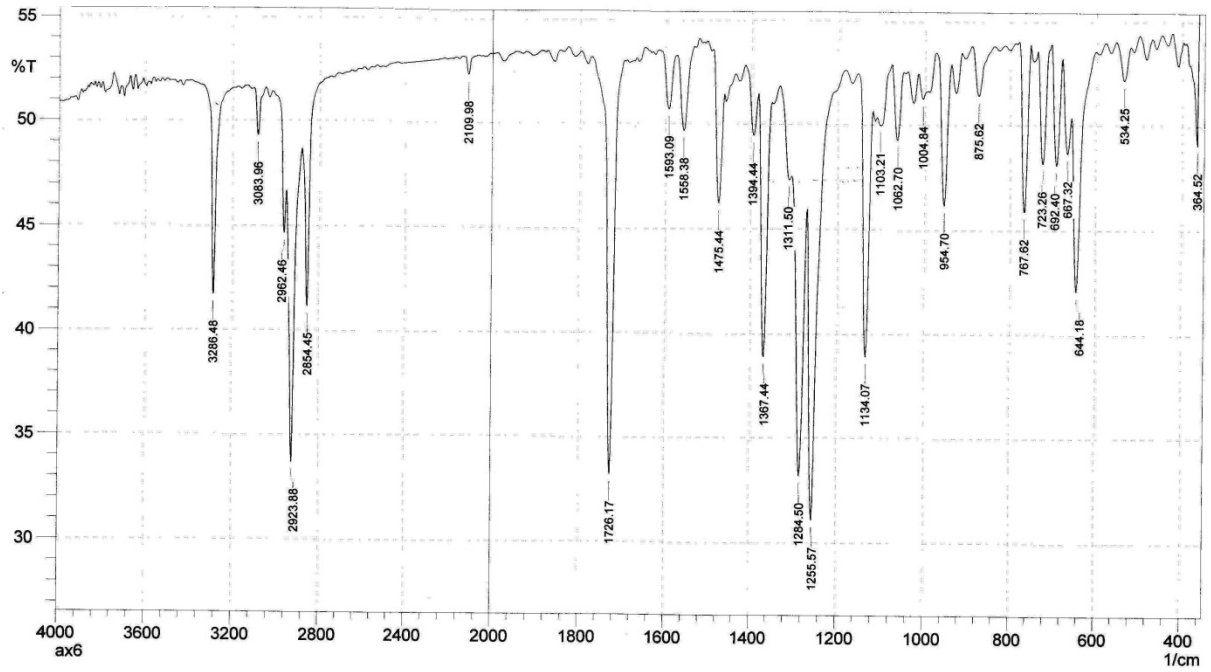

Figure 17S: ESI- MS of **Axle8**

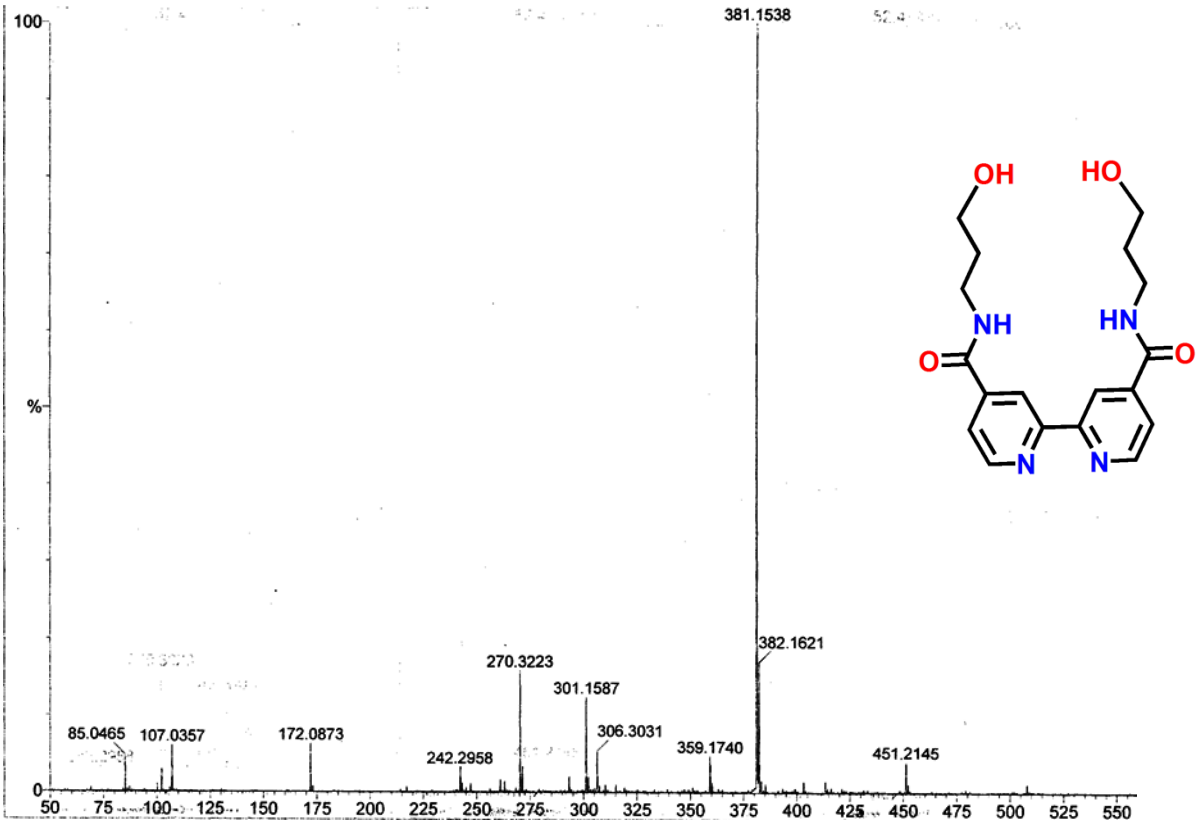

Figure 18S: ^{1}H-NMR Spectrum of **Axle8** in DMSO-d_6 (400 MHz).

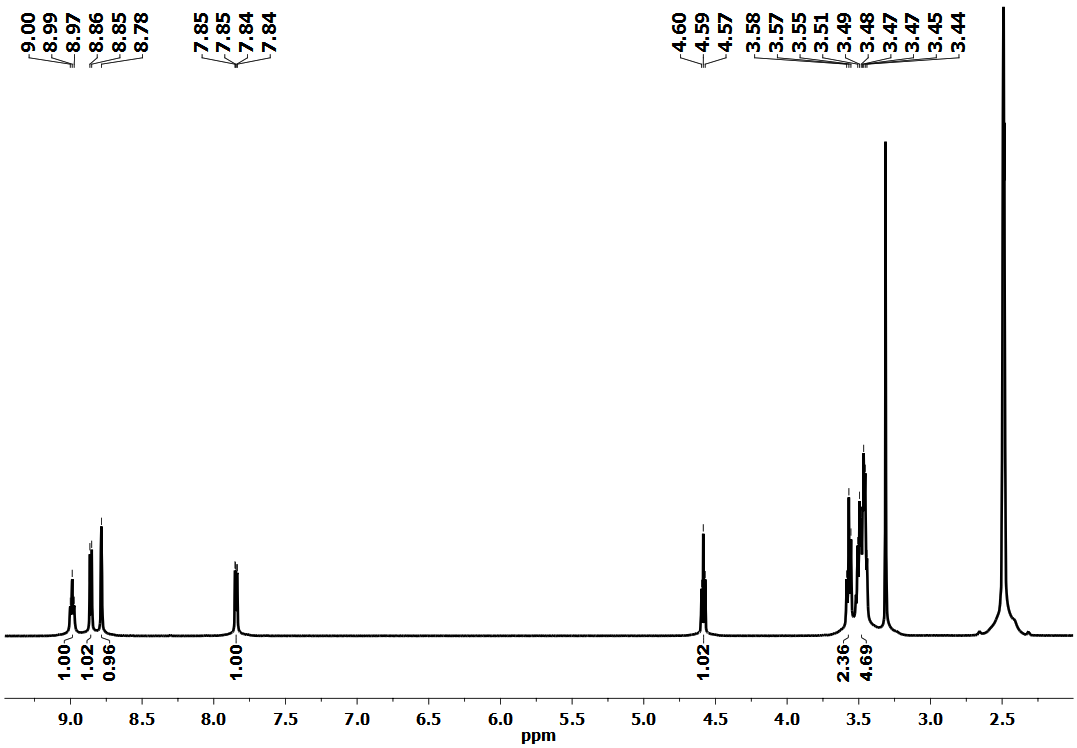

Figure 19S: ^{13}C-NMR Spectrum of **Axle8** in DMSO-d_6 (400 MHz).

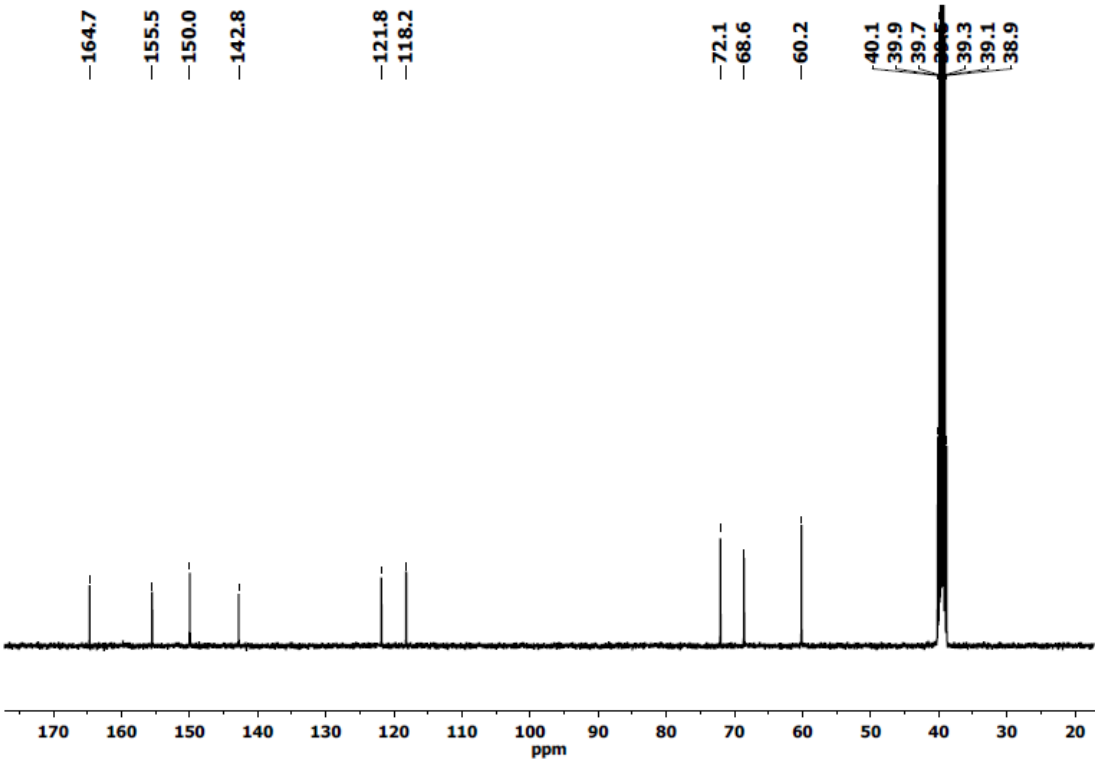

Figure 20S: FT-IR Spectrum of **Axle8**

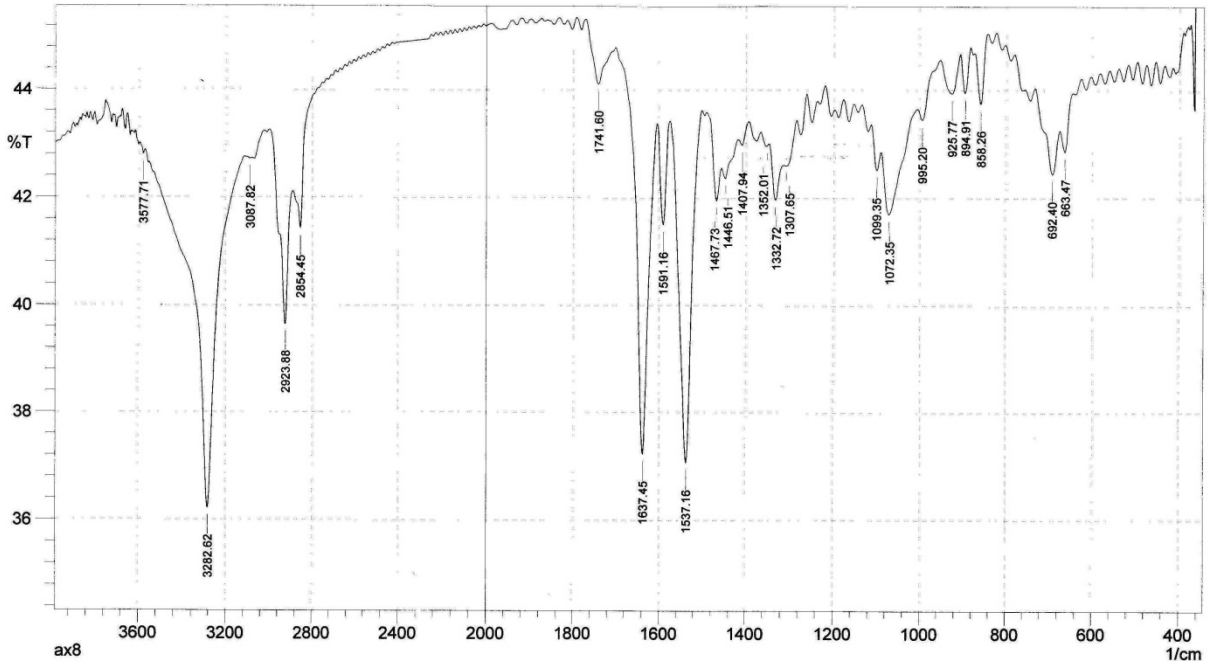

Figure 21S: ESI- MS of **Axle9**

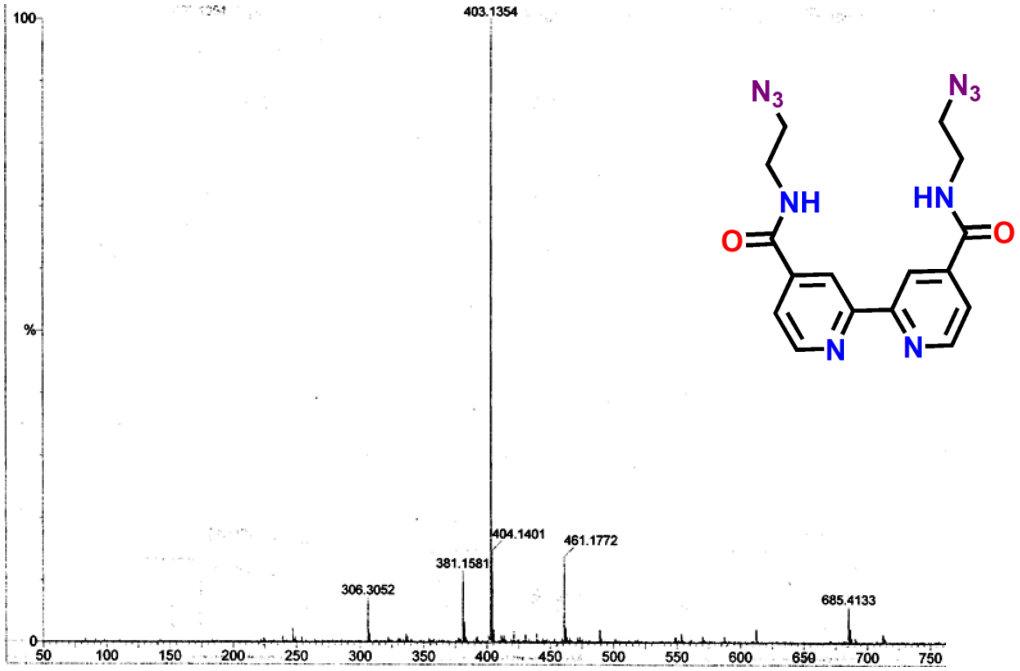

Figure 22S: ^{1}H-NMR Spectrum of **Axle9** in DMSO-d^{6} (400 MHz).

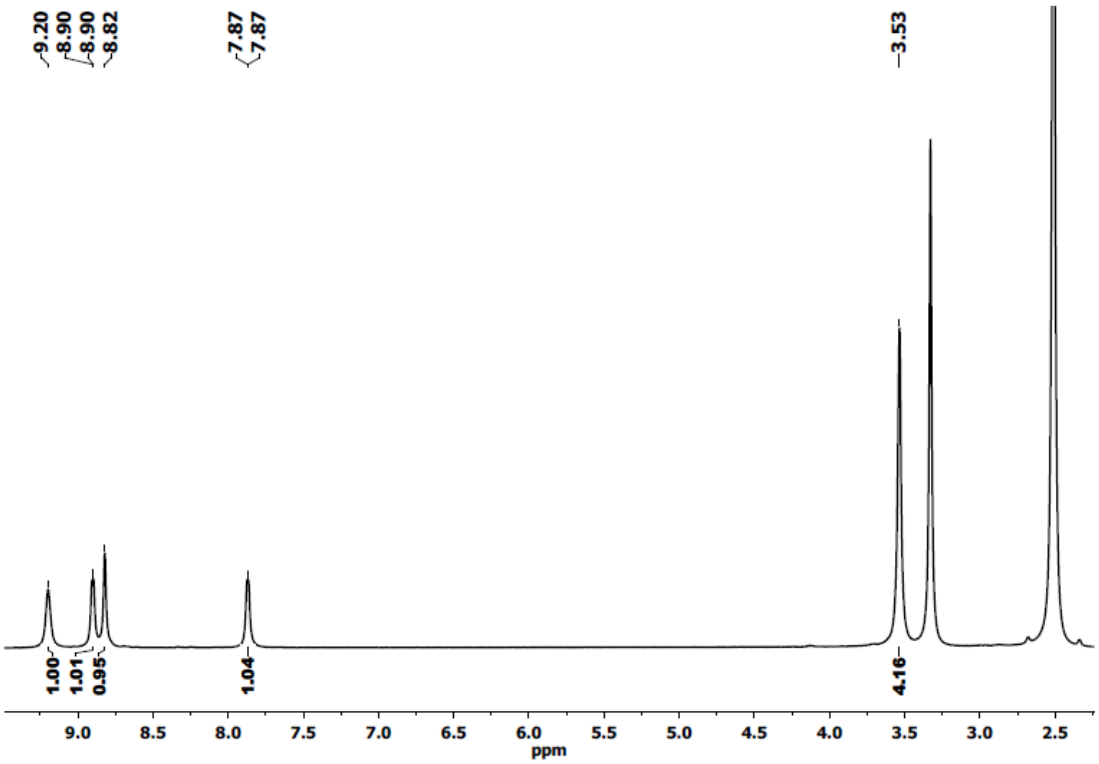

Figure 23S: ^{13}C-NMR Spectrum of **Axle9** in DMSO-d^{6} (400 MHz).

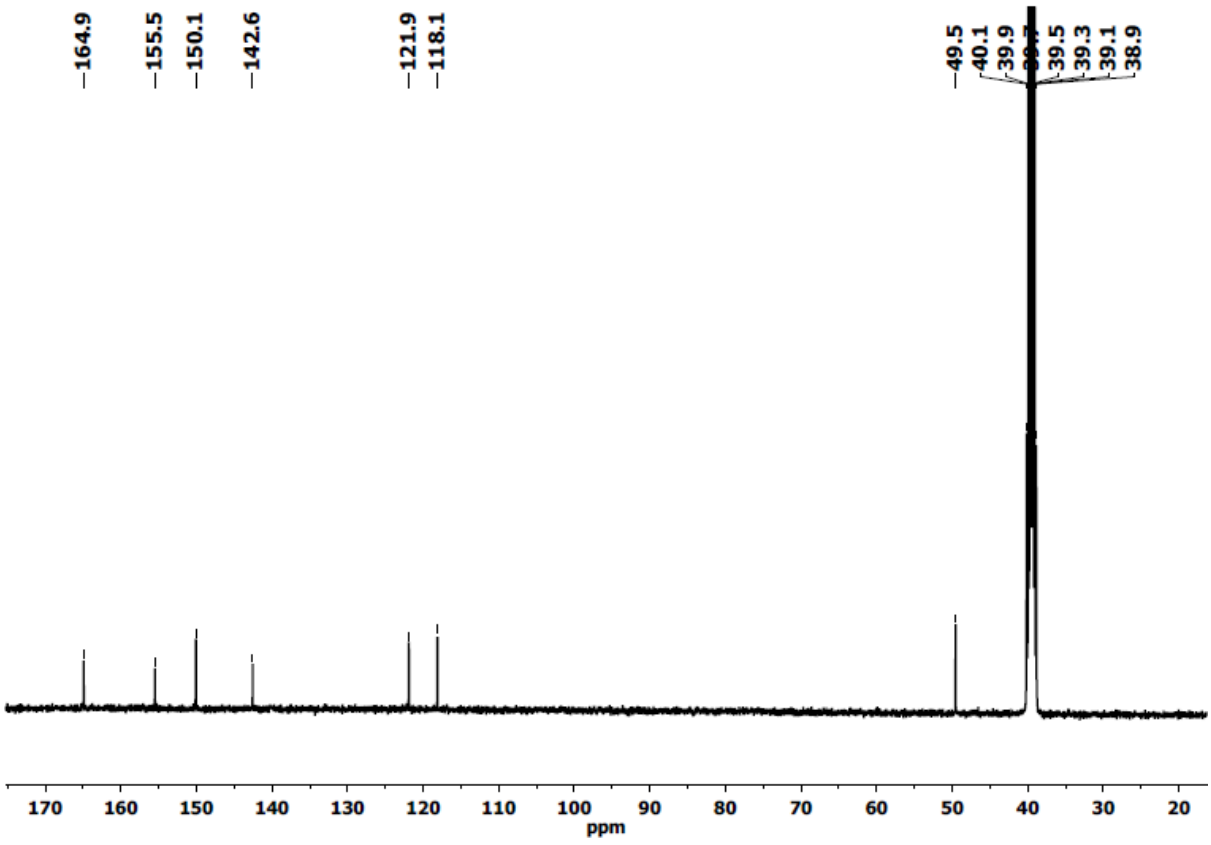

Figure 24S: FT-IR Spectrum of **Axle9**

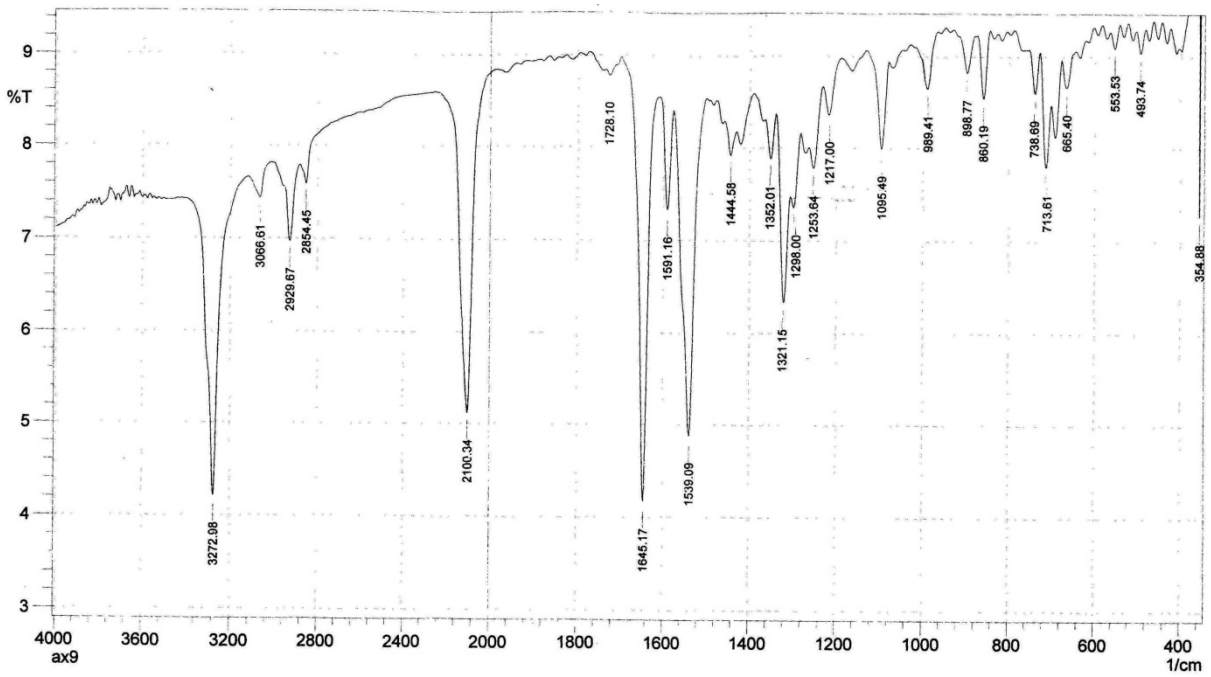

Figure 25S: ESI- MS of **Axle10**

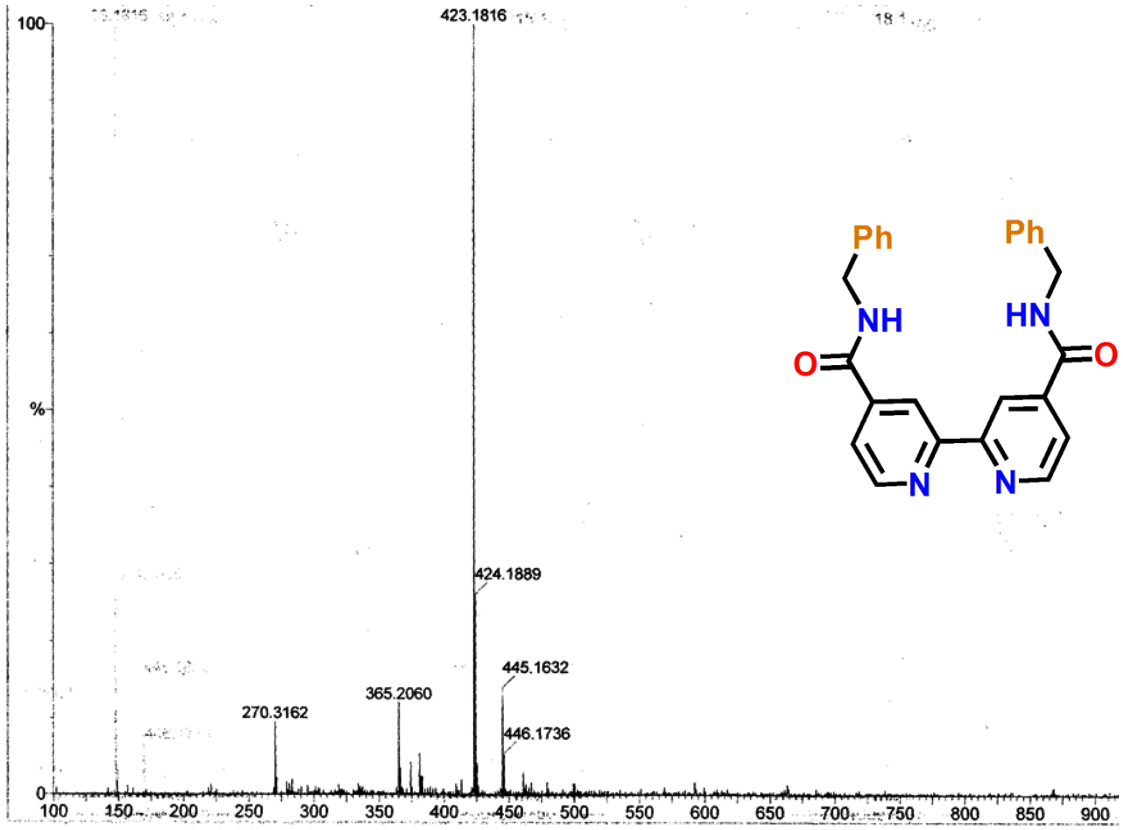

Figure 26S: ^{1}H-NMR Spectrum of **Axle10** in DMSO-d^{6} (400 MHz).

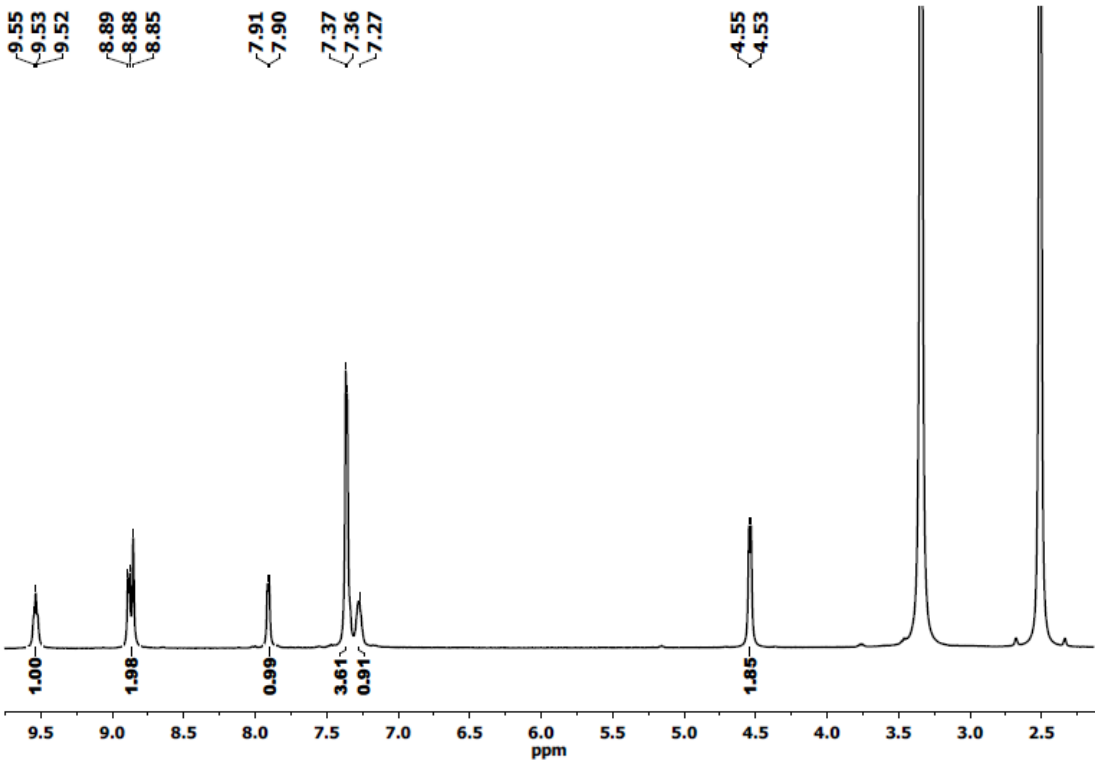

Figure 27S: ^{13}C-NMR Spectrum of **Axle10** in DMSO-d^{6} (400 MHz).

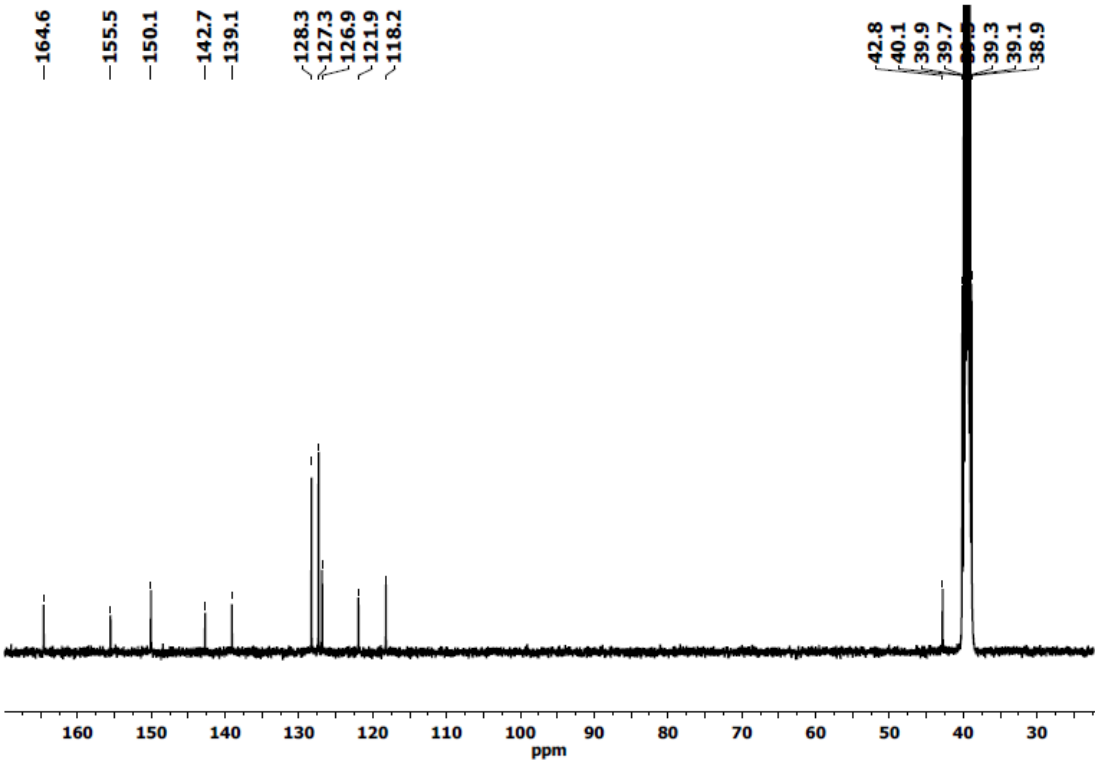

Figure 28S: FT-IR Spectrum of **Axle10**

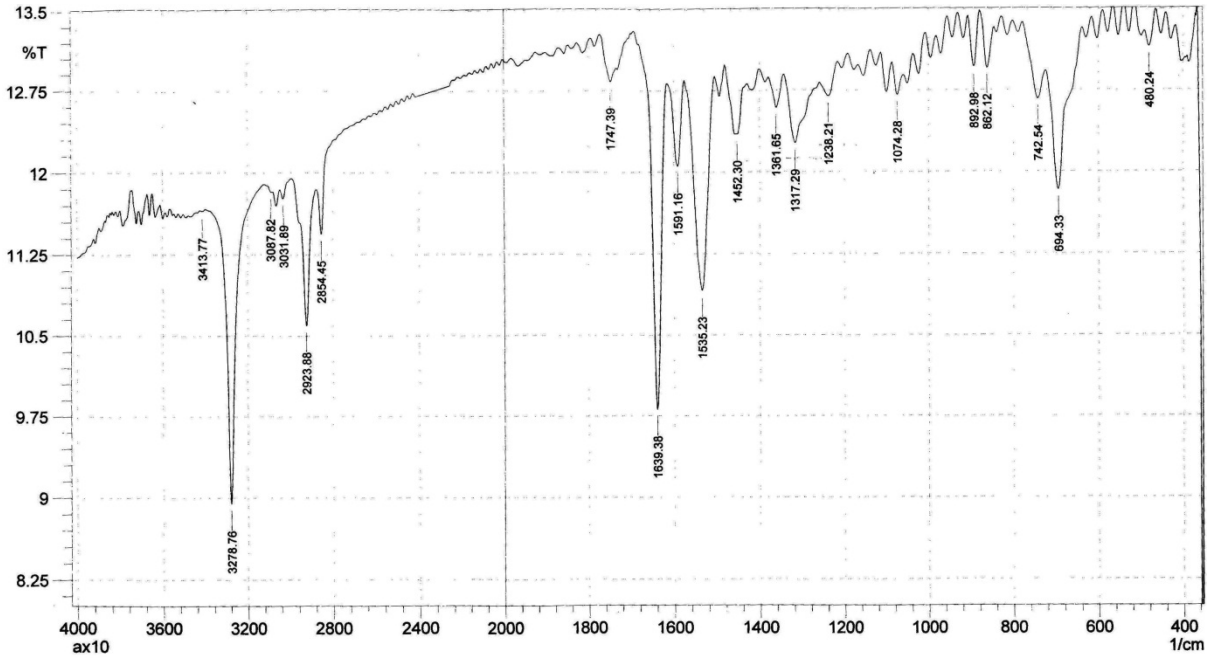

Figure 29S: ESI-MS of **PR1**

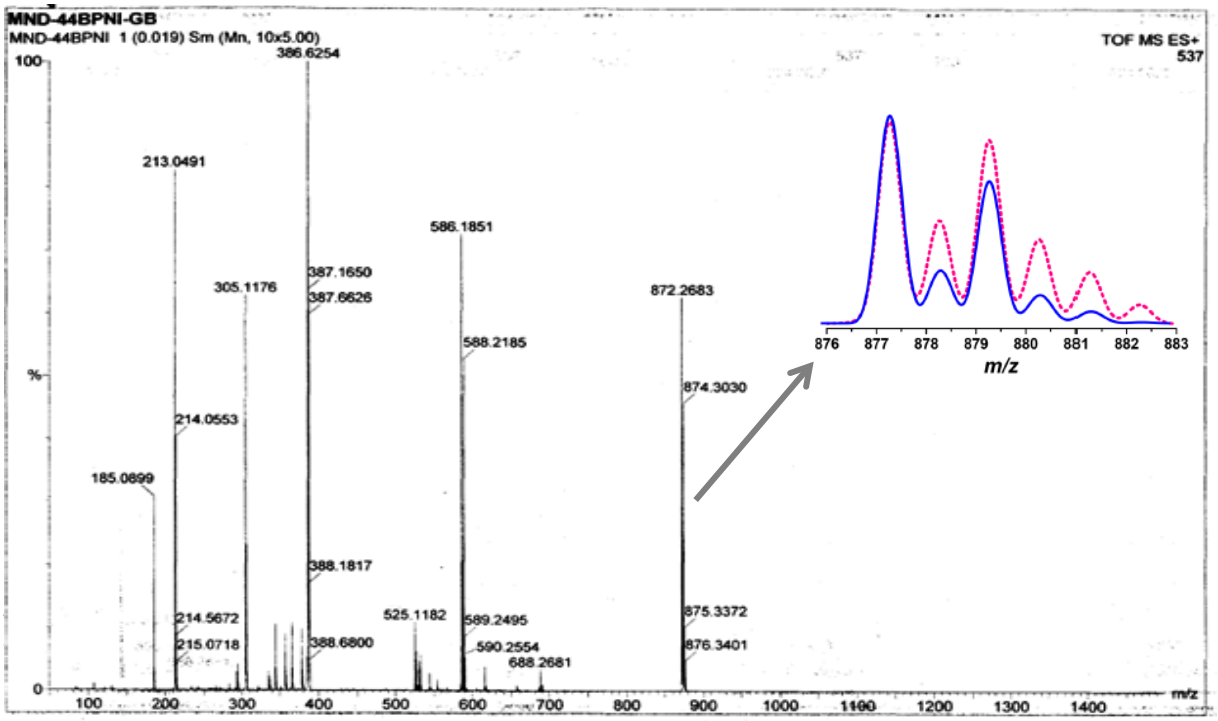

Figure 30S: ESI-MS of **PR2**

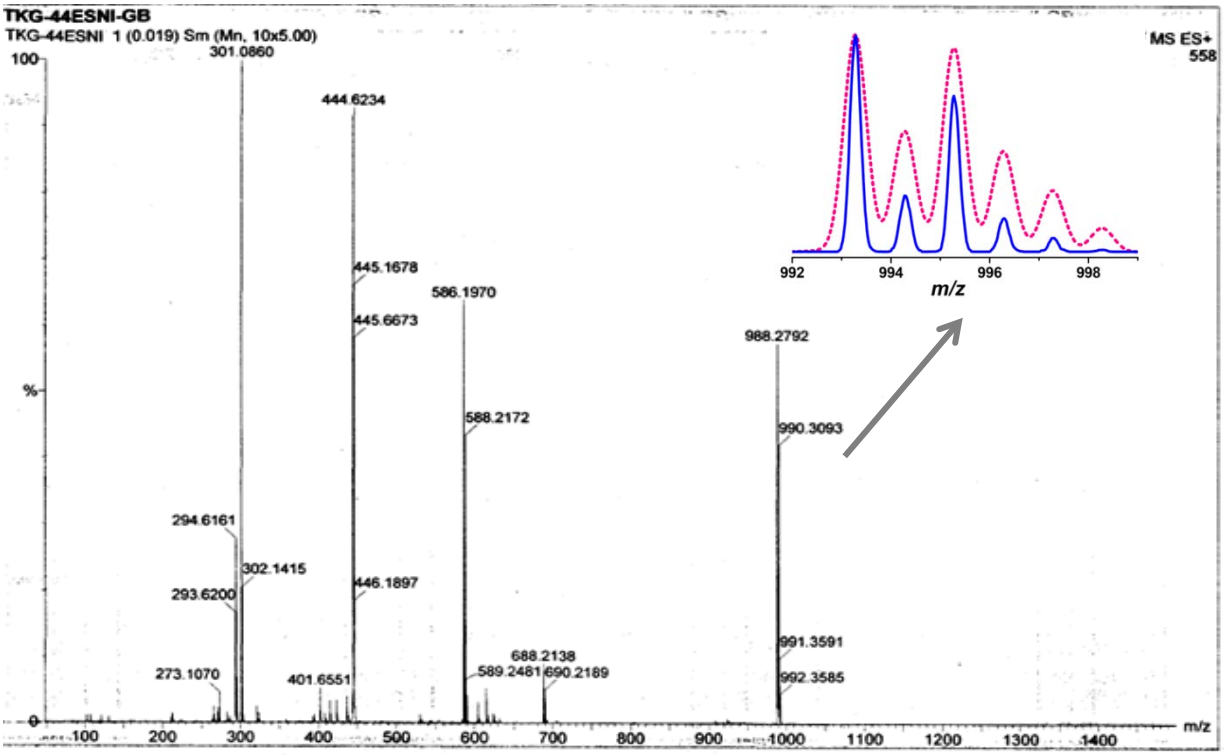

Figure 31S: ESI-MS of **PR3**

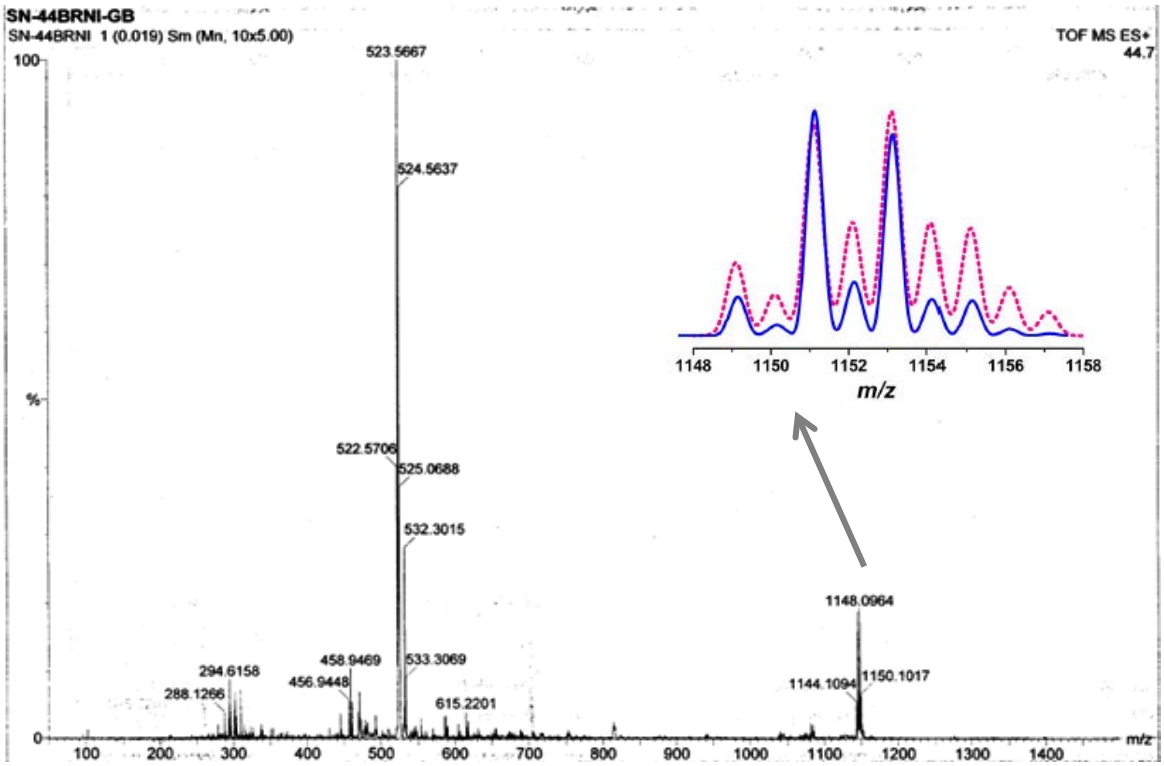

Figure 32S: ESI-MS of **PR4**

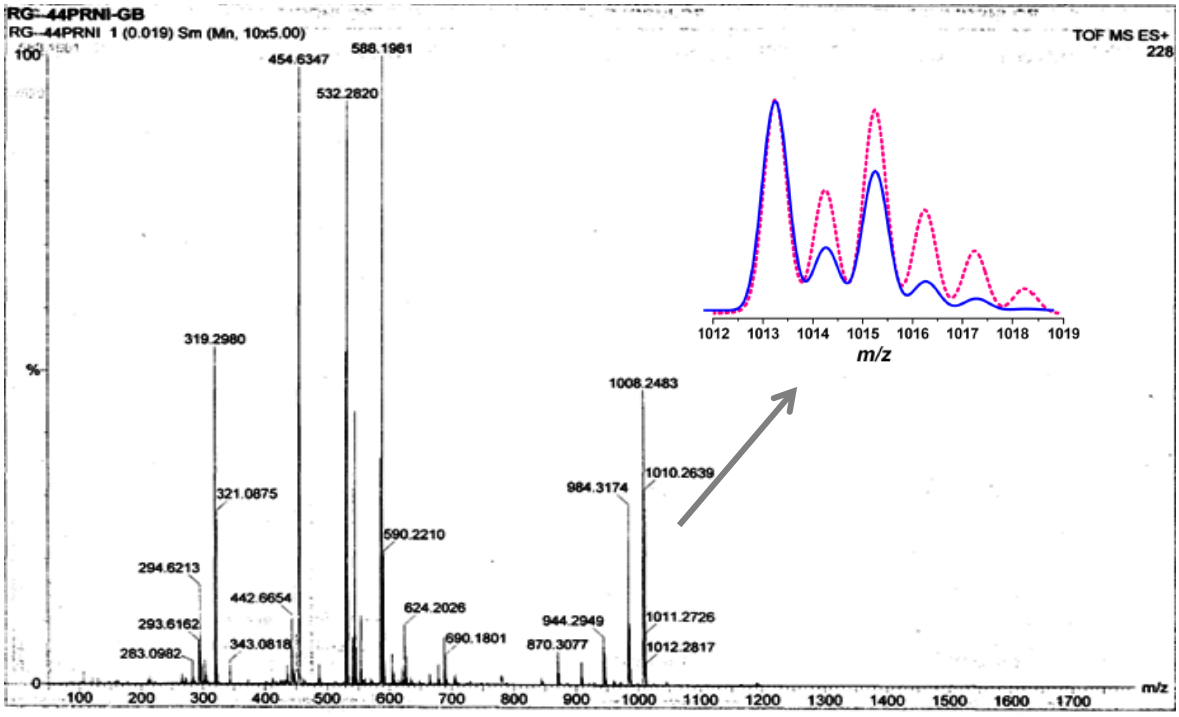

Figure 33S: ESI-MS of **PR5**

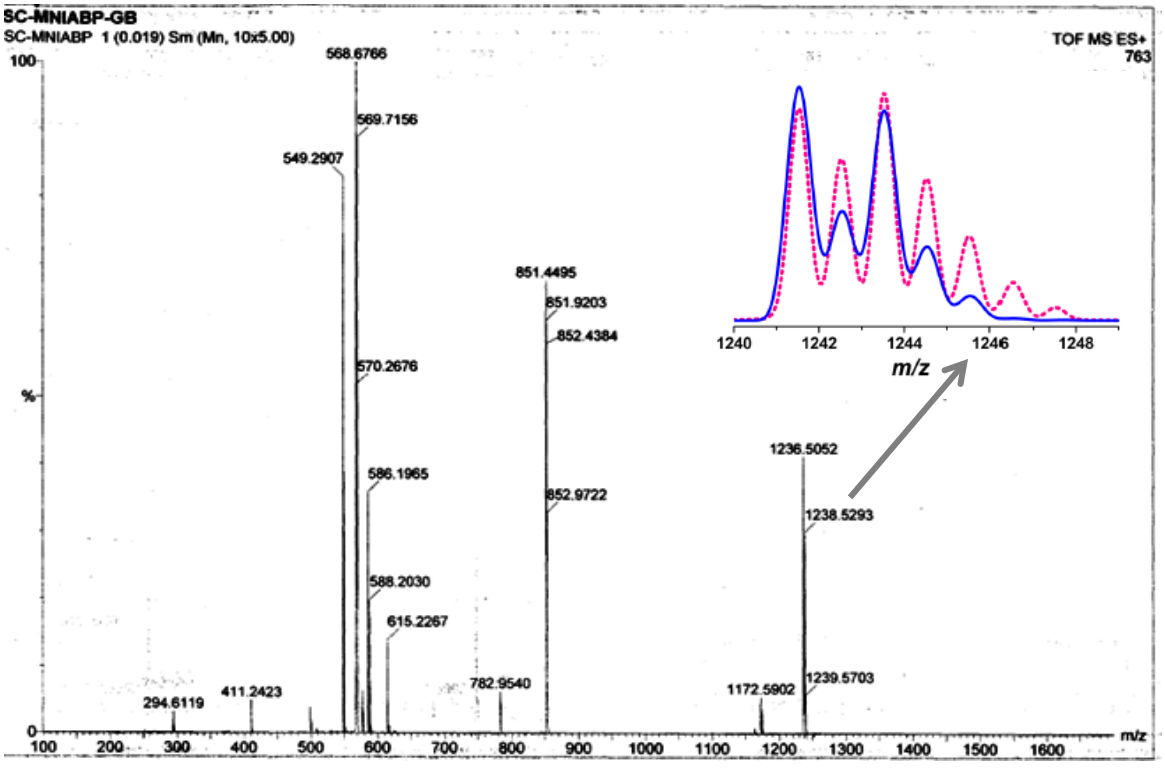

Figure 34S: ESI-MS of **PR6**

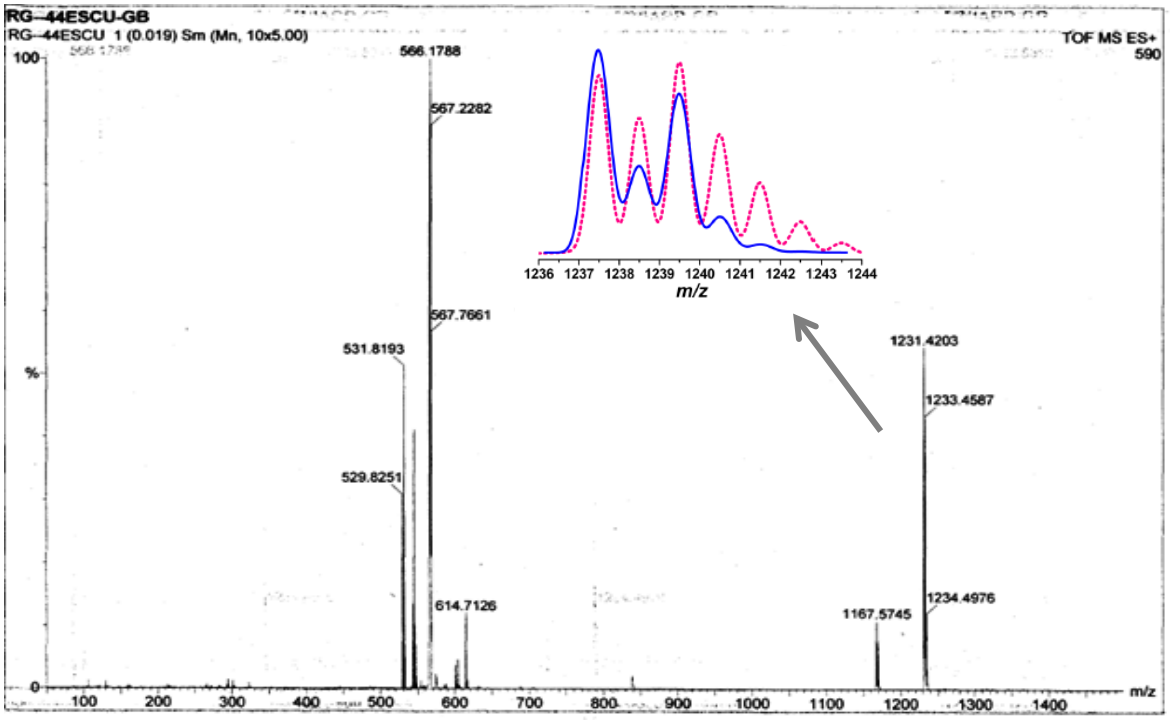

Figure 35S: ESI-MS of **PR7**

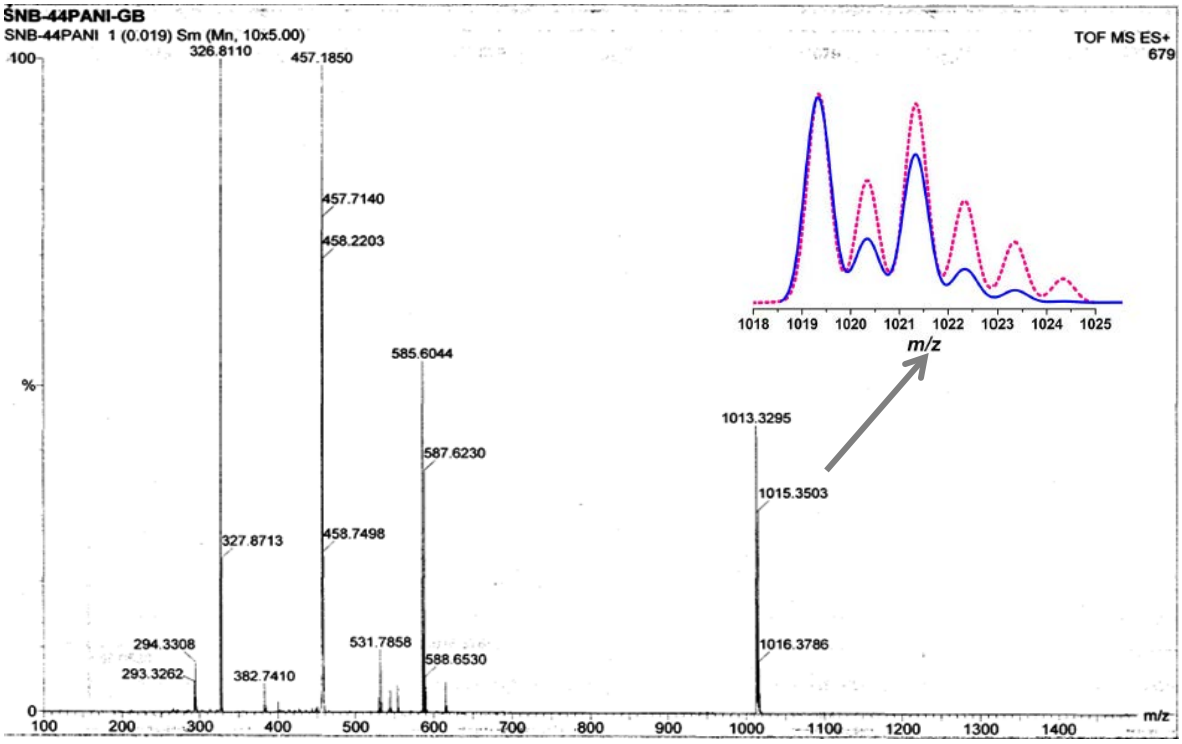

Figure 36S: ESI-MS of **PR8**

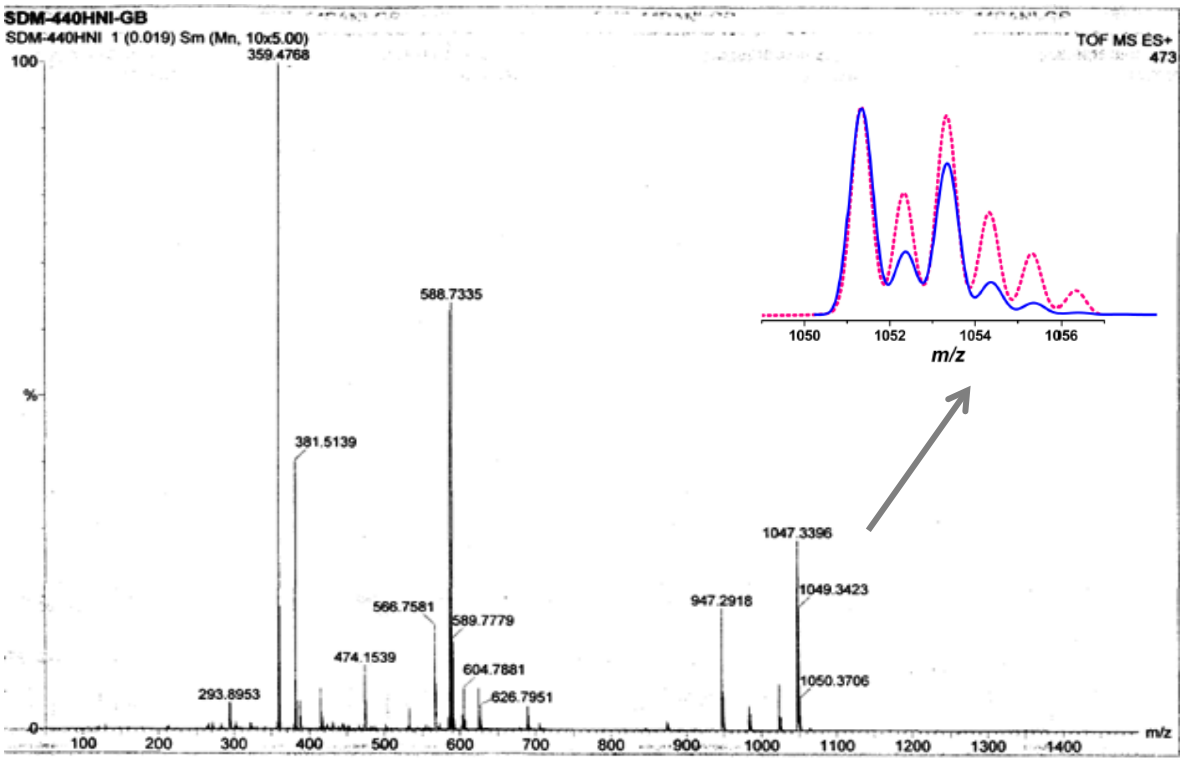

Figure 37S: ESI-MS of **PR9**

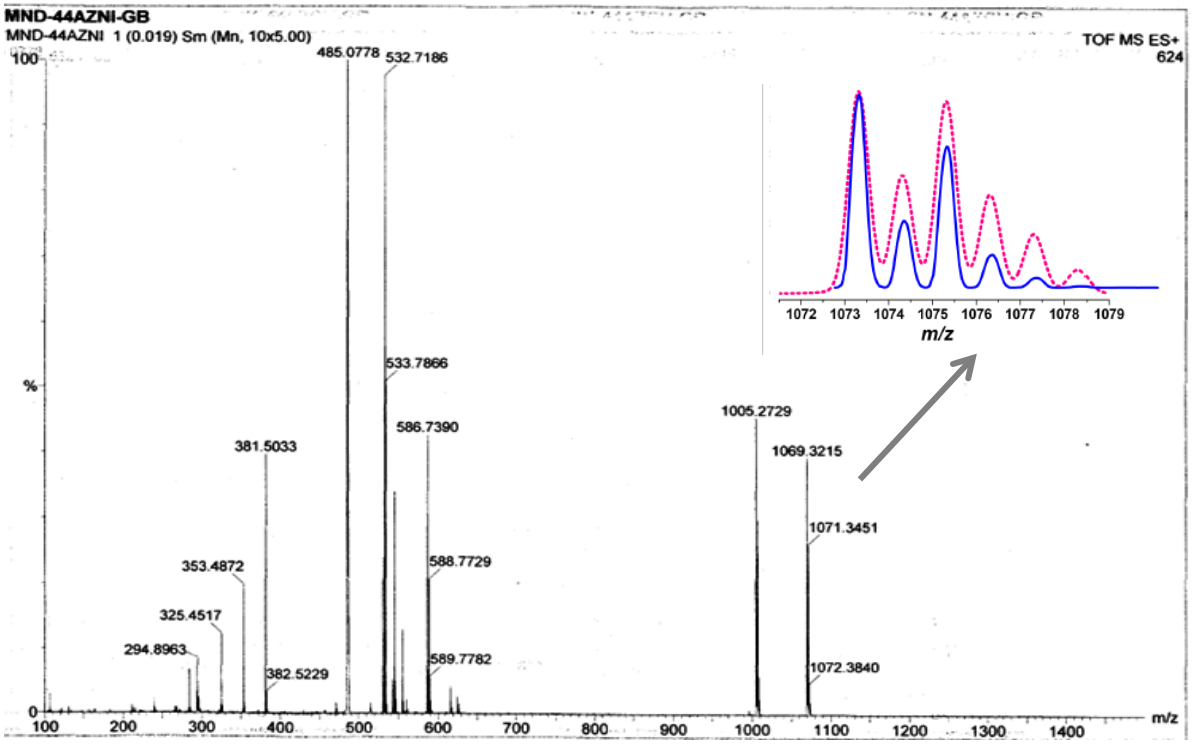

Figure 38S: ESI-MS of **PR10**

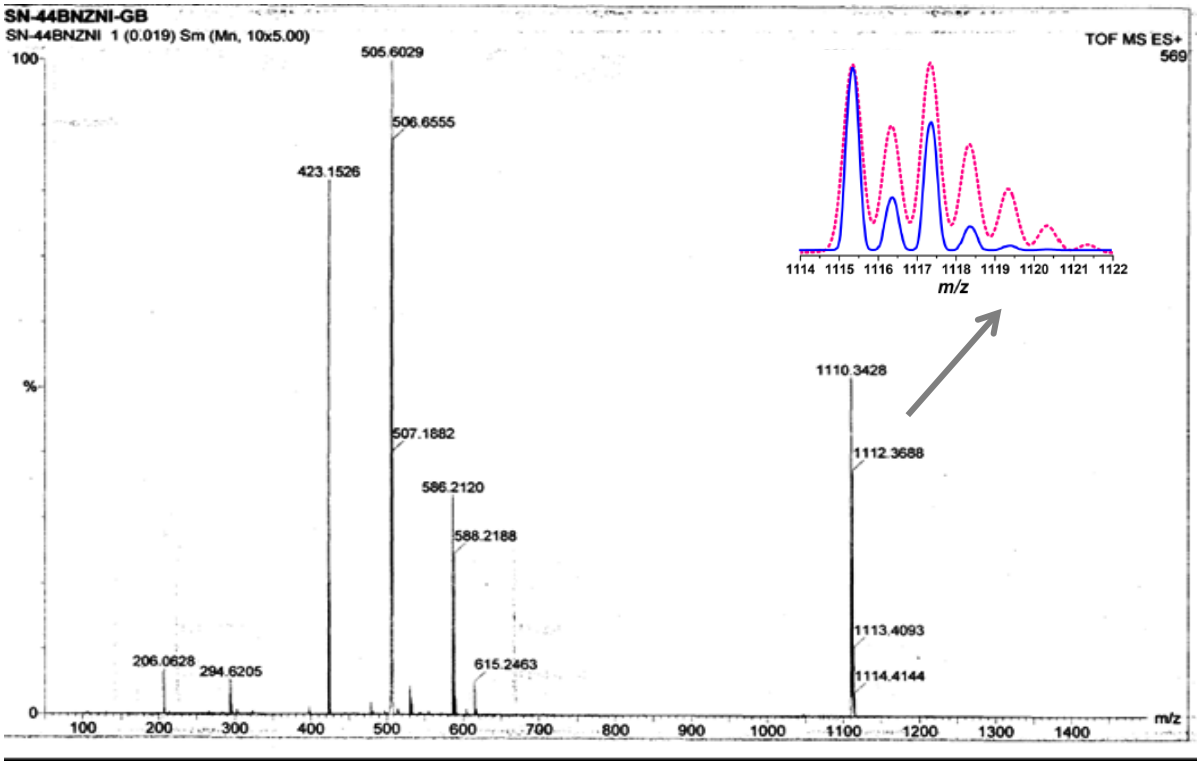

Figure 39S: ESI-MS of **PR1'**

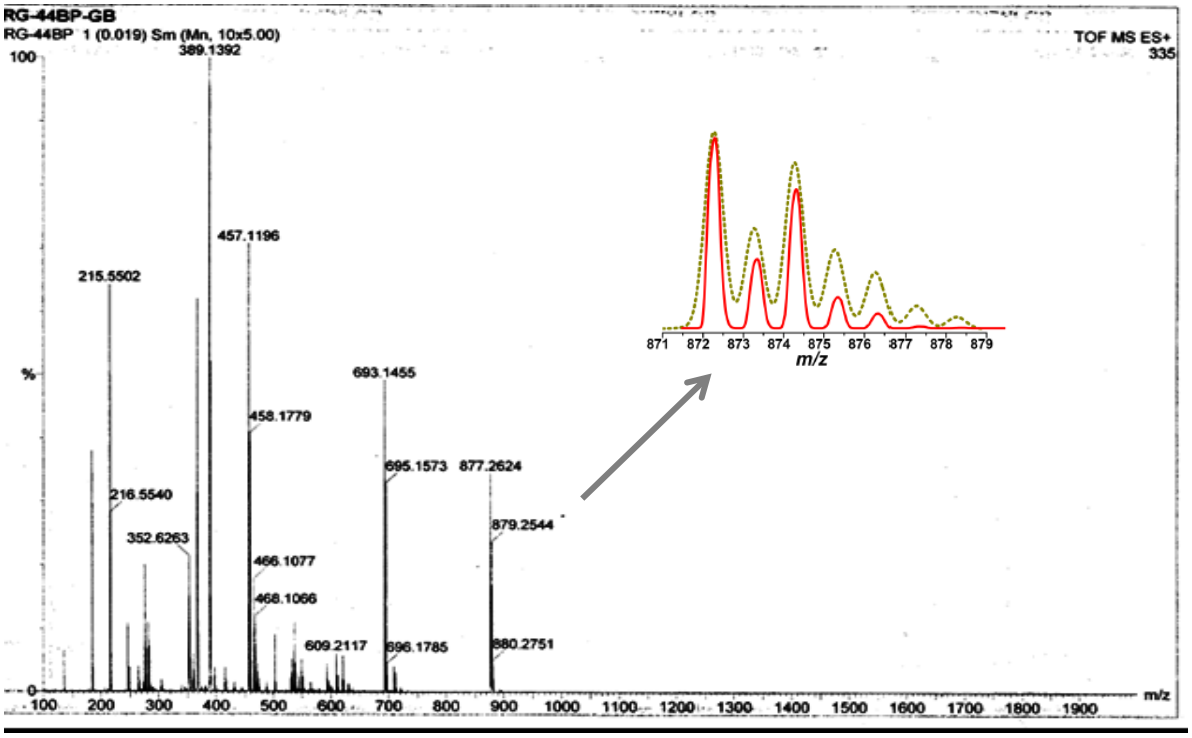

Figure 40S: ESI-MS of **PR2'**

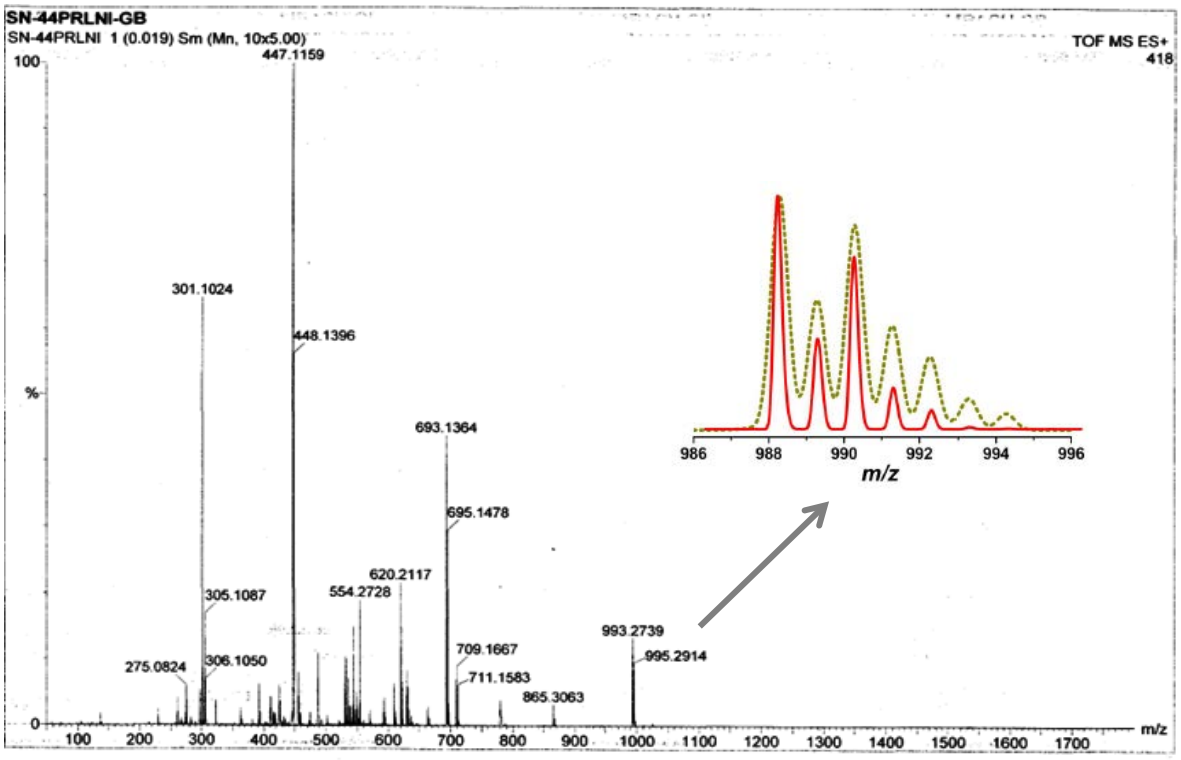

Figure 41S: ESI-MS of **PR3'**

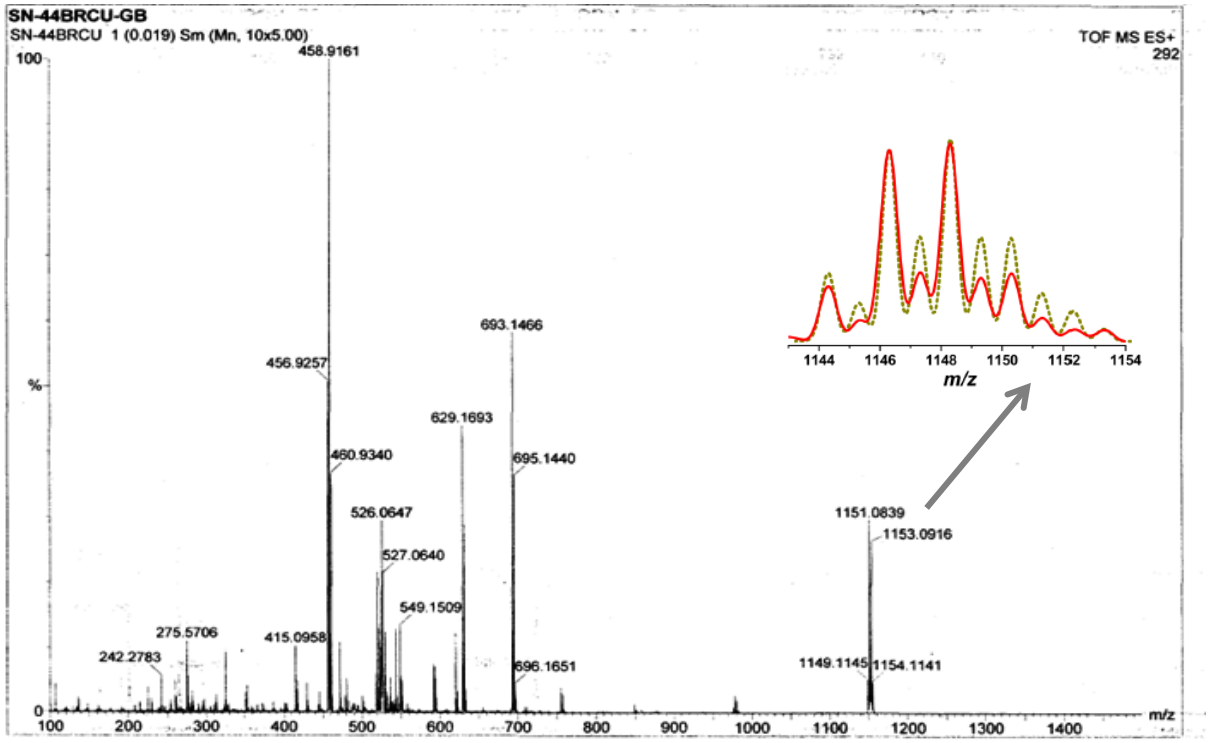

Figure 42S: ESI-MS of **PR4'**

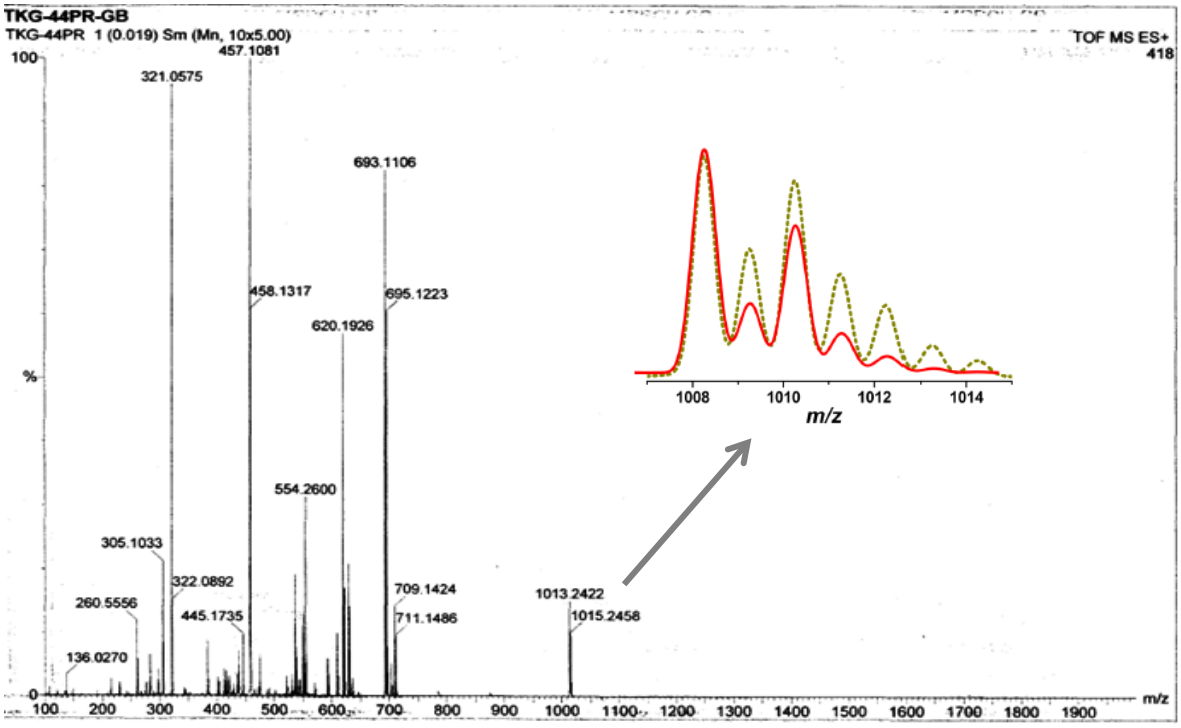

Figure 43S: ESI-MS of **PR5'**

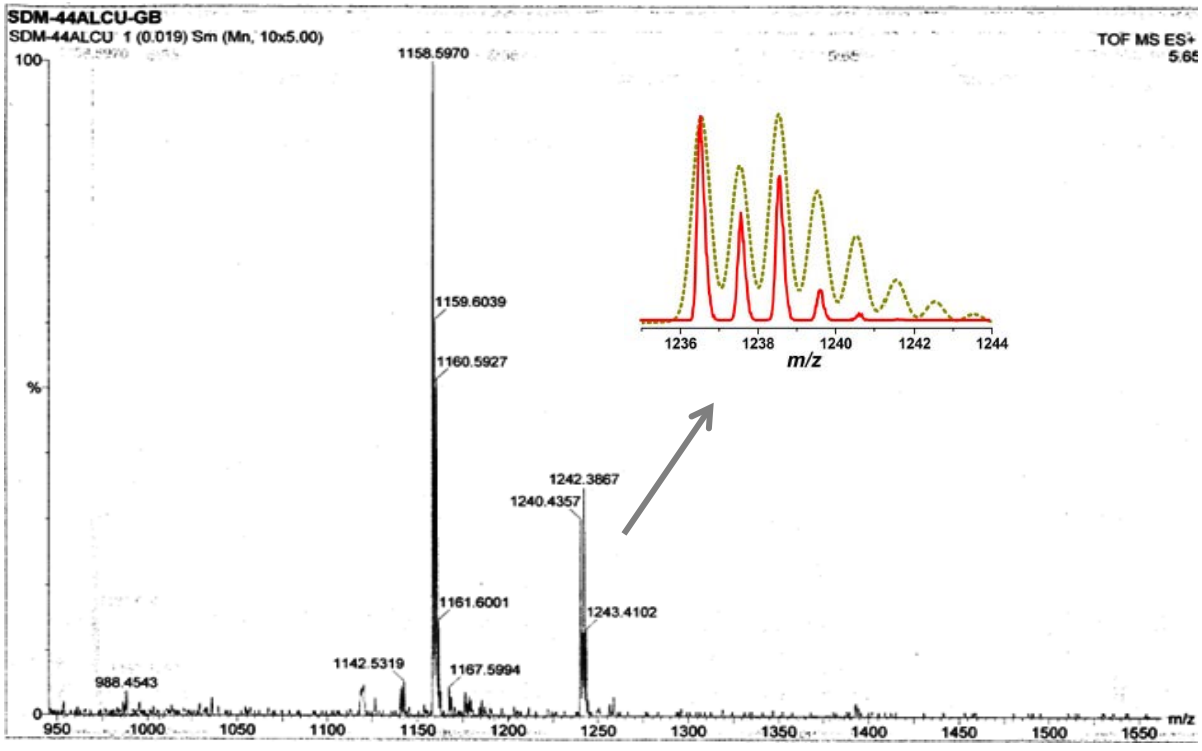

Figure 44S: ESI-MS of **PR6'**

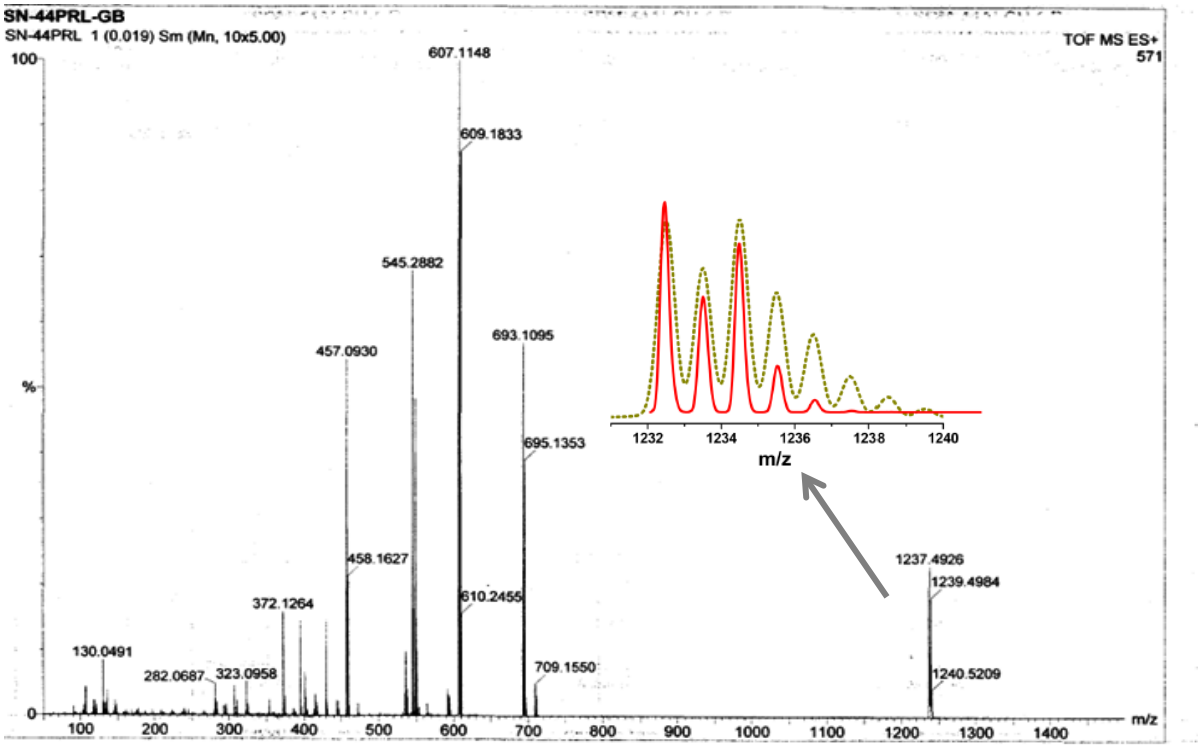

Figure 45S: ESI-MS of **PR7'**

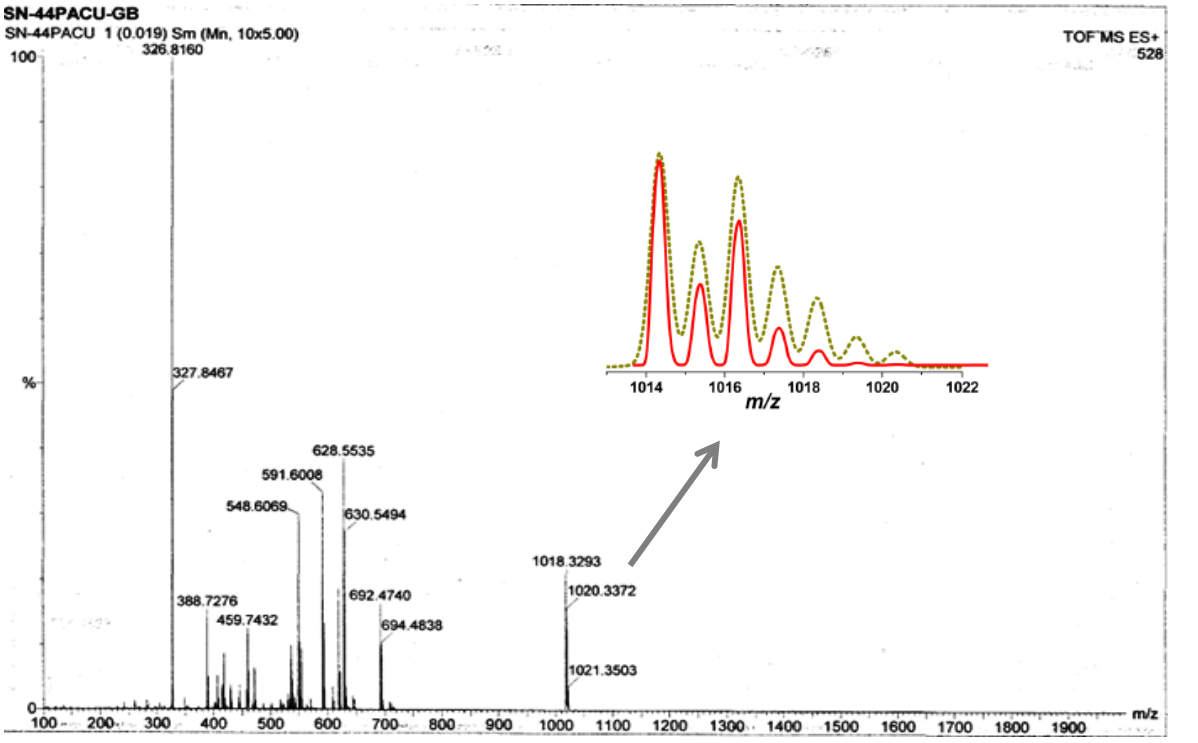

Figure 46S: ESI-MS of **PR8'**

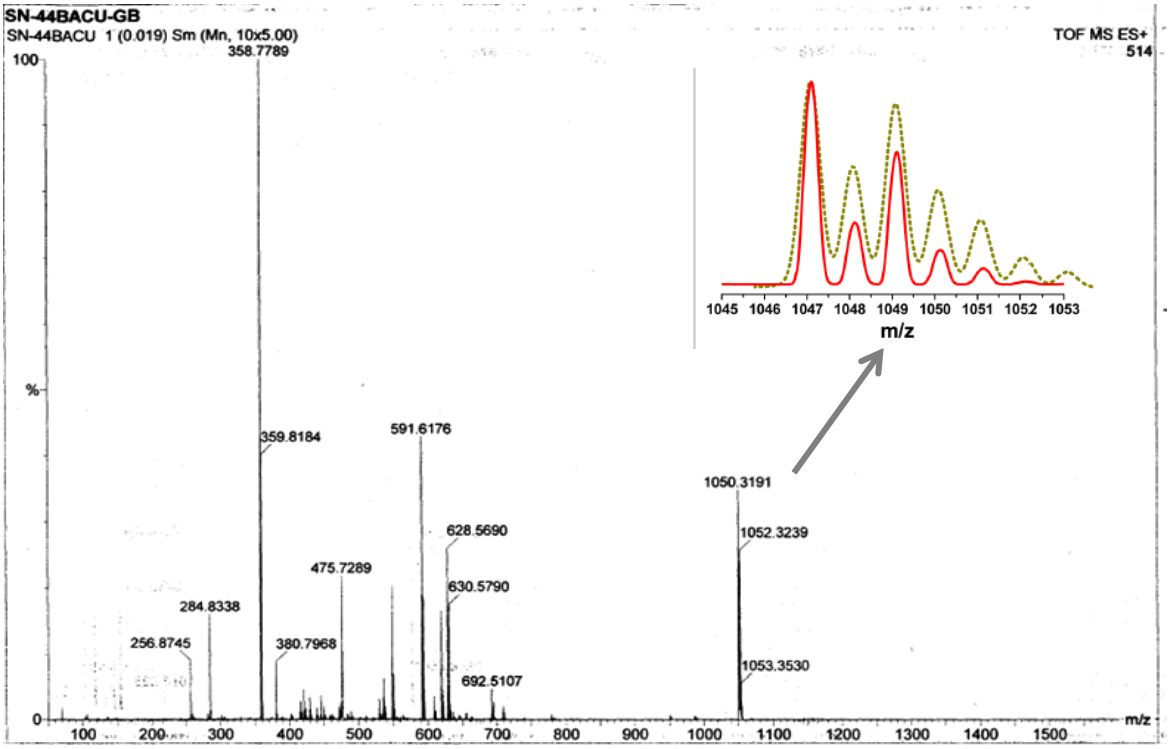

Figure 47S: ESI-MS of **PR9'**

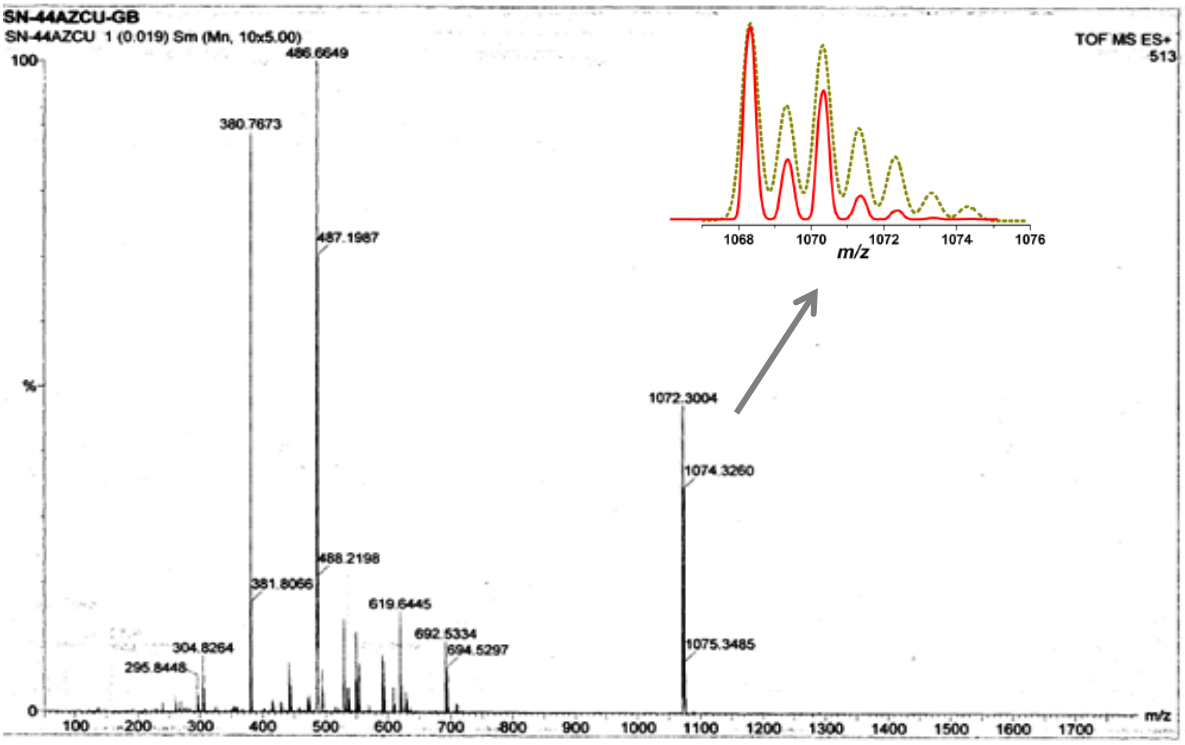

Figure 48S: ESI-MS of **PR10'**

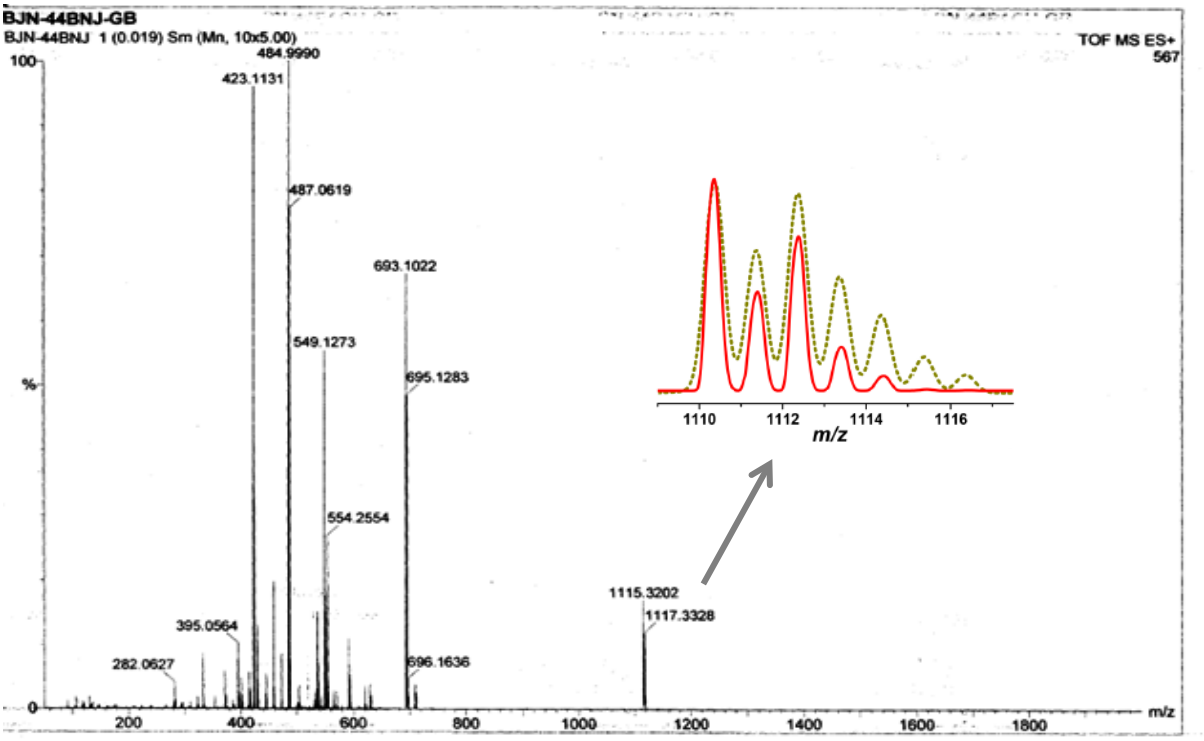

Figure 49S: EPR spectra of **PR2', PR3', PR4', PR6', PR8'** and **PR10'** with their corresponding $\mathbf{g}_{\|}$ and $\mathbf{g}_{\perp}$ values in CH_3CN at 80K.

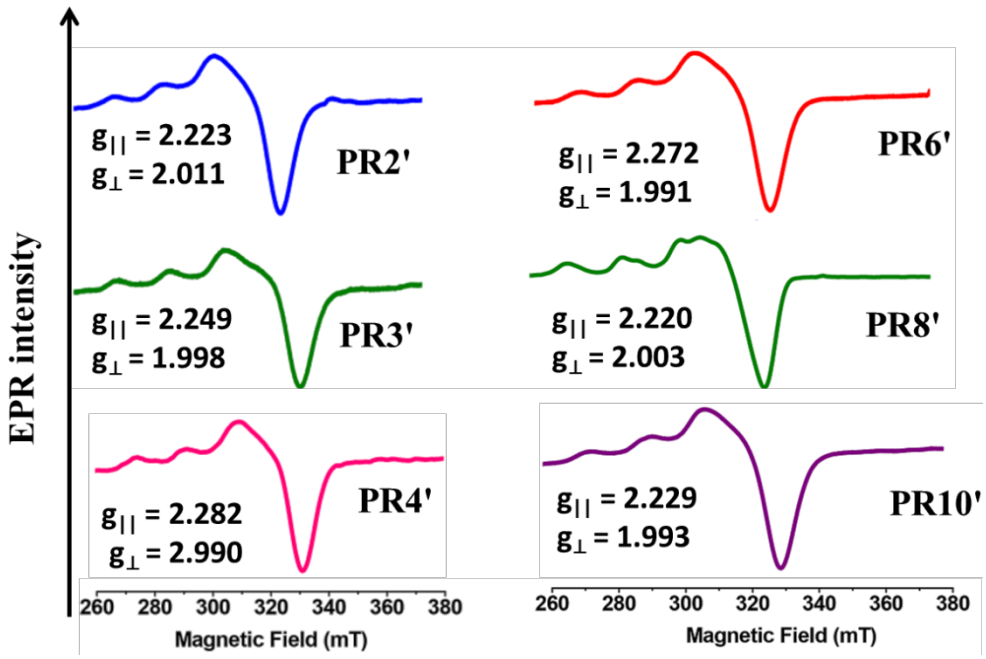

Figure 50S: UV-Vis titration profile of (a) **PR1,** (c) **PR2,** (e) **PR4,** (g) **PR5,** (i) **PR7** , (k) **PR9** and (b), (d), (f), (h), (j), (l) are their corresponding **1:1** equivalence plots.

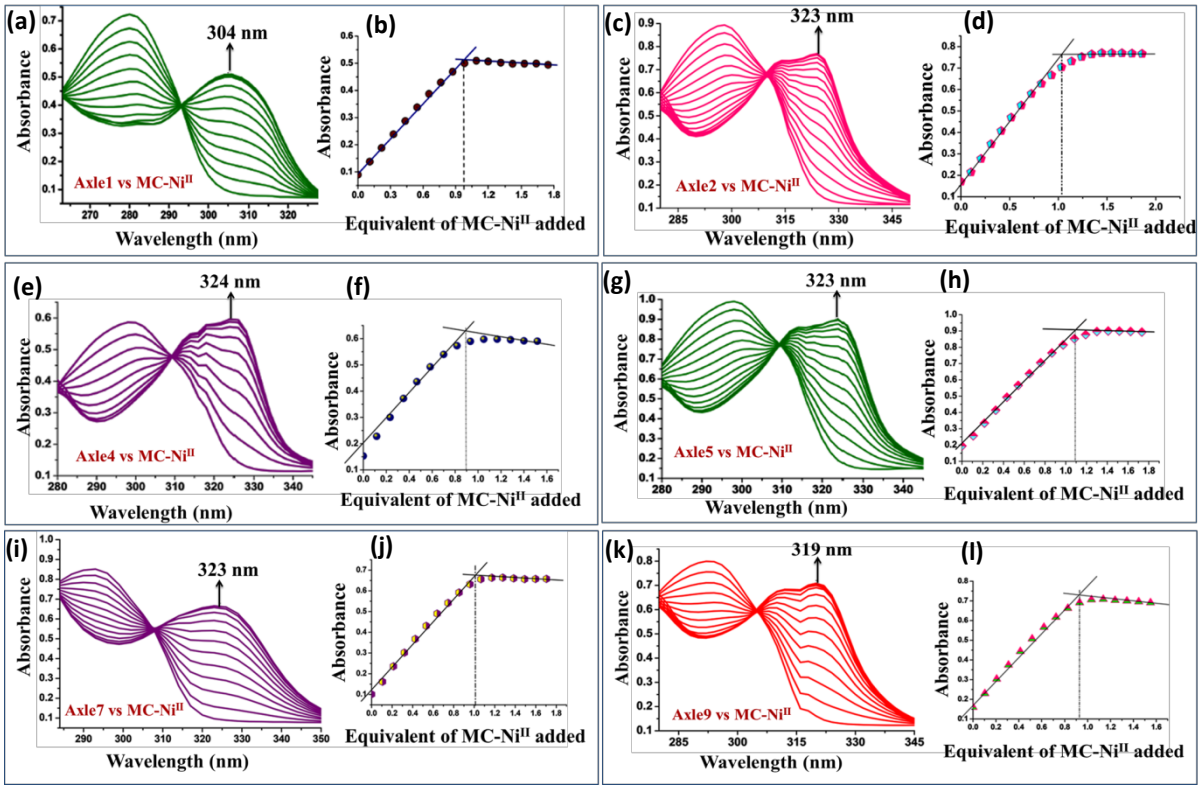

Figure 51S: Nonlinear 1:1 curve fitting of (a) **PR1,** (b) **PR2,** (c) **PR4,** (d) **PR5,** (e) **PR7** and (f) **PR9** absorption titration data with corresponding association constant values ($\mathbf{K_a}$).

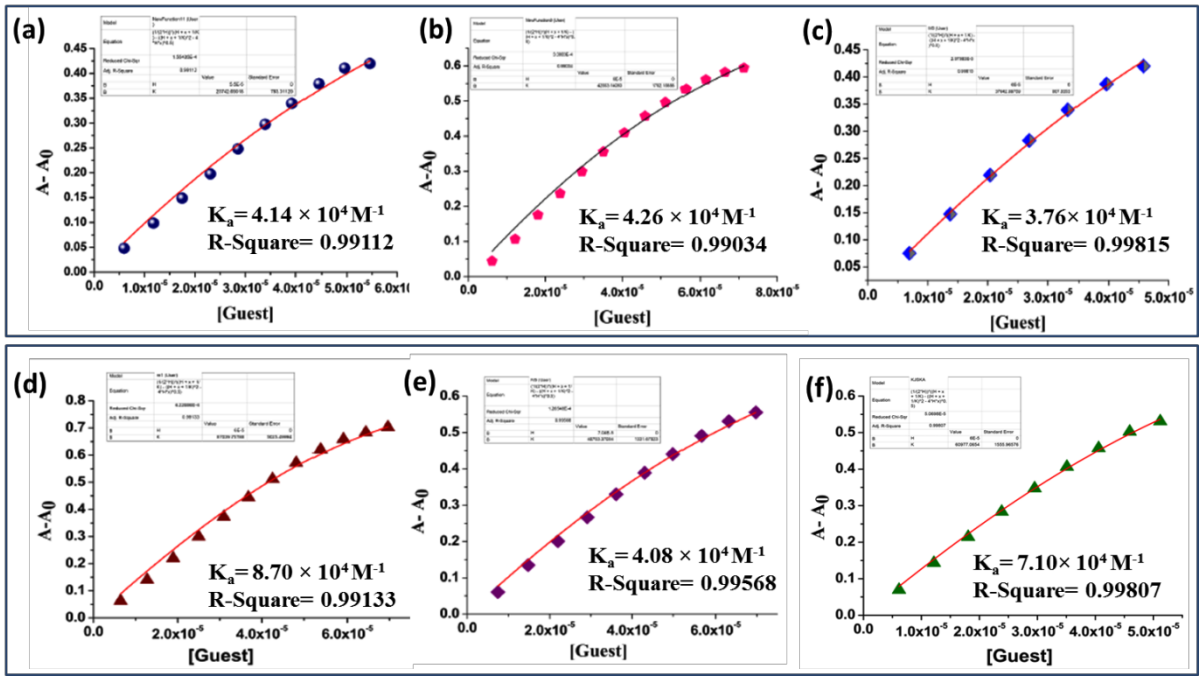

Figure 52S: UV-Vis spectra of (a) **PR3',** (b) **PR4', (c) PR6',** (d) **PR7',** (e) **PR9'** and (f) **PR10'** complexes having ClO_4^- counter anion in CH_3CN.

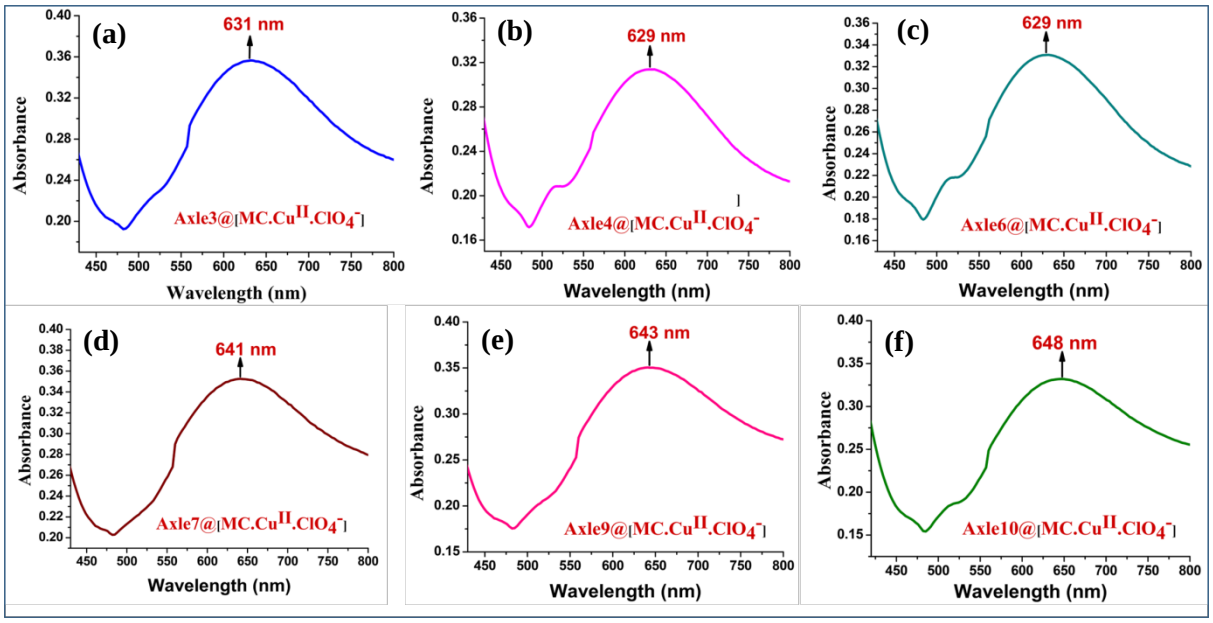

Figure 53S: UV-Vis titration profile of (a) **MC** - Cu^{II} (1×10^{-3}) vs **Axle1** (1.06×10^{-2}) in CH_3CN with corresponding (b) **1:1** equivalence plot.

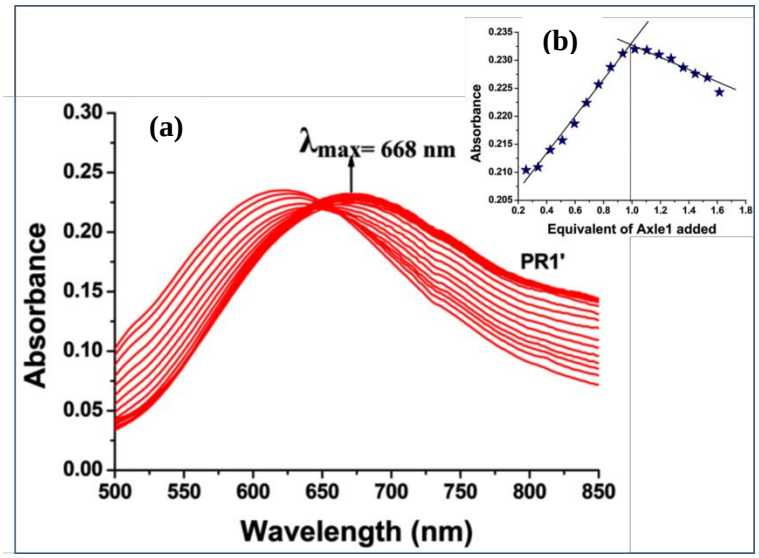

Figure 54S: FT-IR spectra of **PR1**

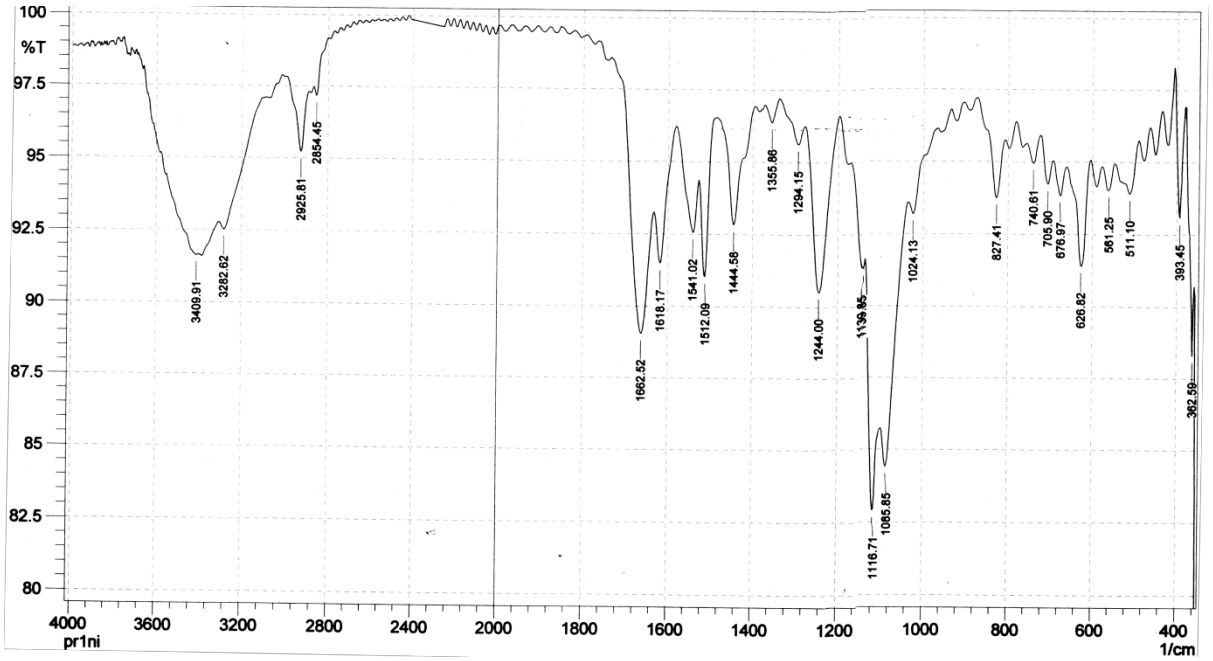

Figure 55S: FT-IR spectra of **PR2**

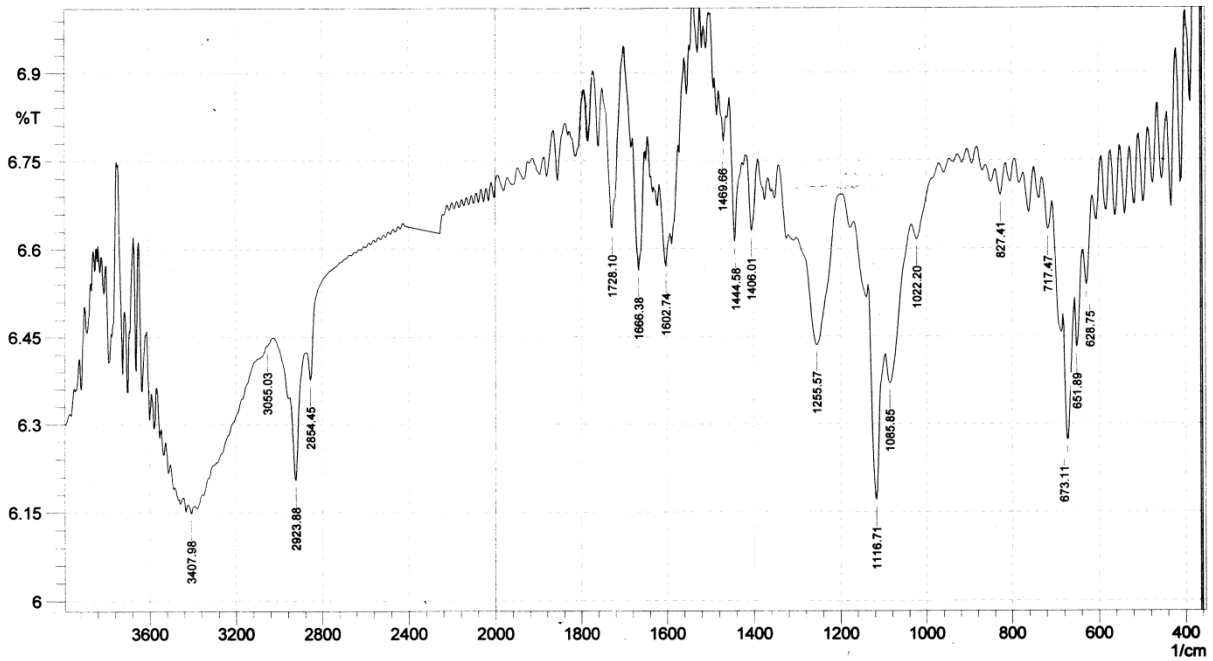

Figure 56S: FT-IR spectra of **PR3**

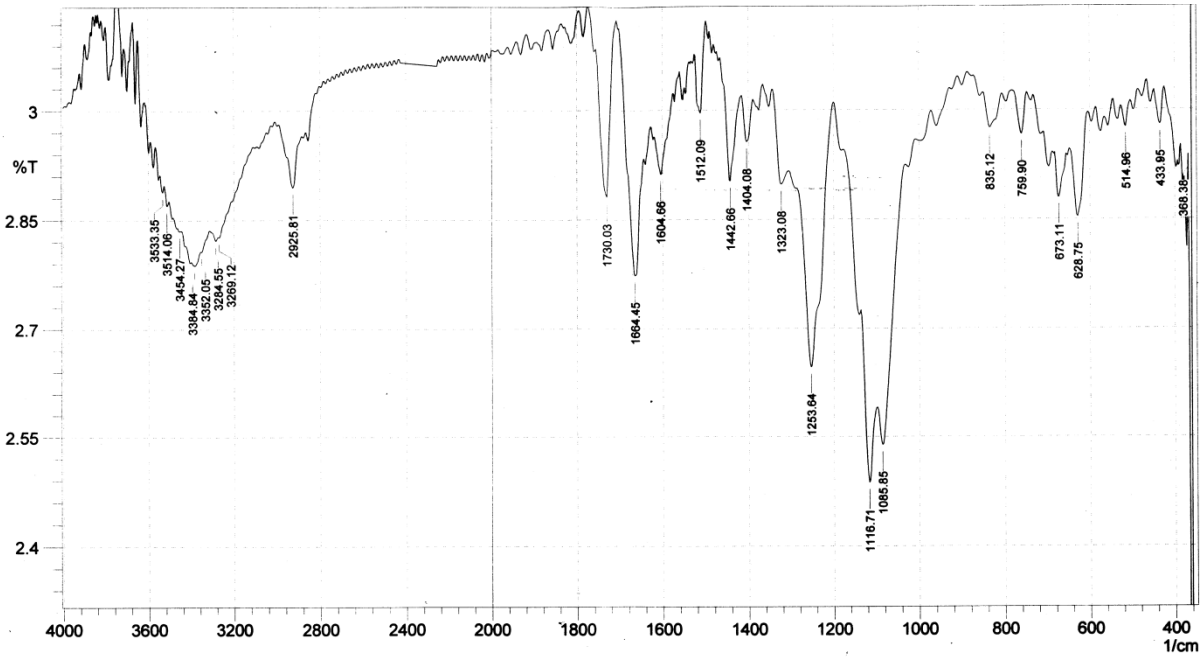

Figure 57S: FT-IR spectra of **PR4**

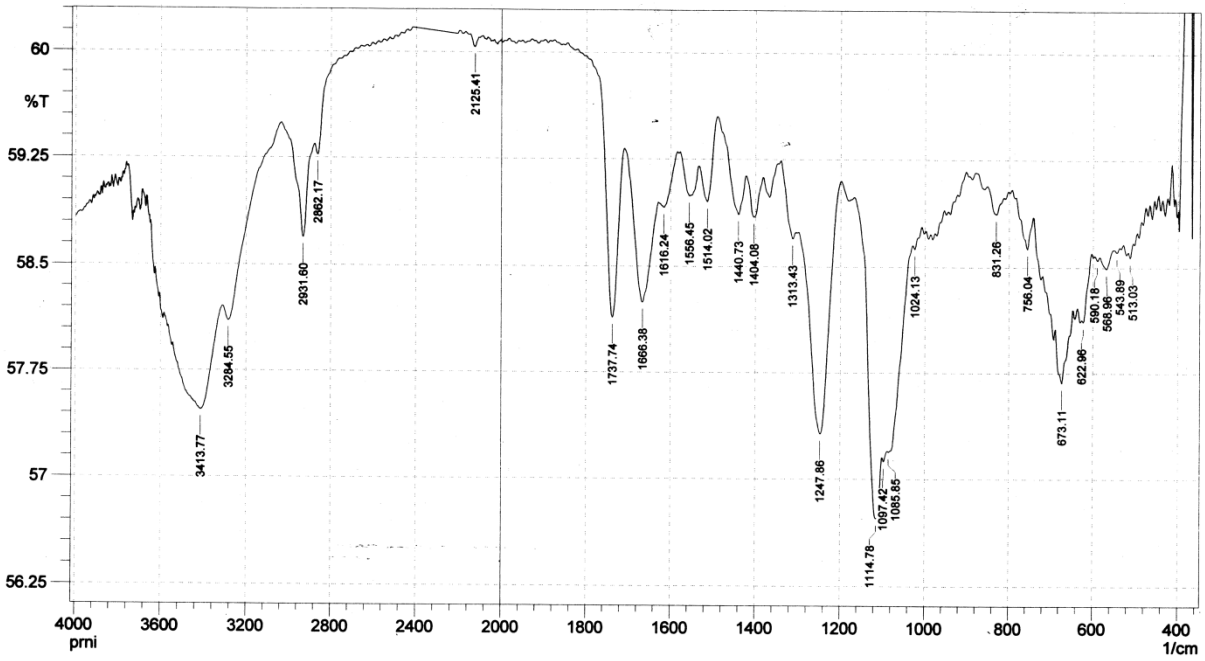

Figure 58S: FT-IR spectra of **PR5**

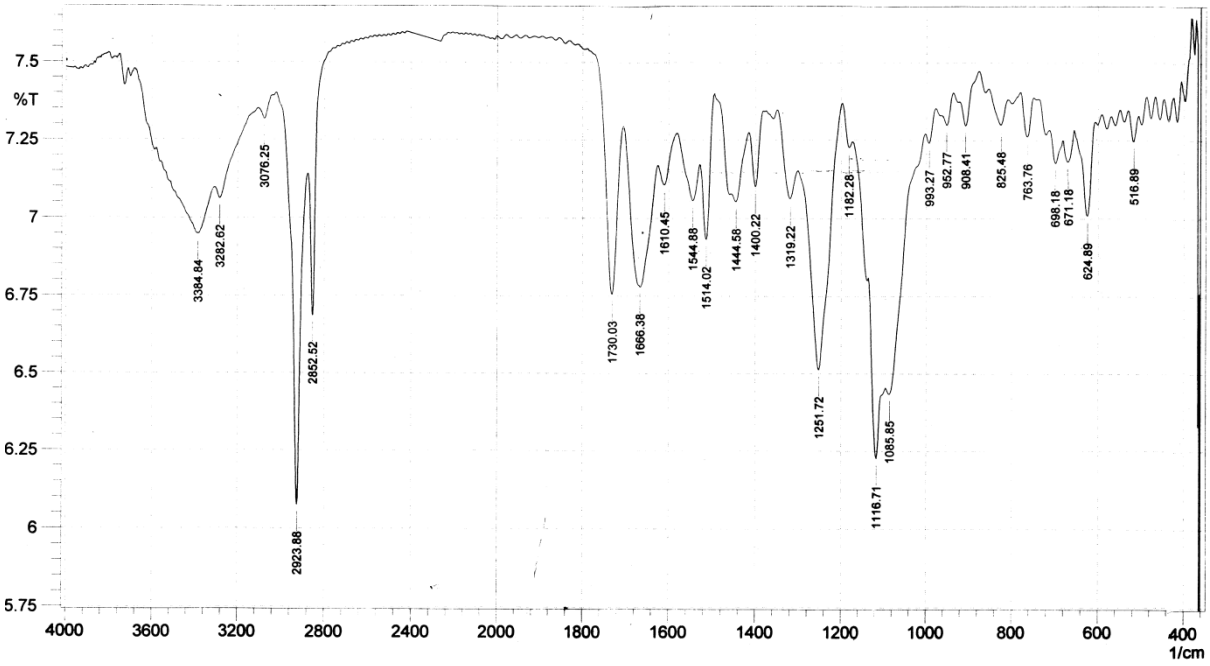

Figure 59S: FT-IR spectra of **PR6**

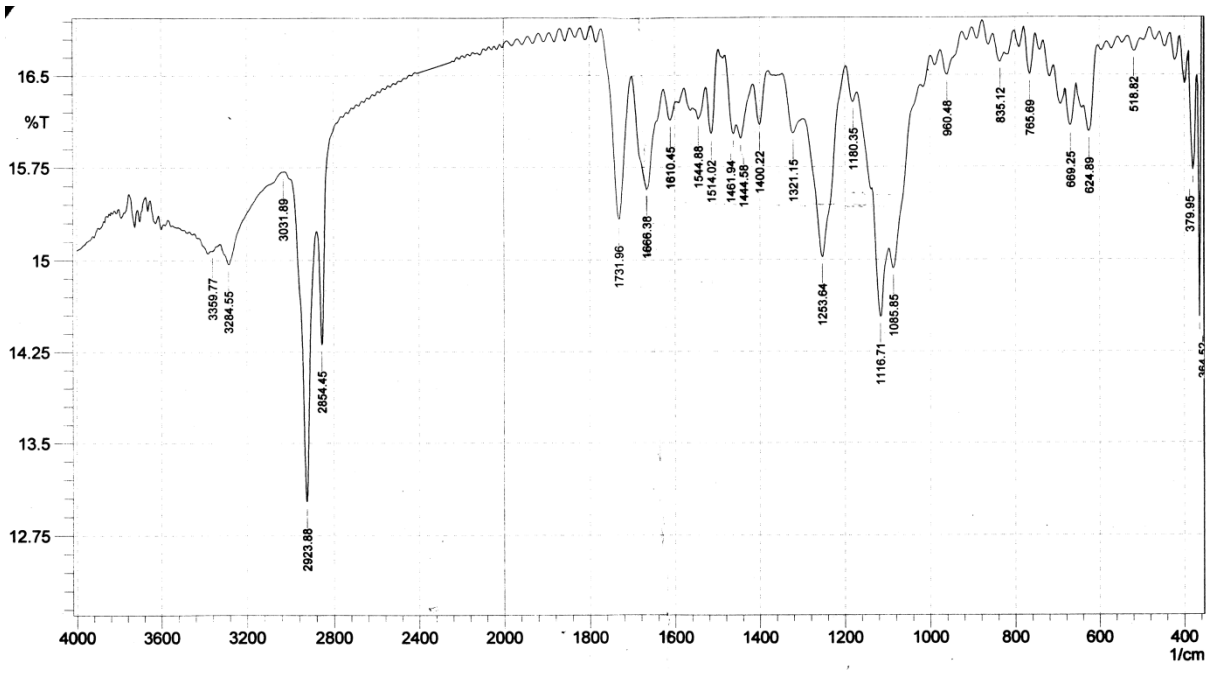

Figure 60S: FT-IR spectra of **PR7**

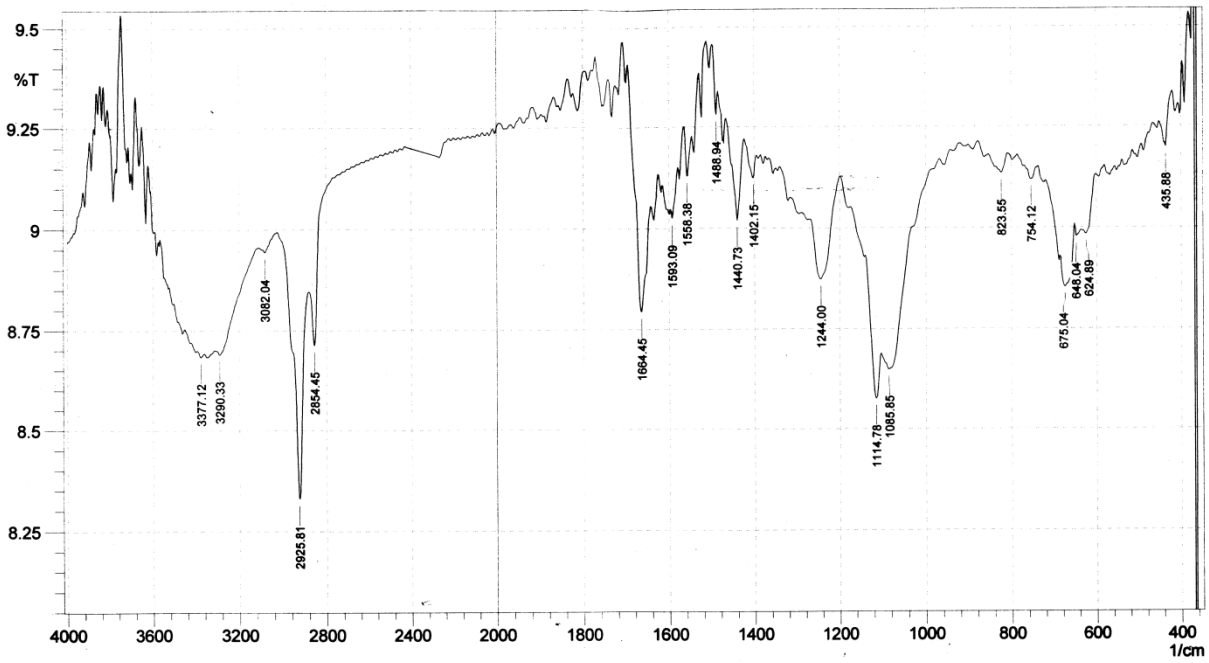

Figure 61S: FT-IR spectra of **PR8**

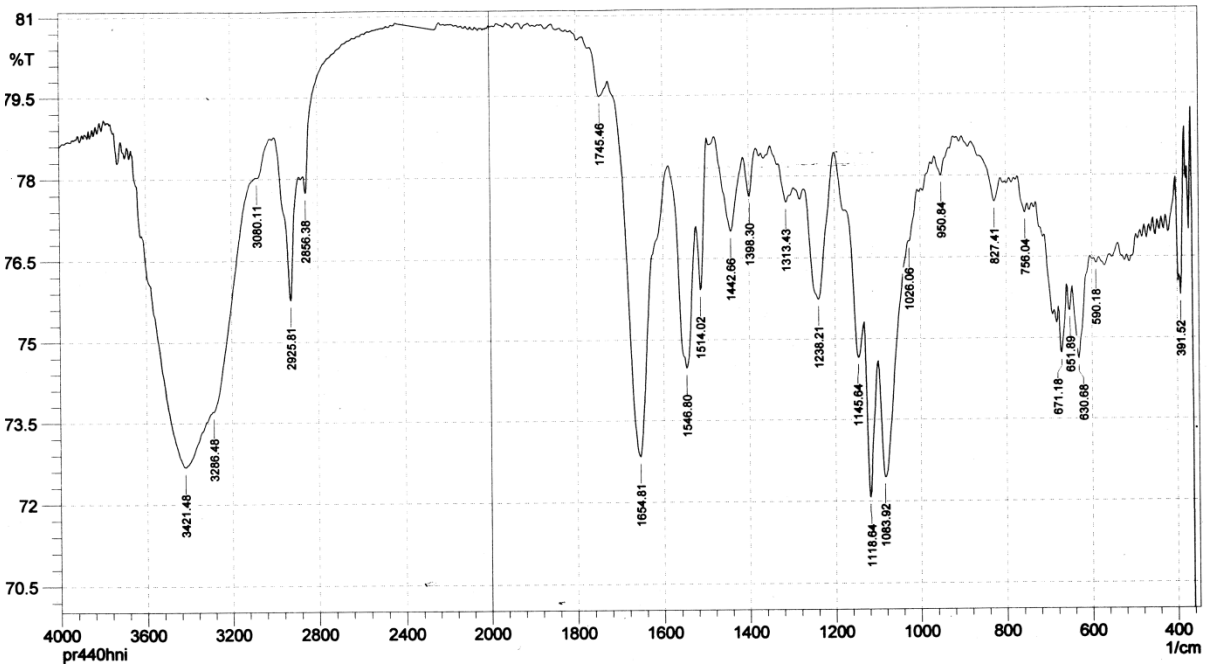

Figure 62S: FT-IR spectra of **PR9**

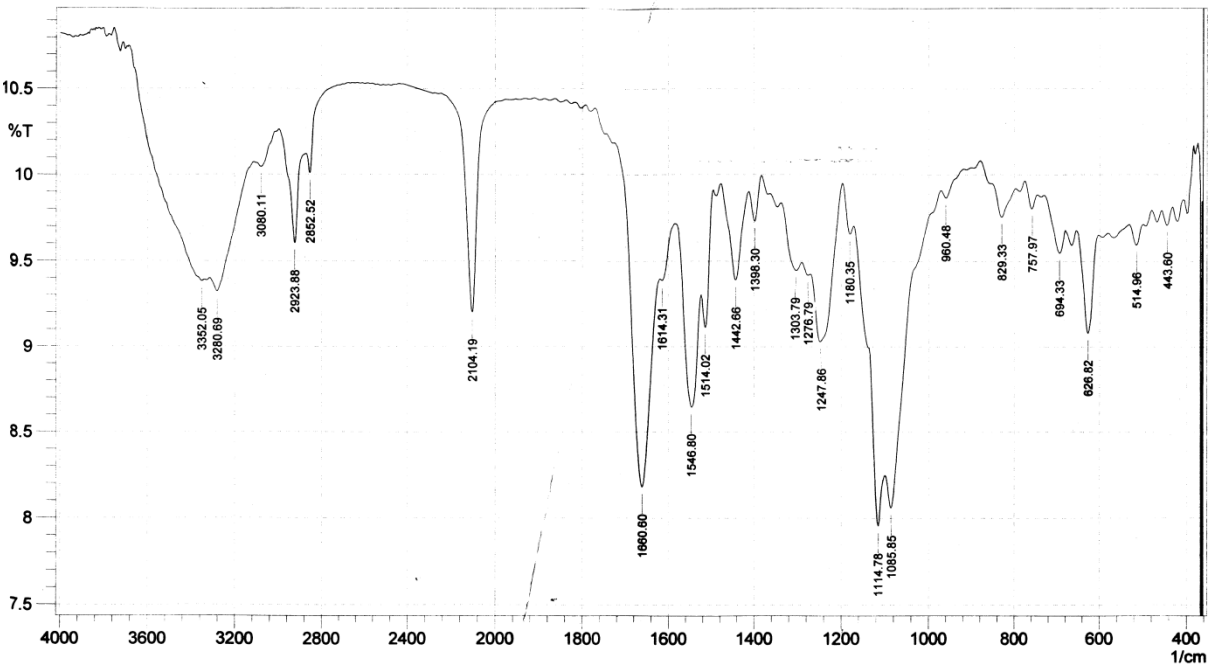

Figure 63S: FT-IR spectra of **PR10**

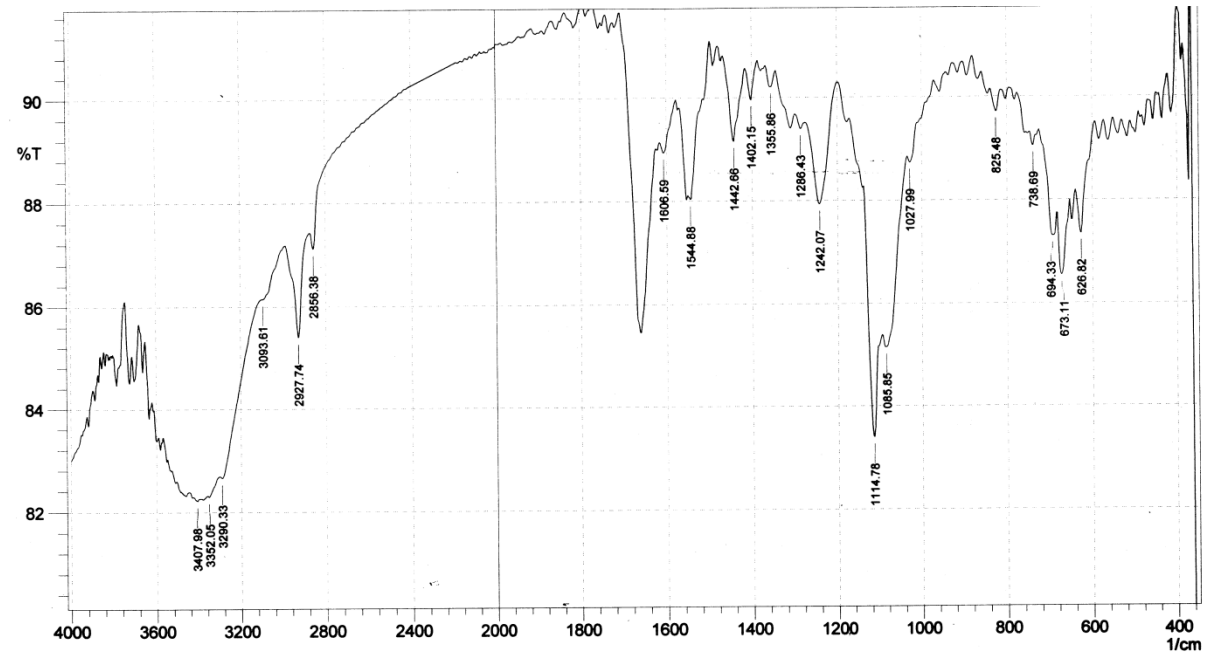

Figure 64S: FT-IR spectra of **PR1'**

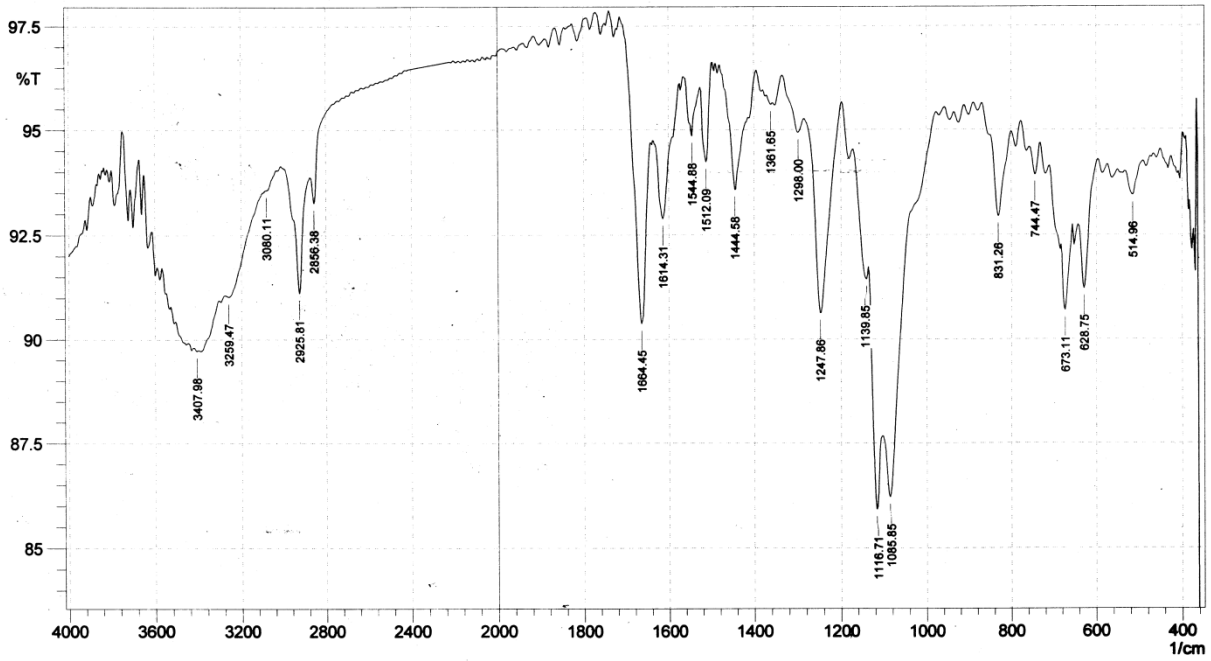

Figure 65S: FT-IR spectra of PR2'

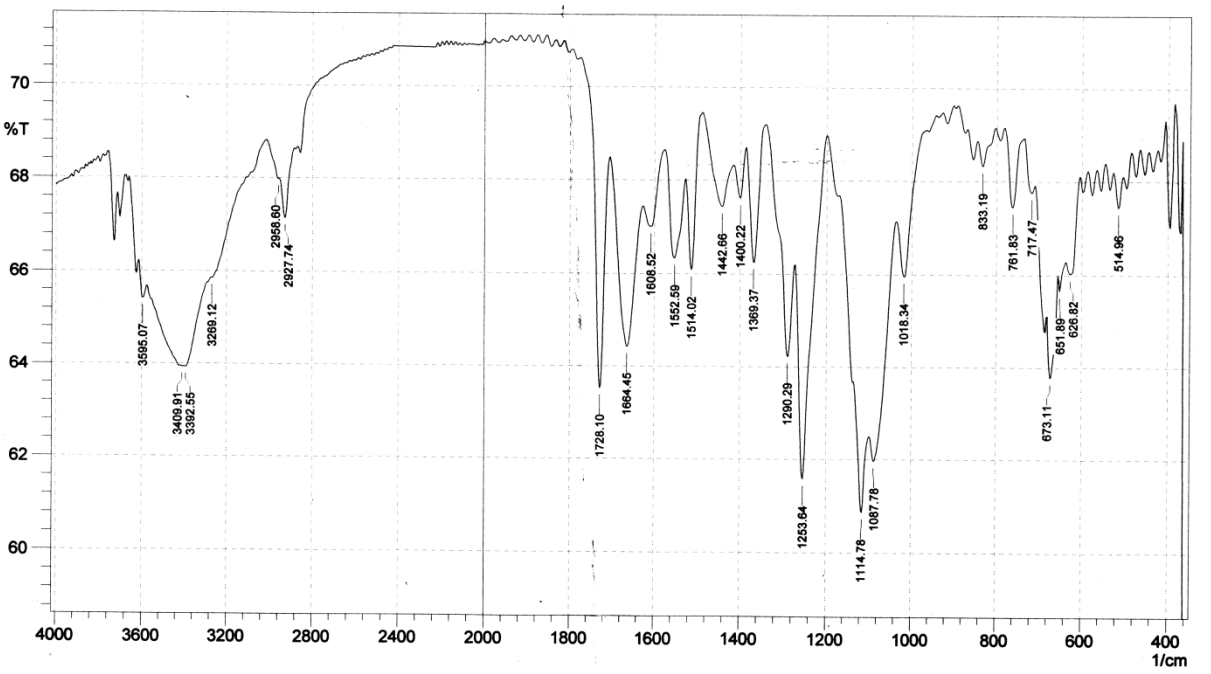

Figure 66S: FT-IR spectra of **PR3'**

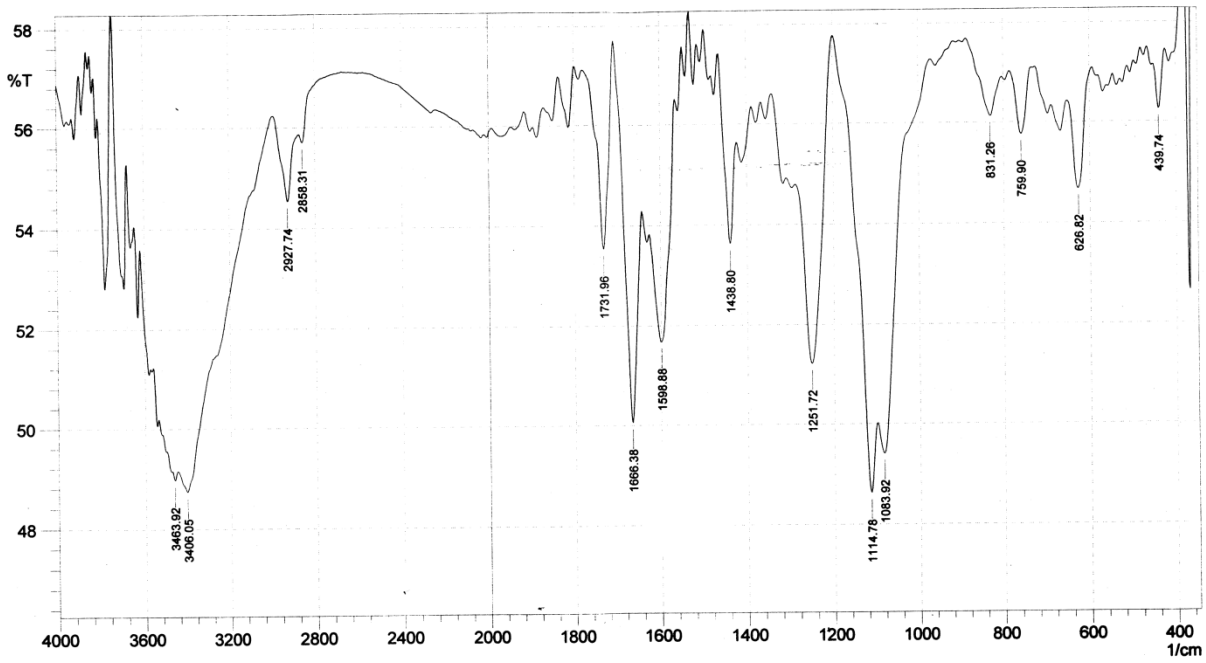

Figure 67S: FT-IR spectra of **PR4'**

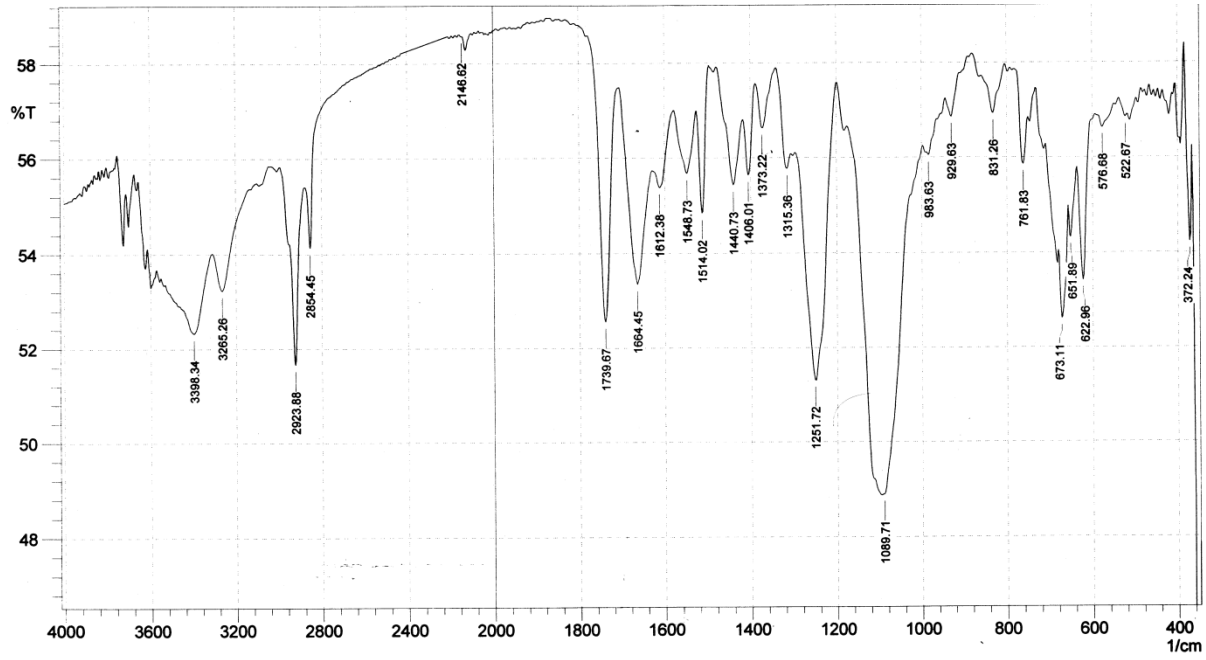

Figure 68S: FT-IR spectra of **PR5'**

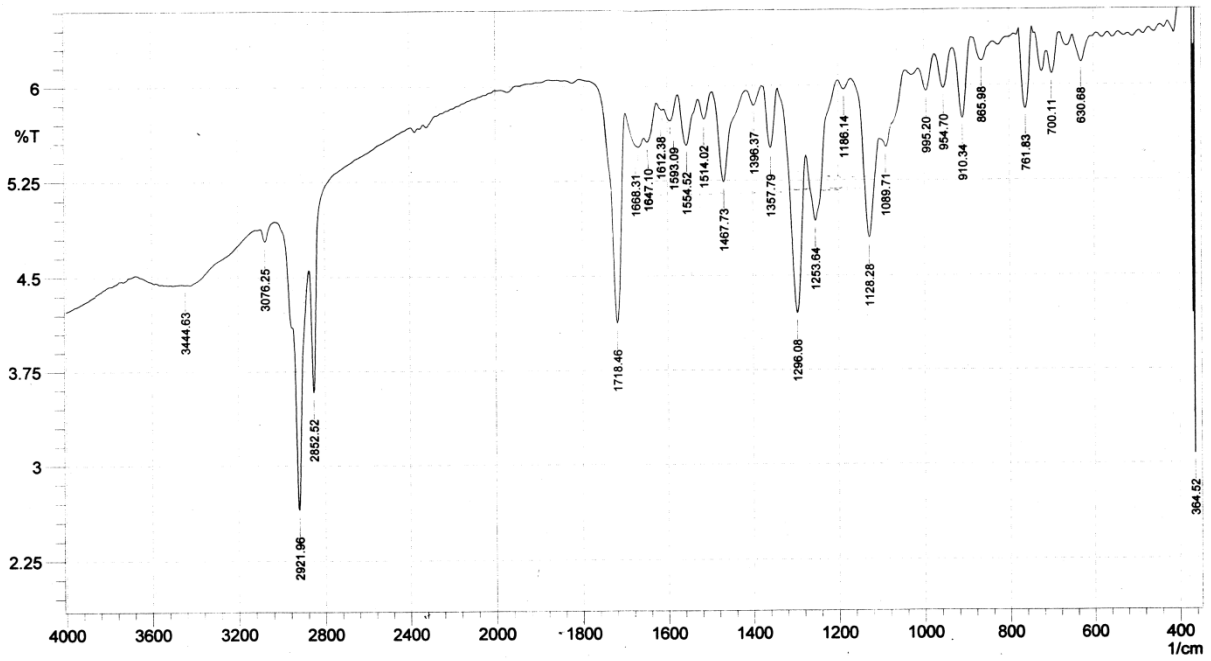

Figure 69S: FT-IR spectra of **PR6'**

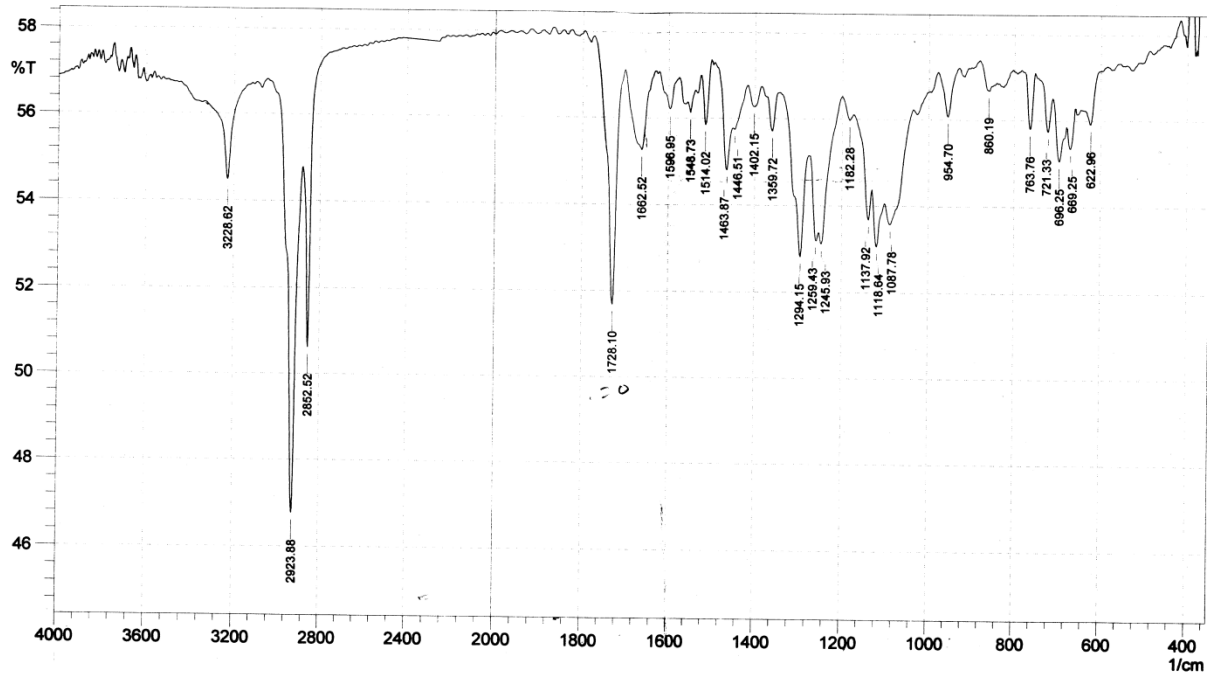

Figure 70S: FT-IR spectra of **PR7'**

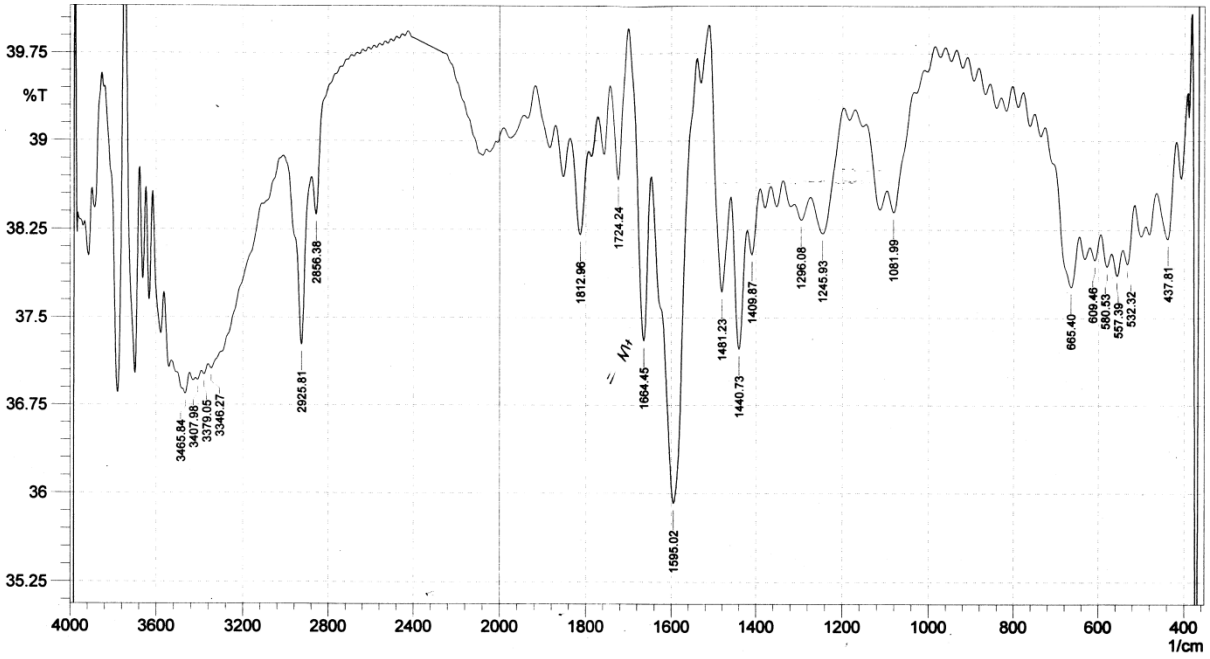

Figure 71S: FT-IR spectra of **PR8'**

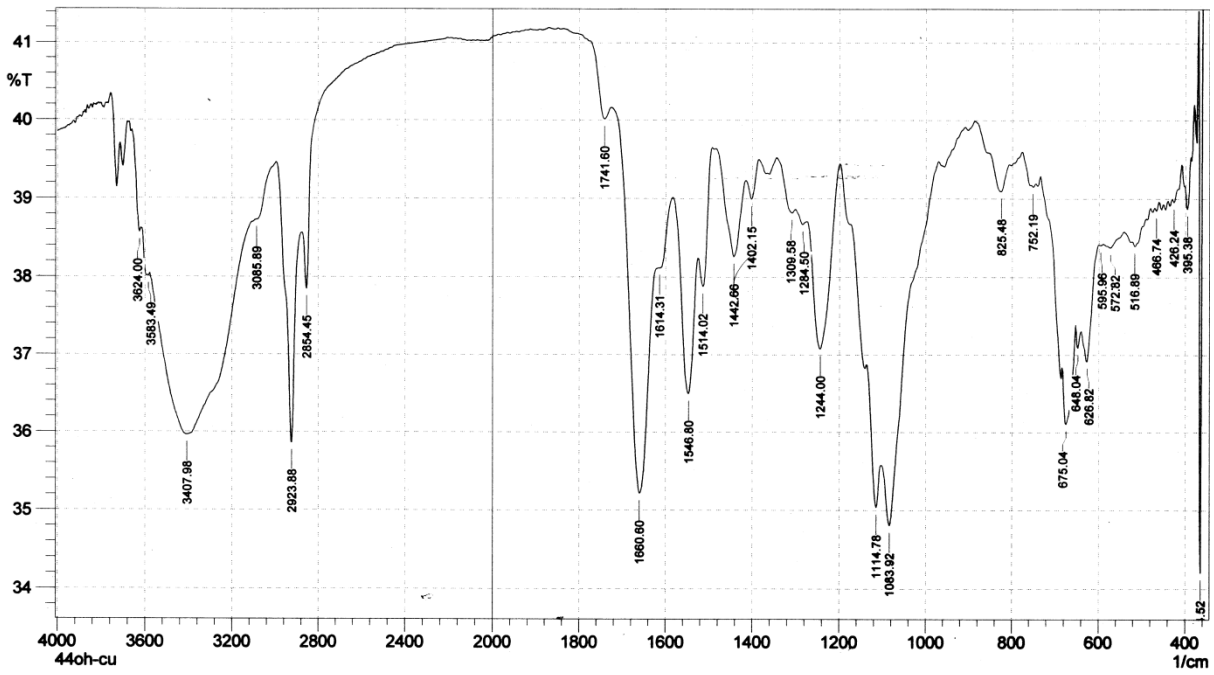

Figure72: FT-IR spectra of **PR9'**

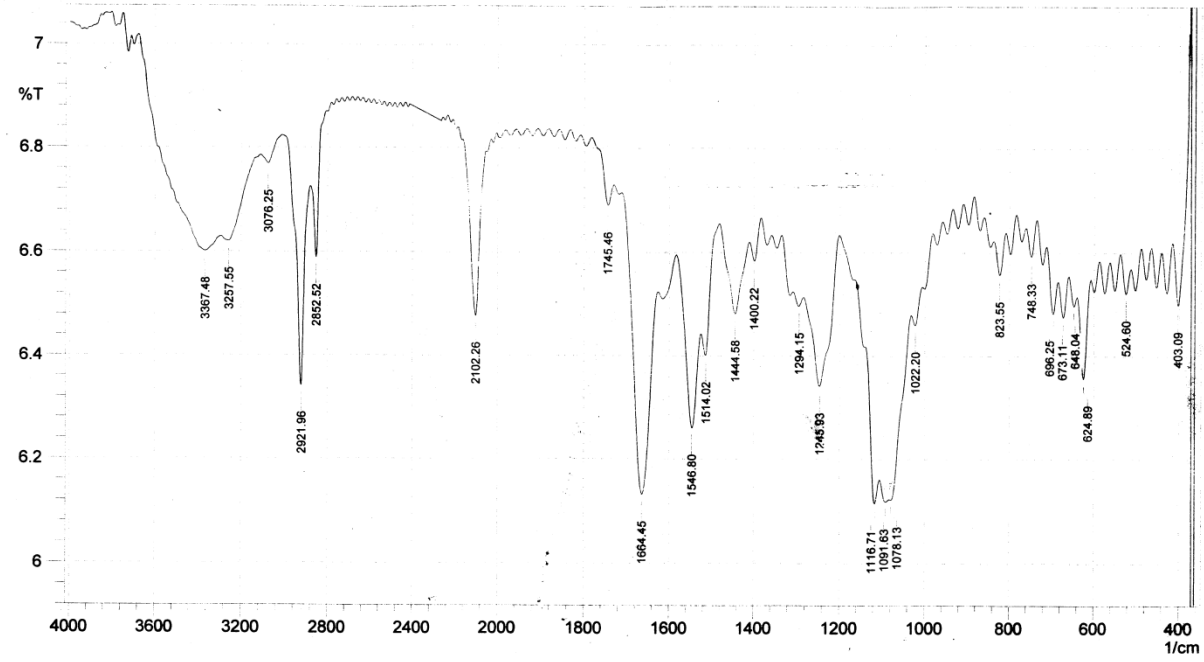

Figure 73S: FT-IR spectra of **PR10'**

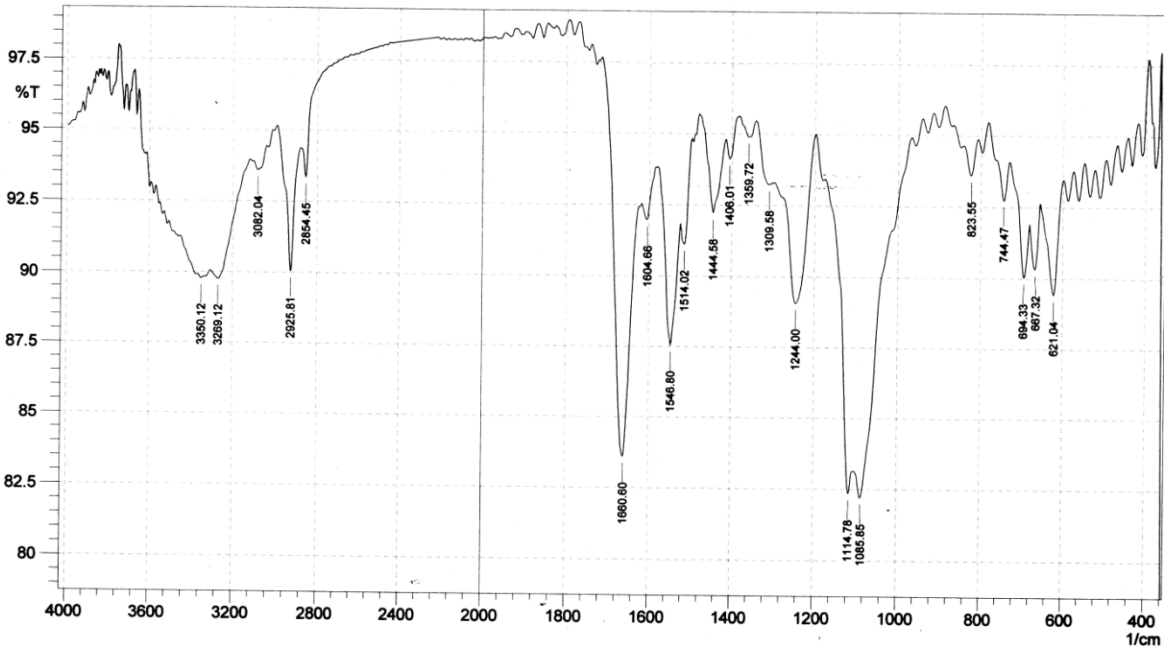

Single crystal data analysis:

Detailed structural analysis shows that, three isolated crystal structures have adopted pentacoordinate geometry around Cu^{II} centre, where three coordination sites are occupied by three NH groups of **MC** and other two coordinating sites are occupied by two N atoms of the pyridine moiety present in the bidentate axles. The Cu-N bond distances (Table S1) are found to have different values in the structures, which is within the range of 1.985Å - 2.170Å. However, these values match well with the ranges, obtained in cases of other Cu^{II}-bipyridine complexes in literature.[1a, b] Bipyridine moieties with the dihedral angle of 3.9˚, -2.3˚ and 2.7˚ as well as chelating amine groups with the angles ranging from -55.3 to 58.3 (Table S3) have indicated that both the bipyridine units and chelating amine groups are in cis configuration.[2] All the N-Cu-N bond angles ranging between 80.6˚ and 176.5˚ (Table S2) assist to calculate the $\boldsymbol{\tau}$ index values that determine the coordination geometry around the metal centre. Calculated $\boldsymbol{\tau}$ index values **0.76**, **0.40** and **0.86** (Table S6) for the respective three crystal structures, confirm the distorted trigonal bipyramidal geometry around the Cu^{II} metal ions in **PR1'** and **PR7'** threaded complexes, whereas **PR3'** crystal structure adopts distorted square pyramidal geometry (Fig. 75S, ESI†**)**. Importantly in each of the crystal structures, the centroid of the arene moieties of the **MC** and one of the pyridine moieties of the bipyridine chelating axles are in the distance of π - π stacking interactions which is within the range of 3.469Å - 4.339Å (Table S6). Such π - π stacking distances vary for different crystal structures may be due to the presence of structural orientation or steric crowding in the bidentate axles around the Cu^{II} metal centre. Such as in **PR1'** absence of any functional substituent suppress the steric hindrance around the arene moieties and decrease the π - π stacking distances. Interestingly, in case of **PR7'** crystal structure, along with the metal ion coordination and π - π stacking interactions, a secondary H bonding interaction is also detected between **N1-H1** amide bond of **Axle7** and carbonyl **O3** atom of **MC** having **O⋯N** distance of 2.880Å (Fig.

74S, ESI†). However, the presence of such secondary H bonding interaction in **PR7'** may cause slight enhancement of π - π stacking distances as compared to **PR1'** and **PR3'**. Thus solid state X-Ray crystal structure analysis assists to demonstrate that, along with metal chelation also other non-covalent interactions are cooperating in 1:1 threading of 'U' shaped bent axles into the cavity of **MC**-Cu^{II}.

Figure 74S: (Top) Chemical structures of (a) **PR1'**, (b) **PR3'**, and (c) **PR7'** in ball and stick model (oxygen= red, nitrogen= blue, violet= carbon, orange= Cu , brown= Br). (Bottom) (**d**), (**e**) and (**f**) showing the space-filling models of the respective pseudorotaxanes. For transparency all the axles are remained in same colours in space filling model. H atoms, counter anions, and solvent molecules are omitted for clarity.

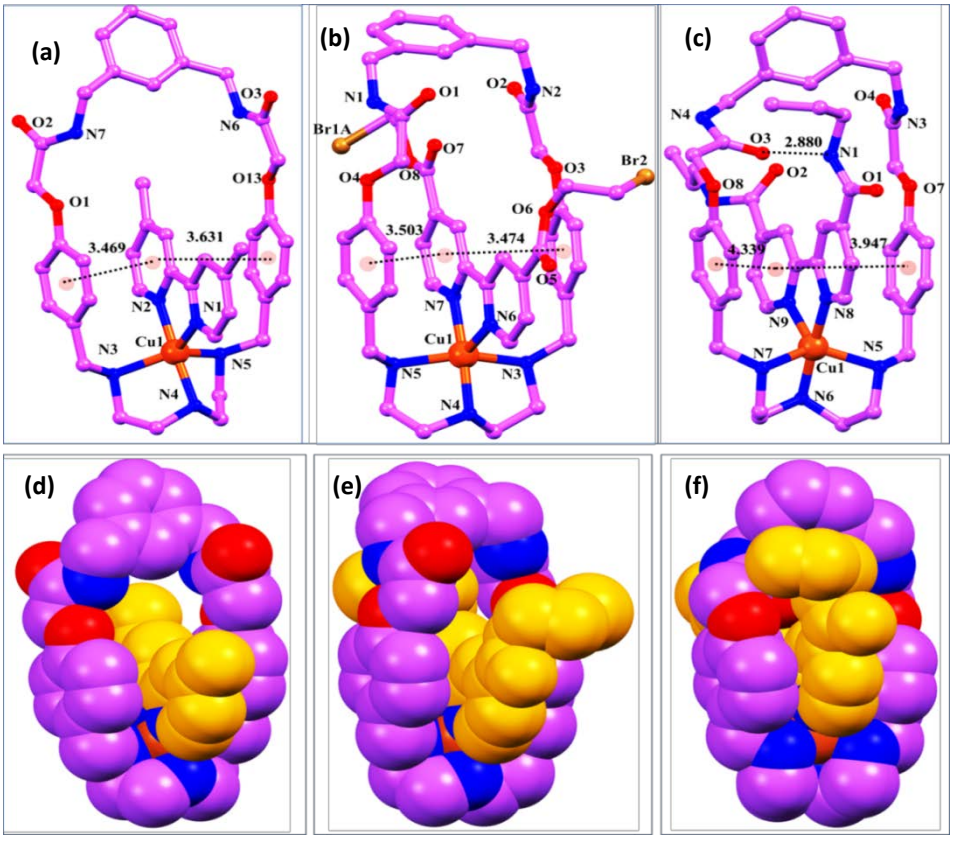

Figure 75S: Coordination geometry around the Cu^{II} metal centre in (a) **PR1',** (b) **PR3'** and (c) **PR7'** single X- Ray crystal structure.

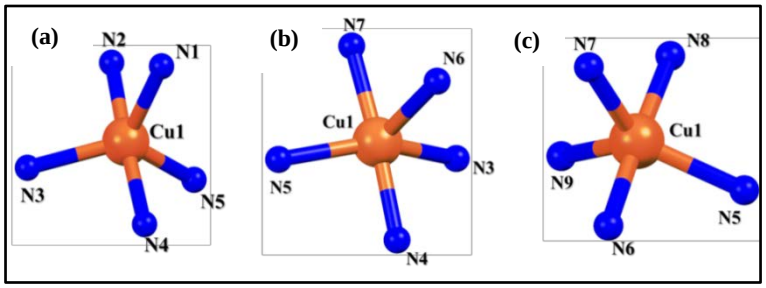

Table S1. *Calculated* Cu-N *bond lengths of **PR1'**, **PR3'** and **PR7'** single X- ray crystal structures.*

PR1'		**PR3'**		**PR7'**	
Cu1 - N1	2.093(8)	Cu1 - N3	2.104(5)	Cu1 - N5	2.078(7)
Cu1 - N2	1.985(9)	Cu1 - N4	1.994(6)	Cu1 - N6	2.026(7)
Cu1 - N3	2.102(10)	Cu1 – N5	2.079(5)	Cu1 - N7	2.119(7)
Cu1 - N4	2.024(10)	Cu1 – N6	2.170(5)	Cu1 - N8	2.013(6)
Cu1 - N5	2.084(11)	Cu1 – N7	2.002 (5)	Cu1 - N9	2.092(6)

Table S2: N-Cu-N bond angles (deg) in **PR1', PR3'** and **PR7'**

PR1'		**PR3'**		**PR7'**	
N1 - Cu1 - N2	80.6(4)	N3 - Cu1 - N4	84.2 (2)	N5 - Cu1 - N6	83.5(3)
N1 - Cu1 - N3	117.5(3)	N3 - Cu1 - N5	152.1(2)	N5 - Cu1 - N7	124.9(3)
N1 - Cu1 - N4	102.5(4)	N3 - Cu1 - N6	97.22(19)	N5 - Cu1 - N8	94.2(2)
N1 - Cu1 - N5	113.5(4)	N3 - Cu1 - N7	97.48(19)	N5 - Cu1 - N9	124.3(2)
N2 - Cu1 - N3	96.5(4)	N4 - Cu1 - N5	85.7(2)	N6 - Cu1 - N7	84.8(3)
N2 - Cu1 - N4	174.7(4)	N4 - Cu1 - N6	104.01(19)	N6 - Cu1 - N8	176.5(3)
N2 - Cu1 - N5	90.9(4)	N4 -Cu1 - N7	176.0 (2)	N6 - Cu1 - N9	103.8(3)
N3 - Cu1 - N4	86.0(4)	N5 - Cu1 - N6	110.45(19)	N7 - Cu1 - N8	94.4(2)
N3 - Cu1 - N5	129.0(4)	N5 - Cu1 - N7	91.3(2)	N7 - Cu1 - N9	110.8(3)
N4 - Cu1 - N5	83.9 (4)	N6 - Cu1 - N7	79.45(19)	N8 - Cu1 -N9	79.7(2)

Table S3. *Calculated* N-C-C-N *torsional angles of* ***PR1'***, ***PR3'*** *and* ***PR7'*** *single X- ray crystal structures.*

PR1'		**PR3'**		**PR7'**	
N1- C6- C7- N2	3.9(14)	N7- C35- C36- N6	-2.2(7)	N9- C32- C33- N8	2.7(9)
N4- C39- C40- N3	-55.3(15)	N4- C3AA- C18- N5	-52.3(7)	N7- C8- C9- N6	58.3(9)
N4- C43- C44- N5	39.9(17)	N4- C20- C21- N3	-48.5(7)	N5- C46- C47- N6	-48.8(9)

Table S4: H bonding table for **PR7'**

D-H…A	**d(H-A) Å**	**d(D-A) Å**	**<DHA (º)**
N1 -- H1... 03	2.0000	2.880(8)	173.00
NOAA -- HOAA.. F12	2.2400	3.061(10)	162.00
N4 -- H4... F9	2.1400	2.971(14)	157.00
N4 -- H4... F11	2.3900	3.107 (8)	139.00
N5 -- H5... O1	1.9500	2.920(8)	168.00
N6 -- H6... O4	2.2400	3.041(10)	139.0
N6 -- H6... N10	2.4600	3.208(10)	134.00
N6 -- H6... F5	2.3300	3.290(10)	170.00
C9 -- H9B .. F25	2.4000	3.385(2)	175.00
C24 -- H24 .. O1	2.4200	3.288(10)	153.00
C25 -- H25 .. F3	2.4800	3.359(12)	155.0
C30 -- H30 .. F7	2.4800	3.428(12)	172.00
C31 -- H31 .. N10	2.5300	3.458(19)	166.00
C34 -- H34 .. O3	2.3000	3.082(9)	140.00
C37 -- H37 .. F4	2.4900	3.391(10)	157.00
C45 -- H45B .. F2	2.4300	3.197(12)	134.00
C46 -- H46B .. F4	2.3400	3.196(10)	145.00

Table S5: Crystallographic table for single X- ray crystal structure of **PR1'** (MCCU44BP), **PR3'** (MCCU44BR) and **PR7'** (MCCU44PA)**.**

Compound reference	MCCU44BP	MCCU44BR	MCCU44PA
Chemical formula	$2(C_{42}H_{49}CuN_7O_4)\bullet4(ClO_4)\bullet2(C_{1.50}H_3N_{0.50})$	$2(ClO_4)\bullet C_{46}H_{51}Br_2CuN_7O_8\bullet2(CH_4O)\bullet C_2H_3N$	$C_{48}H_{58}CuN_9O_6\bullet2(F_6P)\bullet2(C_2H_3N)\bullet CH_4O$
Formula Mass	2012.75	1357.33	1324.63
Crystal system	Orthorhombic	Triclinic	Monoclinic
a/Å	13.300(3)	11.0692(17)	12.872(6)
b/Å	18.907(4)	14.524(2)	16.090(7)
c/Å	19.051(4)	18.154(3)	28.825(12)
α/°	90	88.317(2)	90
β/°	90	73.458(2)	95.239(11)
γ/°	90	89.479(2)	90
Unit cell volume/Å^3	4790.7(17)	2796.5(8)	5945(5)
Temperature/K	150(2)	150(2)	150(2)
Space group	*P*212121	$P\bar{1}$	*P*21/*c*
No. of formula units per unit cell, *Z*	2	2	4
Radiation type	MoKα	MoKα	MoKα
No. of reflections measured	19974	25433	34925
No. of independent reflections	4170	6763	5645
R_{int}	0.0542	0.0464	0.0537
Final R_1 values ($I > 2\sigma(I)$)	0.0490	0.0655	0.0780
Final $wR(F^2)$ values ($I > 2\sigma(I)$)	0.1178	0.1628	0.1899
Final R_1 values (all data)	0.0556	0.0814	0.0900
Final $wR(F^2)$ values (all data)	0.1215	0.1746	0.1989
Goodness of fit on F^2	1.079	1.024	1.060
CCDC number	1534186	1534187	1534188

Table S6: Calculated (i) τ values and (ii) π-π stacking distances of single X- ray crystal structures of **PR1'**, **PR3'** and **PR7'**

Crystal Structures	*τ* values	π-π stacking distances (Å)
PR1'	0.76	3.469 and 3.631
PR3'	0.40	3.503 and 3.474
PR7'	0.86	3.947 and 4.339

Synthesis: Details synthetic procedure of axles

Axle3: To the stirring solution of 2-bromoethanol (0.156 ml, 2.2 mmol) and dry Et_3N (0.306 ml, 2.2 mmol) in dry THF (20 ml), 4BPyCOCl (281 mg, 1 mmol) in dry THF (25 ml) was added with pressure-equalizing-funnel. The solution mixture was allowed to stir at room temperature in ice cold condition for 24h under N_2 atmosphere, followed by removal of solvent in *vaccuo*. The reaction mixture was stirred with saturated $NaHCO_3$ solution (25 ml) for 6h, then appearing precipitate was collected by filtration. Finally after drying the precipitate **Axle3** was obtained as light pink solid (199 mg, 71%).

Axle4: To the stirring solution of propargyl alcohol (0.128 ml, 2.2 mmol) and dry Et_3N (0.306 ml, 2.2 mmol) in dry THF (20 ml), 4BPyCOCl (281 mg, 1 mmol) in dry THF (25 ml) was added with pressure-equalizing-funnel. The solution mixture was allowed to stir at room temperature in ice cold condition for 24h under N_2 atmosphere, followed by removal of solvent in *vaccuo*. The reaction mixture was stirred with saturated $NaHCO_3$ solution (25 ml) for 6h, appearing precipitate was collected by filtration. Finally after drying the precipitate, purification was done by silica gel column chromatography using Petroleum ether/ Ethylacetate (70: 30) as eluent to afford **Axle4** as light pink solid (199 mg, 80%).

Axle5: To the stirring solution of BPy4COOH (244 mg, 1 mmole) in dry THF (20 ml), TBAF (946 mg, 3 mmol) was added and allowed to stir for few minutes. Then AllI **(**616 mg, 2.2 mmol**)** in dry THF (25 ml) was added dropwise to the previous mixture with a pressure

equalizing funnel. The mixture was allowed to reflux under N_2 atmosphere at 70°C for 48h followed by removal of solvent in *vaccuo*. The reaction mixture was extracted 3 times with $CHCl_3$ from the aqueous layer (50 X 3). Organic extracts were combined and washed several times by using saturated $NaHCO_3$ solution (200ml) and brine solution (200 ml), dried over Na_2SO_4 and concentrated under reduced pressure. Final purification was done by silica gel column chromatography using petroleum ether/ ethyl acetate (96: 4) as eluent to afford off white coloured solid **Axle5** (438 mg, 80%).

Axle6: To the stirring solution of BPy4COOH (244 mg, 1 mmol) in dry THF (20 ml), TBAF (946 mg, 3 mmol) was added and allowed to stir for few minutes. Then PropI **(**611 mg, 2.2 mmol**)** in dry THF (25 ml) was added dropwise to the previous mixture with a pressure equalizing funnel. The mixture was allowed to reflux under N_2 atmosphere at 70°C for 48h followed by removal of solvent in *vaccuo*. The reaction mixture was extracted 3 times with $CHCl_3$ from the aqueous layer (50 X 3). Organic extracts were combined and washed several times by using saturated $NaHCO_3$ solution (200ml) and brine solution (200 ml), dried over Na_2SO_4 and concentrated under reduced pressure. Final purification was done by silica gel column chromatography using petroleum ether/ ethyl acetate (94 : 6) as eluent to afford yellowish coloured solid **Axle6** (397 mg, 73%).

Axle8: To the stirring solution of 3-amino-1-propanol (0.168 ml, 2.2 mmol) and dry Et_3N (0.306 ml, 2.2 mmol) in dry THF (20 ml), 4BPyCOCl (281 mg, 1 mmol) in dry THF (25 ml) was added with pressure-equalizing-funnel. The solution mixture was allowed to stir at room temperature in ice cold condition for 24h under N_2 atmosphere, followed by removal of solvent in *vaccuo*. The reaction mixture was stirred with saturated $NaHCO_3$ solution (25 ml) for 6h, appearing precipitate was collected by filtration. Finally after drying the precipitate, **Axle8** was obtained as white coloured solid (243 mg, 68%).

Axle9: To the stirring solution of 2-aminoethyl azide (189 mg, 2.2 mmol) and dry Et_3N (0.306, 2.2 mmol) in dry THF (20 ml), 4BPyCOCl (281 mg, 1 mmol) in dry THF (25 ml) was added with pressure-equalizing-funnel. The solution mixture was allowed to stir at room temperature in ice cold condition for 24h under N_2 atmosphere, followed by removal of solvent in *vaccuo*. The reaction mixture was stirred with saturated $NaHCO_3$ solution (25 ml) for 6h, appearing precipitate was collected by filtration. Finally after drying the precipitate, **Axle9** was obtained as light pink solid (228 mg, 60%).

Axle10: To the stirring solution of benzylamine (0.240 ml, 2.2 mmol) and dry Et_3N (0.306, 2.2 mmol) in dry THF (20 ml), 4BPyCOCl (281 mg, 1 mmol) in dry THF (25 ml) was added with pressure-equalizing-funnel. The solution mixture was allowed to stir at room temperature in ice cold condition for 24h under N_2 atmosphere, followed by removal of solvent in *vaccuo*. The reaction mixture was stirred with saturated $NaHCO_3$ solution (25 ml) for 6h, appearing precipitate was collected by filtration. Finally after drying the precipitate, **Axle10** was obtained as a white coloured solid (337 mg, 80%).

References:

1. (a) E. C. Constable, A. H. Redondo, C. E. Housecroft, M. Neuburger and S. Schaffner, *Dalton Trans*., 2009, **33**, 6634–6644; (b) R. D. Willett, G. Pon and C. Nagy, *Inorg. Chem*., 2001, **40**, 4342–4352.

2. R. M. Williams, L. D. Cola, F. Hartl, J.-J. Lagref, J.-M. Planeix, A. D. Cian and M. W. Hosseini, *Coord. Chem. Rev.*, 2002, **230**, 253–261.